Space Environment Corporation

1010 Eastridge Drive, Logan, UT USA 84321-4990 435-752-6567

December 12, 2020

Defense Technical Information Center
8725 John J Kingman Road Suite 0944
Fort Belvoir, VA 22060-6218

Subject: Final Report Delivery under Award N00014-17-1-2156.

Greetings,

We at Space Environment Corporation have delivered the Final Report, which is also the final year Technical Report to the Technical Representative, Daniel Eleuterio of the Ocean, Atmosphere, and Space Research Division of the Office of Naval Research in fulfilling the requirements of Grant12231256 under Award N00014-17-1-2156 entitled ***"New Ionosphere Model for the Global Bottom-Side Ionosphere from 50 to 350 km: TIDS, Metal Ion Layers, D Region, and Severe Disturbance."*** This delivery to you includes the following:

1. Final Technical Report transmittal letter.
2. Final Report with SF298 Document Report cover. This is also the Performance/Technical Report for the final year of the grant.

This delivery is in fulfillment of the requirements of the Award mentioned in the subject line.

Sincerely,

James Vincent Eccles

James Vincent Eccles (vince.eccles@sdl.usu.edu, 435-757-2499)

enclosed:
Final Report transmittal letter
The Final Report with SF298 cover letter

REPORT DOCUMENTATION PAGE

Form Approved
OMB No. 0704-0188

1. REPORT DATE *(DD-MM-YYYY)*	2. REPORT TYPE	3. DATES COVERED *(From - To)*
13-12-2020	FINAL REPORT	02/01/2017-09/30/2020

4. TITLE AND SUBTITLE
New Ionosphere Model for the Global Bottom-Side Ionosphere from 50 to 350 km: TIDs, Metal Ion Layers, D Region, and Severe Disturbances

5a. CONTRACT NUMBER

5b. GRANT NUMBER
N00014-17-2156

5c. PROGRAM ELEMENT NUMBER
ONR BAA N00014-16-S-BA10

6. AUTHOR(S)
J. V. Eccles, J. J. Sojka, and D. Rice

5d. PROJECT NUMBER
701 BSION

5e. TASK NUMBER

5f. WORK UNIT NUMBER

7. PERFORMING ORGANIZATION NAME(S) AND ADDRESS(ES)
Space Environment Corporation
1010 Eastridge Drive
Logan, UT USA 84321-4990

8. PERFORMING ORGANIZATION REPORT NUMBER
SEC-2020-BSION-FINAL

9. SPONSORING/MONITORING AGENCY NAME(S) AND ADDRESS(ES)
Office of Naval Research
Ocean Atmosphere and Space Research Division
875 North Randolph Street
Arlington, VA 22203-1995

10. SPONSOR/MONITOR'S ACRONYM(S)

11. SPONSOR/MONITOR'S REPORT NUMBER(S)

12. DISTRIBUTION/AVAILABILITY STATEMENT
Approved for public release: Distribution unlimited

13. SUPPLEMENTARY NOTES

14. ABSTRACT
The bottom-side ionosphere is a structured component of the upper atmosphere in vertical and horizontal directions as well as temporally. This effort will create a new ionosphere model capable of reproducing observed structures and temporal variations in the bottom-side ionosphere from 40 to 400 km altitude. The new bottom-side ionosphere model will respond with proper temporal variations and phasing of traveling ionospheric wave phenomena driven by atmospheric waves, winds, & tides and ionospheric electric fields. Bottom-side physics and chemistry will be included to properly model (1) the D, E, & F regions, (2) ion layers in response to atmospheric tides and gravity waves, (3) sporadic E layers, (4) response to solar x-ray flares and energetic particles fluxes. Space Environment Corporation will deliver the new ionosphere model software, documentation of chemistry-physics-numerical methods, and User's Manual.

15. SUBJECT TERMS
Ionosphere model, D region, metal ion layers, traveling ionospheric disturbances

16. SECURITY CLASSIFICATION OF:			17. LIMITATION OF ABSTRACT	18. NUMBER OF PAGES	19a. NAME OF RESPONSIBLE PERSON
a. REPORT	b. ABSTRACT	c. THIS PAGE			James Vincent Eccles
U	U	U	U	101	19b. TELEPHONE NUMBER *(Include area code)* 435-757-2499

New Ionosphere Model for the Global Bottom-Side Ionosphere from 50 to 500 km: TIDs, Metal Ion Layers, D Region, and Severe Disturbance

Award No. N00014-17-1-2156

Technical Report for
2nd Option Year with No-Cost Extension
3D BIWXM Model Development
02/01/2019 to 09/30/2020

James Vincent Eccles (PI), Donald Rice, and Jan J. Sojka

Space Environment Corporation
1010 Eastridge Drive
Logan, Utah 84321

Vince.eccles@spacenv.com
(435) 752-6567 (corporate office)
(435) 757-2499 (Vince Eccles contact number)

New Ionosphere Model for the Global Bottom-Side Ionosphere from 50 to 500 km: TIDs, Metal Ion Layers, D Region, and Severe Disturbance

Table of Contents

Table of Contents

1. Introduction of BSION/BIWXM Effort Summary

Scientists at Space Environment Corporation in collaboration with Dr. Titus Yuan of Utah State University (USU) are developing a new ionosphere model called the ***Bottom-side Ionosphere with Winds, X-rays, and Metals*** or ***BIWXM***. It is being designed to have a full complement of physics and chemistry necessary to model the bottom-side ionosphere from 50 to 500 km as the region that affects radio signal propagation for frequencies from 3kHz to 300 MHz (VLF, LF, MF, HF, VHF). BIWXM will be built on the foundation of existing models, but with improvements and extensions that will enable an increased fidelity through the whole altitude range of the bottom-side ionosphere. The completed effort will address these key issues:

1) The most recent solar ionization physics for quiet and flare conditions,
2) D region chemistry and physics including a physics-based model of nitric oxide and metastable neutrals necessary for the accurate determination of the D region profiles,
3) Secondary electron physics to ensure proper responses to disturbance conditions,
4) Ion transport with sufficient chemistry for E-F1 region
5) Altitudes to include wind-altered profiles and metal ion layers including a neutral metal layer model to support the metal ion layer physics, and
6) Appropriate transport response of F region plasma to capture TIDs and F region modulations.

The ionosphere model design will be suitable for massively parallel computer systems for global high-resolution solutions of electron and ion density specifications as well as very high-resolution regional specifications. The ionosphere model will be developed for coupling with atmosphere models through a suitable modeling framework. The final ionosphere model will be delivered for producing 3D ionospheric specifications that are suitable for coupling atmosphere and electric field models. This will be accompanied by the following documentation:

1) User's Manual,
2) Physics-Chemistry-Numerics Document,
3) Full BIWXM Code Distribution, and
4) Three standard runs for model deployment validation. These three standard runs will be chosen from the validation tests with data associated with effects in the D region, metal layers, and TIDs.

2. BSION/BIWXM Development Task Charts

Base Year Task Chart for BWIXM Model Development (February 2017 to January 2018)

TASK 1: Field Line Model	Feb-Apr	May-Jul	Aug-Oct	Nov-Jan
Subtask 1.0: Meetings		VE		VE
Subtask 1.1: Create numerical engine of 1D BIWXM	VE	VE		
Subtask 1.2: Collect & test D-Region chemistry		VE	VE	
Subtask 1.3: Collect metal ion chemistry			VE	VE
Subtest 1.4: Validation of chemistry for D & E Reg.				VE
Subtest 1.5: Solar spectrum refinement	JS	JS	JS	
Subtask 1.6: Collect validation data		DR	DR	DR
Subtask 1.7: Maintain documents	SS	SS	SS	SS
Subtask 1.8: Atmosphere model			TY	TY

VE – Vince Eccles, JS – Jan Sojka, DR –Donald Rice, SS – Susan Sojka, TY – Titus Yuan

* Completed work in blue

1st Option Year Task Chart for BIWXM Model Development (February 2018 to January 2019)

TASK 2: Global BIWXM Model	Feb-Apr	May-Jul	Aug-Oct	Nov-Jan
Subtask 2.0: Meetings		VE		
Subtask 2.1: Create global overarching framework	VE	VE		
Subtask 2.2: Create grid-interpolation modules		VE	VE	VE
Subtask 2.3: Create global atmosphere module			VE	VE
Subtest 2.4: Create neutral metal layer module		VE	TY	VE
Subtest 2.5: Define Nitric Oxide module			JS	JS
Subtask 2.6: Create Nitric Oxide module				JS,VE
Subtask 2.7: Collect TID and TAD observations			DR	DR
Subtask 2.8: (1) User, (2) I/O, (3) Physics Docs	SS, All	SS, All	SS, All	SS, All
Subtask 2.9: Test metal layers & TID simulations				TY

VE – Vince Eccles, JS – Jan Sojka, DR –Donald Rice, SS – Susan Sojka, TY – Titus Yuan

2nd Option Year Task Chart for BIWXM Model Development (February 2019 to January 2020)

TASK 2: Global BIWXM Model	Feb-Apr	May-Jul	Aug-Oct	Nov-Jan
Subtask 3.0: Meetings		VE		
Subtask 3.1: Create 3D BIWXM Model			VE	VE
Subtask 3.2: Create Solar Flare Model for EUV			JS	JS
Subtask 3.3: Implement MSIS 2.0			VE	VE
Subtest 3.4: Create neutral metal layer module		TY,VE	TY,VE	TY,VE
Subtask 3.5: Test neutral/ion metal BIWXM			TY,VE	TY,VE
Subtask 3.6: Create Galactic Cosmic Ray module			VE	VE
Subtask 3.7: Create auroral ionization & convection			VE	VE
Subtask 3.8: Create SPE ionization module			VE	VE
Subtask 3.9: (1) User, (2) I/O, (3) Physics Docs	SS, All	SS, All	SS, All	SS, All
Subtask 3.10: Test BIWXM Components	JS,VE	JS,VE	JS,VE	JS,VE

VE – Vince Eccles, JS – Jan Sojka, DR –Donald Rice, SS – Susan Sojka, TY – Titus Yuan

No-Cost Extension Task Chart for BIWXM Model Development (February 2020 to September 2020)

TASK 2: Global BIWXM Model	Feb-Apr	May-Jul	Aug-Oct	Nov-Jan
Subtask 3.0: Meetings			VE	
Subtask 3.1: Create 3D BIWXM Model			VE	VE
Subtask 3.2: Create Solar Flare Model for EUV		JS	JS	
Subtask 3.3: Implement MSIS 2.0			VE	VE
Subtest 3.4: Create neutral metal layer module		TY,VE	TY,VE	TY,VE
Subtask 3.5: Test neutral/ion metal BIWXM			TY,VE	TY,VE
Subtask 3.6: Create Galactic Cosmic Ray Module	VE	VE		
Subtask 3.7: Create auroral ionization & convection	VE	VE		
Subtask 3.8: Create SPE ionization module	VE	VE		
Subtask 3.9: (1) User, (2) I/O, (3) Physics Docs	SS, All	SS, All	SS, All	SS, All
Subtask 3.10: Test BIWXM Components	JS,VE	JS,VE	JS,VE	JS,VE

VE – Vince Eccles, JS – Jan Sojka, DR –Donald Rice, SS – Susan Sojka, TY – Titus Yuan

Tasks of second option year were not completed due to reduced work effort and spending on the contract. A No-Cost extension was requested and approved. This report presents specifically the tasks accomplished during the 2nd Option year and No-Cost extension period. The combination of this technical report and the BIWXM documents of the Chemistry-Physics-Numerics Document and the User's Guide are the Final Report of the Space Environment Corporation (SEC) effort on the BSION Grant from the Office of Naval Research (ONR). All references are provided in the Chemistry-Physics-Numerics Document.

3. Progress Report on 2nd Option/No-Cost Extension Year Tasks

Subtask 3.0: Meetings. The BSION Review Meeting was attended by Dr. Vince Eccles and Jan Sojka at the Naval Research Laboratory in July 2019. Additionally Dr. Vince Eccles attended the BSION Review Meeting through a Zoom Virtual Meeting hosted by the Naval Research Laboratory in August 2020. Dr. Eccles and Dr. Sojka presented the progress of the development of *"A new bottomside ionosphere model for the ONR BSION program:* ***Bottomside Ionosphere with Winds, X-rays, and Metals (BIWXM).***"

Subtask 3.1: Create 3D BIWXM Model. The 1D BIWXM model was continually updated with new physics components necessary for the modeling of the high latitude ionosphere, in particular, and a 3D version of the BIWXM model was developed. The most suitable implementation of the BIWXM model was for the creation of a high and mid latitude 3D model. This was done in a manner to produce very high-resolution ionosphere representations using parallel capabilities of multi-CPU computers. The 3D code was developed and run on 3 different LINUX machines: 8-core Intel CPU UBUNTU 20.04 LINUX machine, 32-core AMD CPU UBUNTU 18.04 LINUX machine, and a 48-core Intel CPU CENTOS 7 LINUX machine. The debugging of the 3D module has taken longer than anticipated and required the No-Cost. The highest resolution demonstration of the 3D model was 50 km by 50 km cells over the mid and high Northern latitudes (MLAT>45°).

Subtask 3.2: Create Solar Flare Model for EUV. The first implementation of the solar flare response within BIWXM was based on the flare model within the Data-Driven D-Region (DDDR) model, which was primarily a hard X-ray solar flare definition. Jan Sojka demonstrated that this was not sufficient for producing an E and F region response to solar flares. Thus, Dr. Sojka produced an EUV and soft X-ray solar flare module to improve the BIWXM response to solar flares.

Subtask 3.3: Implement Additional Atmosphere Models. This task was related to coupling BIWXM to the Whole Atmosphere Model (WAM). A subroutine was written to read WAM results provided by Timothy Fuller-Rowell. However, the coupled atmosphere-ionosphere-electric field modeling system produced unusable plasma drifts. The subroutine to couple the WAM model with BIWXM is available, but we moved to implement the MSIS 2.0 atmosphere with the Nitric Oxide (NO) species, the Horizontal Wind Model, and empirical electric field convection to obtain better results. Additionally, the tasks of adding important physics to the BIWXM model consumed significant work effort. These physics components are isolated in subroutines and can be used for any other ionospheric model development. This turns out to be a very capable ionosphere model for magnetic latitudes above 30° magnetic latitude. The NO species within MSIS 2.0 is still a pre-release version provided by Dr. Emmert of NRL, but it provides suitable quiet-time ionization profiles in the D region with demonstratable improvements to the electron density profiles when compared to the results of the Data-Driven D-Region model of Eccles et al. [2004].

Subtask 3.4: Create Neutral Metal Layer Module. The neutral metal layer model was developed within a second effort associated with Xuguang Cai and Tao Yuan of Utah State University. With this SEC version of the BIWXM we prefer the speed of using an empirical representation of the metal neutral layers to permit more efficient ionosphere calculations.

Subtask 3.5: Test neutral/ion metal layer module. Two papers were written describing the development of the neutral-ion metal layer modules with coauthors Xuguang Cai, Tao Yuan, and Vince Eccles [Xugaung et al, 2018; 2019].

Subtask 3.6: Create Galactic Cosmic Ray module. To produce a rigorous model of the D region it was important to create a new Galactic Cosmic Ray (GCR) module for BIWXM. This was accomplished and tested.

Subtask 3.7: Create auroral ionization and high latitude convection modules. To extend BIWXM to high latitudes an electron precipitation module and an electric field convection module were created to enable the modeling of the high-latitude ionosphere. This version improves the DDDR auroral ionization module and provide rigorous transport calculations imposed by the high latitude electric field convection potential. The ionization module for electron precipitation can use non-Maxwellian precipitation descriptions.

Subtask 3.8: Create a Solar Proton Event module. To extend BIWXM to high latitudes an energetic proton ionization module was developed and tested. The solar proton ionization profiles compare very favorably with profiles generated by the HEPPA-II model [Matthes et al., 2017].

Subtask 3.9: User's Manual, Software Version, and Physics/Chemistry/Numerics Document: These documents are completed and included with the Final Report delivery.

Subtask 3.10: Test BIWXM Components: The new components of the GCR, electron precipitation, solar proton ionization profiles were tested against published profiles. These were tested within the BIWXM using the EISCAT incoherent scatter radar during an event that measured the ionization due to a solar flare, auroral precipitation, and a solar proton event. Additional, tests were performed against Millstone Hill Incoherent scatter radar to test the bottomside solar ionization and the ion/electron temperature calculations. Finally, the BIWXM D region was compared against the community database of rocket flight measurements of D region electron density.

4. Development of the 3D BIWXM

4.1. Completion of 1D BIWXM

The BIWXM one-dimensional model (BIWXM1D) was completed and documents updated for final delivery. The BIWXM1D was updated alongside the development of the 3D version of the BIWXM model. The Base Year development effort was focused on the 1D BWIXM model for efficiently calculate both the transport and chemistry of the ionosphere in the altitude range of 50 to 550 km, which necessarily includes the topside ionosphere. Thus, the practical range of BIWXM is 30 to 3000 km, which is an excellent choice to cover the full range of phenomena of the bottomside ionosphere. Transport and chemistry are performed through all altitudes. This enables the lower E region and D region ionization to respond to modification by neutral winds. The numerics of the BIWXM model includes a sophisticated chemistry solver suitable for 'stiff' differential equations associated with complex chemistries. The transport numerics strives to accurately reproduce density features and wave propagation. The chemistry and transport are solved through spilt timestep methods to permit the transport solution to progress at near the courant stability limit for timesteps, while the chemistry can be calculated at much shorter timesteps for accurate chemical behavior within the complexity of a reactive multi-species gas.

The BIWXM model uses species and reaction setup files to define the chemical and collisional parameters of the ionosphere and atmosphere species required for the solution. There are minimum requirements for the species file to obtain a quality ionosphere solution. The atmosphere neutral species must include H, O, N_2, NO, and O_2. The ions species must include H^+, O^+, N_2^+, NO^+, and O_2^+. Additionally, the O_2^- ion is used to accommodate rapid calculations of

the D region profiles. This provides a very good estimate of the quiet time and disturbance period D region electron densities. Improving these profiles with more complicated chemistry is not efficient. Heterogeneous chemistry with smoke particles and aerosols is required for D region profile improvements. This first-order accuracy of the D region profiles depends more on the ionization source definitions by solar ionization (EUV and X-ray) and particle ionization (auroral and SPE) and on the Nitric Oxide profile. The delivered version of the BIWXM model includes Fe^+, Fe, FeO, FeO_2, and FeN_2 to enable the modeling of a representative metal ion layer. An ad hoc Fe layer is provided to support the development of Fe^+ ions. More complicated ionospheres can be solved by including additional species and different reaction chemistry sets.

Solar Spectrum Upgrades

A part of the BIWXM 1D development effort was to upgrade the solar spectrum binning with associated absorption and ionization cross sections to enable the most accurate ionization profiles for D, E, and F1 regions of the ionosphere. The current status of most ionosphere models depends on the EUVAC solar spectrum [*Richards et al.*, 1994*ab*], which has been shown to be insufficient for the lower E region [*Sojka et al.*, 2016] and does not cover X-rays or Lyman Alpha necessary for D region ionization profiles. The X-ray spectrum is current populated using a quiet and storm time average spectrum developed from TIMED satellite observations and a partitioning of the GOES X-ray bins and the addition of a Lyman Alpha bin. This provides a solar spectrum from 0.5 A to 1214 A that enables a full development of solar ionization profiles for the ionosphere. We note here that He ionization is also calculated in the BIWXM code so He+ can be added to the species.set and reactions.set files.

The TIMED X-ray range and the EUV range both did not response to solar flares indicated within the GEOS X-ray observation stream, which is used by BIWXM to drive the ionospheric solar flare response. The early BIWXM model response did not change the E and F region profiles during solar flares (Figure 1). Thus, Jan Sojka developed an EUV soft X-ray flare model to provide a flare response within the BIWXM. See the BIWXM Physics, Chemistry Numerics for details. Figure 2 presents the BIWXM E and F1 region response using the new EUV/soft X-ray flare model.

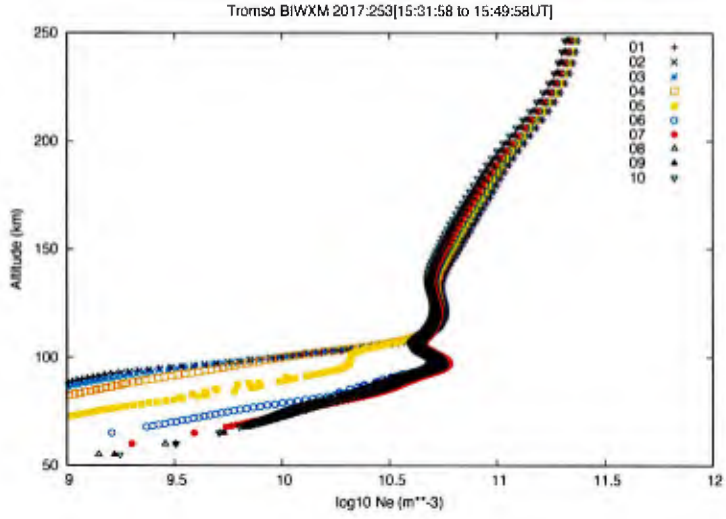

(a)

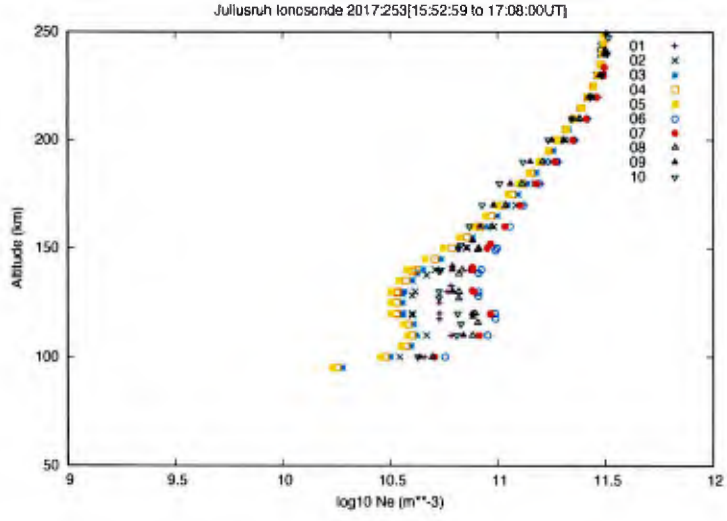

(b)

Figure 1. (a) BIWXM results during flare of 2017/253 at Juliusruh, Germany. The early version of BIWXM response to solar flares only below 100km. (b) Ionosonde measurements demonstrate E region response during same flare. Both present profiles between 15:50 to 17:10UT.

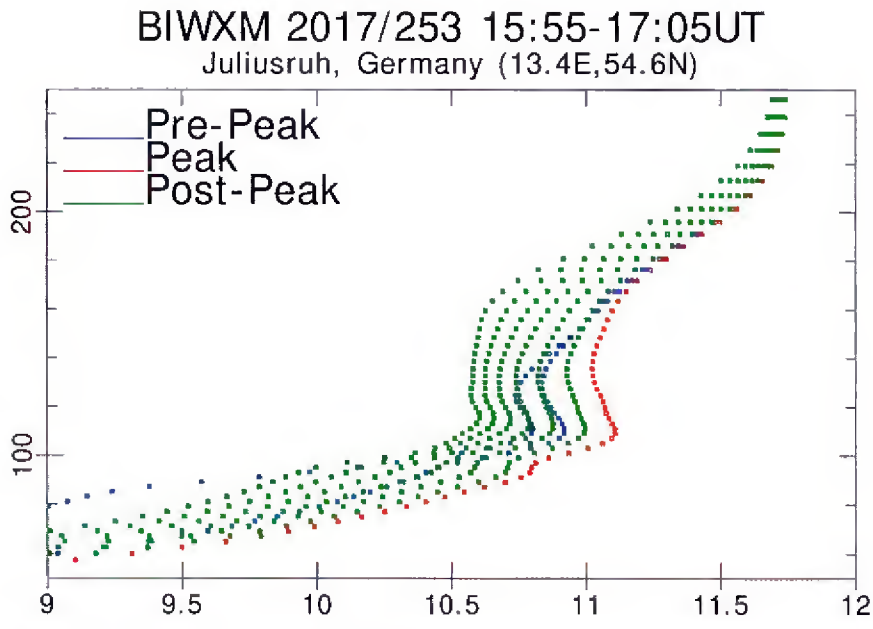

Figure 2. BIWXM profiles from 15:55 to 17:05 UT during flare of 2017/253. Using the new solar Flare soft X-ray/EUV model.

High-Latitude Drivers

To properly model the high latitude ionosphere, a convection module was developed to move plasma through ExB along potential contours of convection potential. The Weimer Convection Model was used to develop the capability. Other models can be used as well. The convection electric field affects the ion velocity calculations and imposes motion along field lines through collisional forcing when the convection velocity is high. This is all properly calculated in the ion velocity module.

Additionally The modules to produce ionization profiles from energetic protons (solar proton events) and from energetic electron precipitation (auroral ionizaiton) were developed and compared against other models and data. The solar proton ionization profiles were compared against results from the HEPPA-II model [Matthes et al., 2017] and the electron precipitation ionization profiles were compared against the GLobal airglOW model (GLOW) of Solomon [2017]. The BIWXM model was used to favorably model results from the EISCAT incoherent scatter radar at 19.5E and 69.5N on the same day as Figures 1 and 2. In Figure 3 we show panels of (top to bottom): the Kp values (Newell formula for Kp), the GOES X-ray fluxes, the GOES solar proton fluxes, and the electron density profiles for a portion of day 2017/253. This particular day showed ionospheric response to solar spectrum, solar flare, solar protons, and auroral precipitation.

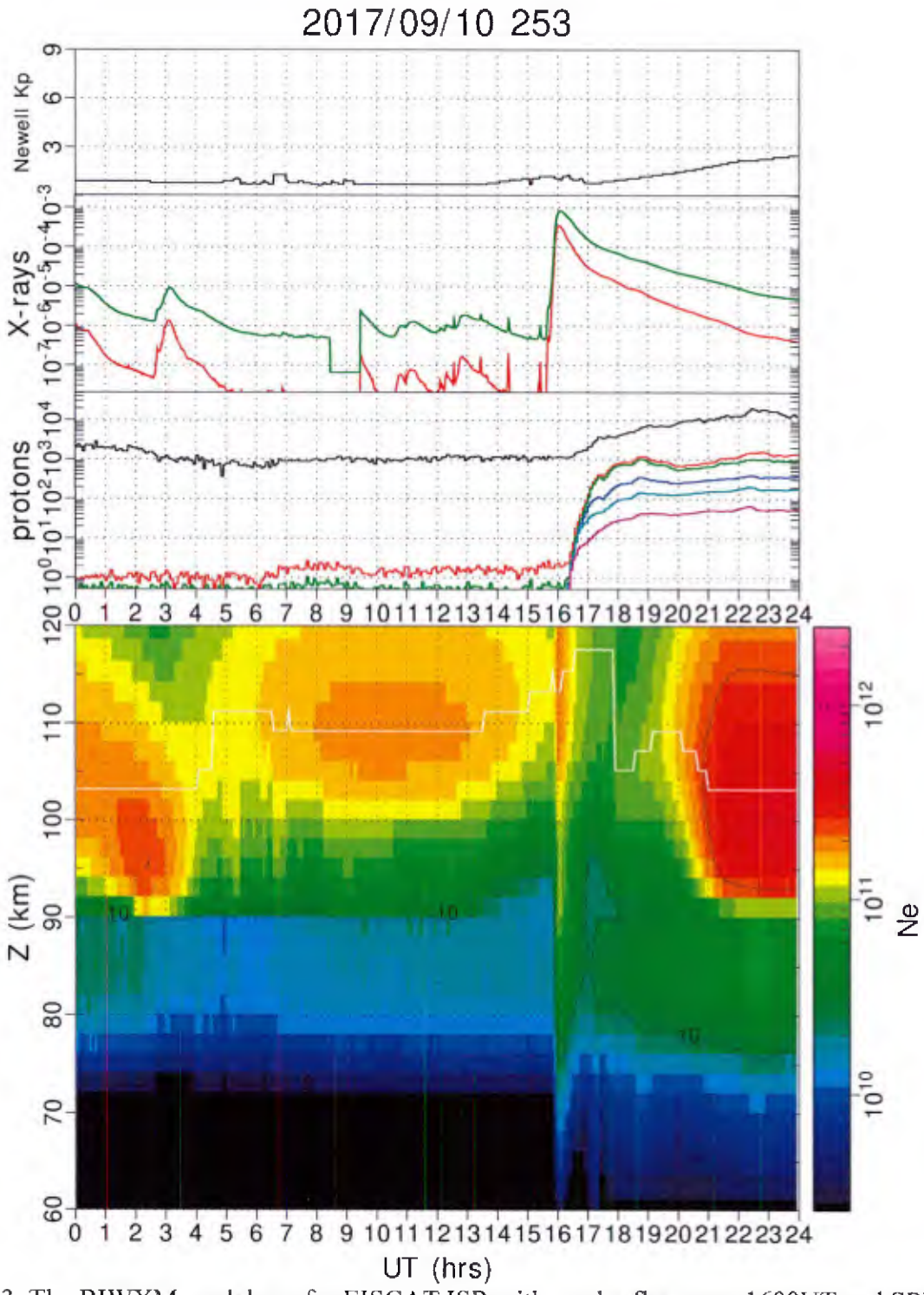

Figure 3. The BIWXM model run for EISCAT ISR with a solar flare near 1600UT and SPE event beginning near 1630UT, and auroral precipitation appearing before 0400UT and after 2000UT. Local Solar Noon occurs near 1030UT.

D Region Improvements and Testing

The D region chemistry was re-examined in detail for the BIWXM V2 delivery. The time-dependence of the BIWXM solution did not perform as well with the night time solutions of the D region electron densities when compared with the Data-Drive D-Region (DDDR) model results. The DDDR model result uses a steady-state solution and the time-dependent BIWXM solution permitted a very slow nighttime decay of the D region after sunset. The BIWXM reaction set updated with ion-electron 3 body recombination which accelerates the D region decay after sunset. The effective recombination has been reported in [Gledhill, 1986] with

$$\alpha = 2.5 \times 10^{-13} \exp(-0.234\, z)$$

for night time and

$$\alpha = 2.5 \times 10^{-13} \exp(-0.165\, z)$$

for day time rates (/cm^3/s) and calculated as a 2-body reaction though it is representing 3-body recombination. The daytime rate should be used during disturbed periods (solar proton events). BIWXM handles this reaction rate using a formula identifier within the reactions.set, `| recom3`. This is an identifier to the BIWXM program to use an internal formula to calculate an altitude dependent value depending on the solar angle. The regular 3-body i-e reaction commented out (#) within the reactions.set provided in the distribution. The higher 3-body reaction rate at night helps remove electrons in the 85 to 50 km altitude range after sunset. This seems to better agree with VLF propagation calculates. These elevated 3-body rates were not needed in the DDDR since it calculated a steady-state profile.

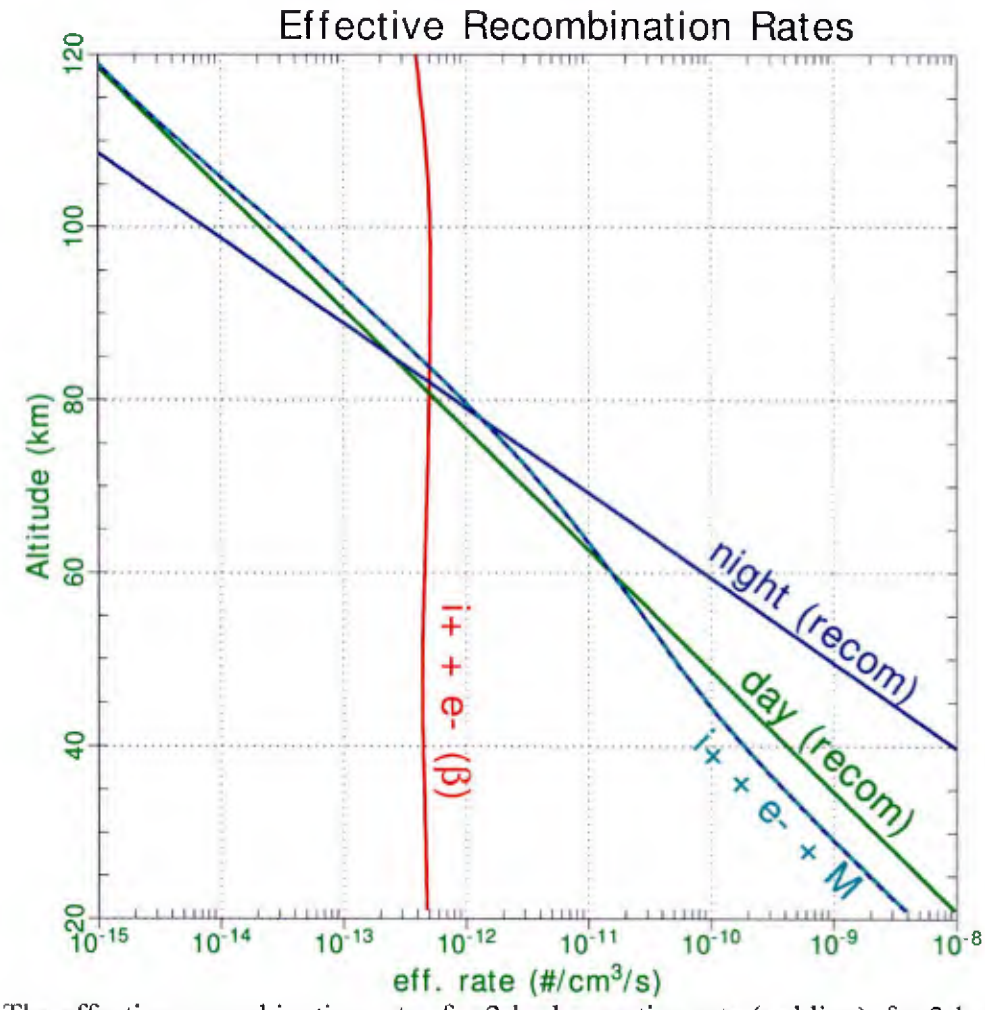

Figure 4. The effective recombination rates for 2-body reaction rate (red line), for 3-body reaction rate (dashed line), for the recom formula for day (green line) and night (blue line).

4.2. Comparison of Rocket Data with BIWXM and DDDR

A comparison of day and night time BIWXM profiles with DDDR profiles for various rocket flights indicate that BIWXM is now performing at least as well as DDDR for quiet time profiles. Figure 5 presents a number of D region rocket flight observations with both models. These profiles show several of the 'good' comparisons. There are many with poor comparisons due to the unknown solar flare conditions of these pre-2000 rocket flights.

The comparison of 50 rocket flights that indicate quiet D region behavior with DDDR and BIWXM models is show in Figure 6. This is an RMS and Difference calculation performed on the log of the electron density in 10 km altitude bins. Doing this on log density permits underestimates to be measured equally with overestimates in density. The resulting comparison demonstrates that BIWXM performs as well or better than DDDR at all altitudes except the lowest altitude bin ($50<z<60$ km). The rocket data begin at 50 km. The night time comparison shows similar improvements for the BIWXM D Region over the DDDR results. However, the

BIWXM night time D Region demonstrates greater variablility than the DDDR model due to the inclusion of ion transport at all altitudes. The neutral wind tides do generate ion motion within the E region and upper D region altitudes. The rocket flight comparisons for this comparison of DDDR and BIWXM D Region profiles are placed on the Final Report delivery DVD.

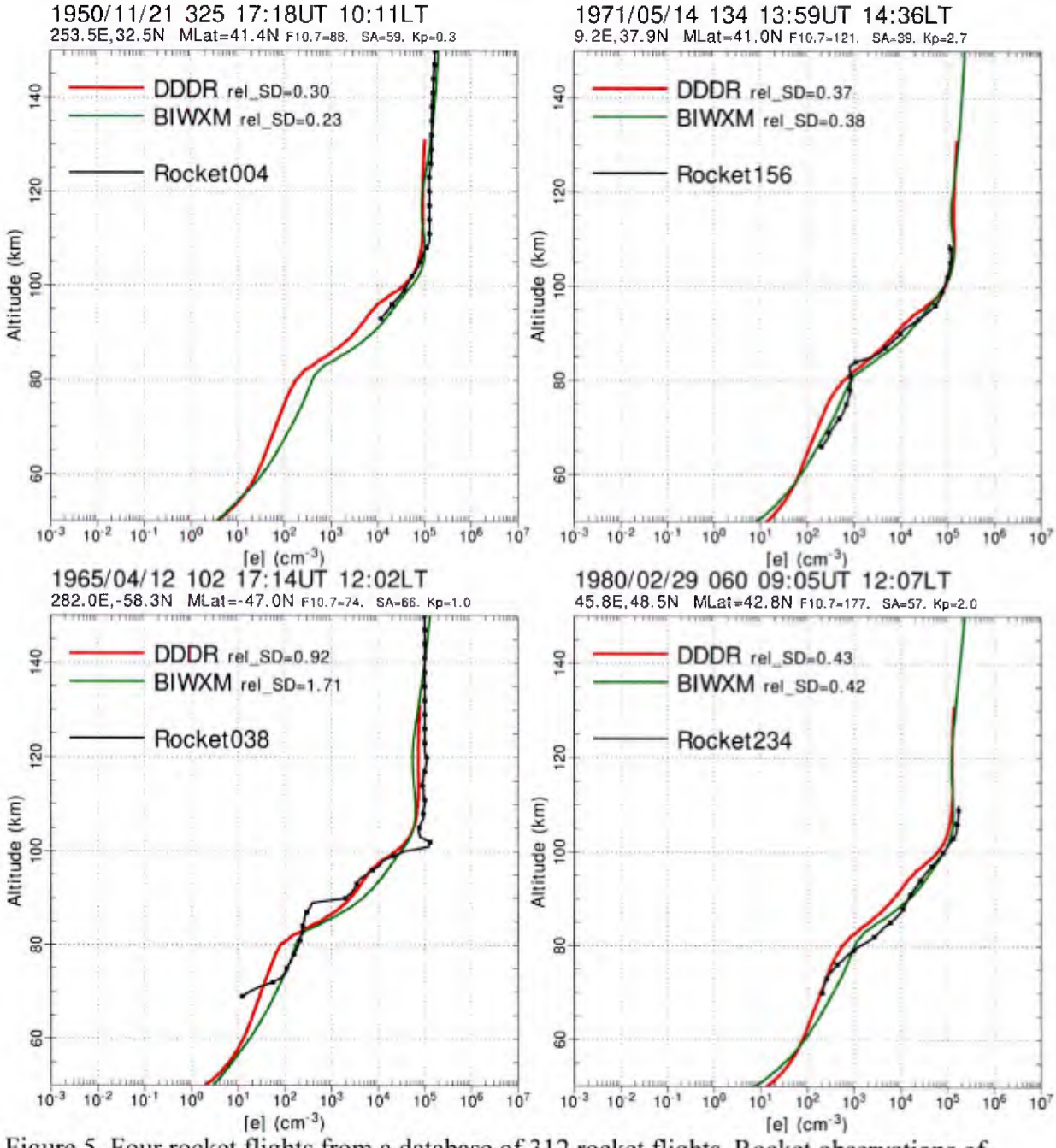

Figure 5. Four rocket flights from a database of 312 rocket flights. Rocket observations of electron density (black lines) are compared against DDDR (red lines) and BIWXM (green lines) profiles.

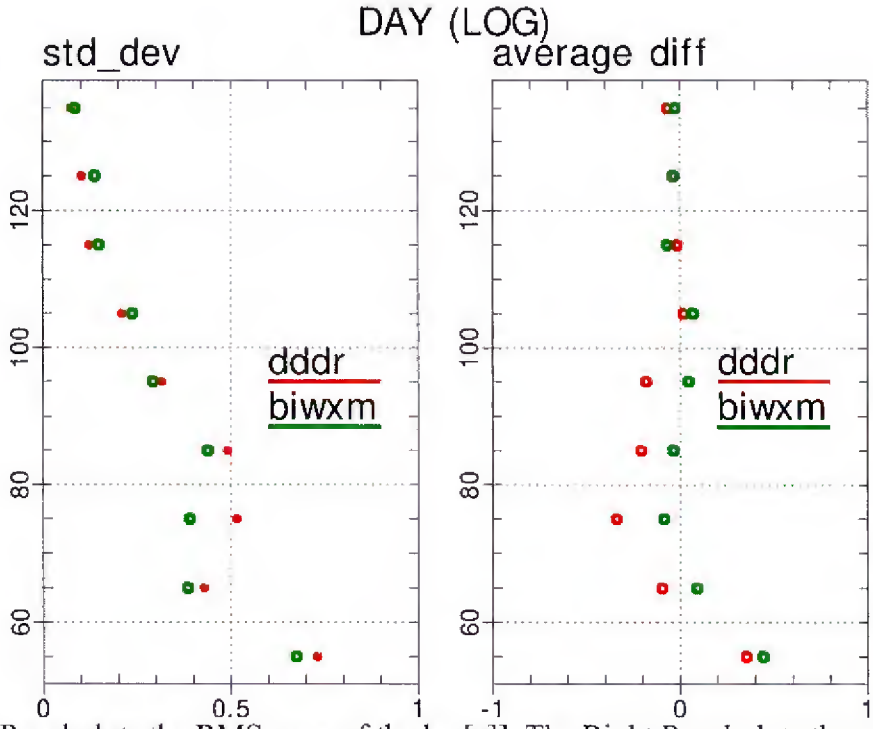

Figure 6. Left Panel plots the RMS error of the log[e]]. The Right Panel plots the average difference of the log[e].

4.3. Development of the 3D BIWXM

The complexities of developing a new ionosphere model that includes all ionizations sources extended the required work effort on the BIWXM1D model. The 3D implementation was delayed. During the No-Cost extension a very high-resolution 3D capability was developed for the mid and high latitude ionosphere. A many trajectory program, *biwxm_tr.x*, was created to take advantage of multi-CPU computer systems. The resulting 3D BIWXM is 'delightfully parallel' and scales directly with the number of available cores in a computer. The user requests a resolution of 2., 1., or 0.5 degrees for the region above 45 degrees magnetic latitude for the 3D BIWXM run. The 3D BIWXM produces two output files that hold the individual profiles and a regular gridded ionospheric representation. The 3D BIWXM has been tested on multiple computers at multiple resolutions and is now ready for delivery to ONR. Parameters from a 3D BIWXM run are shown in Figure 7.

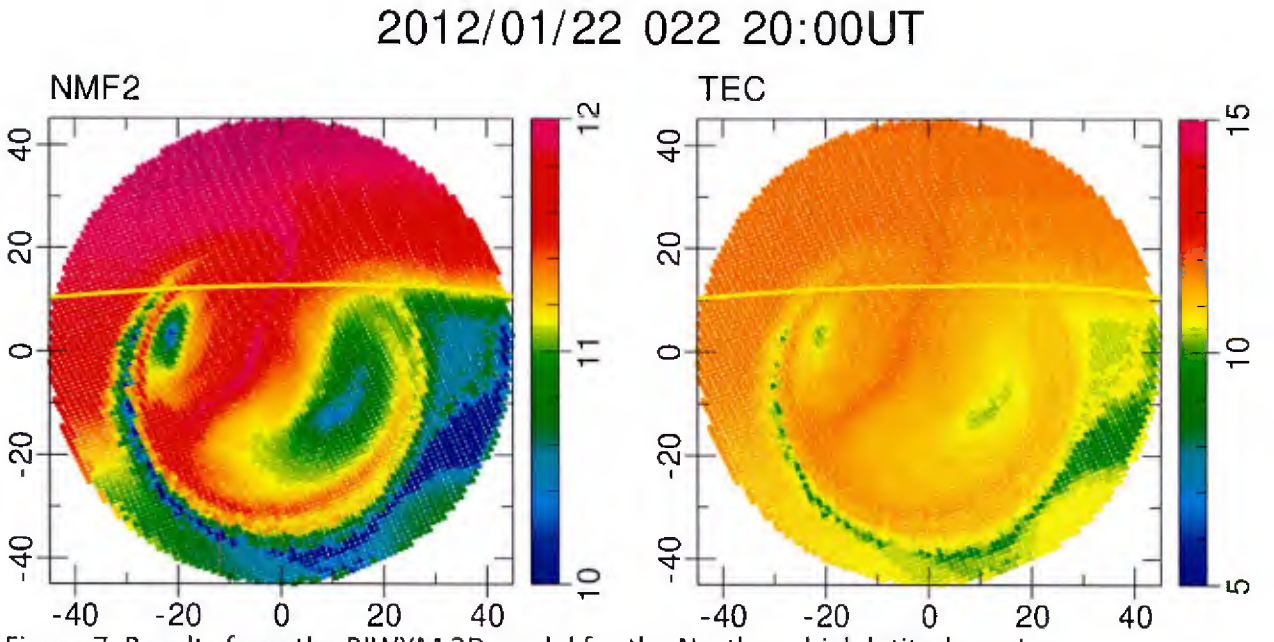

Figure 7. Results from the BIWXM 3D model for the Northern high latitude region.

5. Publications and an Unpublished Manuscript Under BSION Contract

The follow are the publications under this contract:

Cai, X., Yuan, T., Eccles, J. V., Pedatella, N. M., Xi, X., Ban, C., & Liu, A. Z. (2019). A Numerical Investigation on the Variation of Sodium Ion and Observed Thermospheric Sodium Layer at Cerro Pachón, Chile During Equinox. Journal of Geophysical Research: Space Physics, 124, https://doi.org/10.1029/2018JA025927.

Cai, X., Yuan, T., Eccles, J. V., and Raizada, S. (2019). Investigation on the distinct nocturnal secondary sodium layer behavior above 95 km in winter and summer over Logan, UT (41.7°N, 112°W) and Arecibo Observatory, PR (18.3°N, 67°W). Journal of Geophysical Research: Space Physics, 124, https://doi.org/10.1029/2019JA026746.

An unpublished manuscript was submitted and remains unpublished:

Eccles, J. V., J. J. Sojka, D. E. Rice, R. A. Marshall, D. P. Drob, and J. C. Mojica-Decena, Modeling the D Region and VLF Propagation for the Solar Eclipse of 21 August 2017, unpublished manuscript submitted to Geophysical Research Letters.

Copies of these manuscripts are included with the final delivery.

6. FInal Report, Documents, and Software Delivery

This Final Report presents the details the effort of the development of the BIWXM1D and BIWXM3D ionosphere models. The details of the physics and algorithms of BIWXM are provided in the Physics-Chemistry-Numerics Document. For the Final delivery of this ONR Contract N00014-17-1-2156, we include (1) this Final Report and previous Annual Reports, (2) Users Guide, (3) Physics-Chemistry-Numerics Document, (4) Review Meeting Presentations, (5) copies of publications, and (6) the Software Delivery of BIWXM V2.0. These are placed on a DVD for delivery to fulfill the requirements of the BSION contract N00014-17-1-2156 to Space Environment Corporation.

7. APPENDIX: Delivery Documents for BIWXM

7.1. BIWXM – Physics, Chemistry, Numerics

7.2. BIWXM – User's Guide

New Ionosphere Model for the Global Bottom-Side Ionosphere from 50 to 500 km: TIDs, Metal Ion Layers, D Region, and Severe Disturbance

BIWXM -- Physics, Chemistry, and Numerics

James Vincent Eccles (PI), Donald Rice, and Jan J. Sojka

Space Environment Corporation
1010 Eastridge Drive
Logan, Utah 84321

Vince.eccles@spacenv.com
(435) 752-6567 (corporate office)
(435) 757-2499 (Vince Eccles contact number)

Table of Contents

New Ionosphere Model for the Global Bottom-Side Ionosphere from 50 to 500 km: TIDs, Metal Ion Layers, D Region, and Severe Disturbance

1 Introduction

The ***Bottom-side Ionosphere with Winds, X-rays, and Metals*** or ***BIWXM*** ionosphere model has been designed to have the physics and chemistry necessary to model the bottom-side ionosphere from 30 to 3000 km. The 50 to 500 km altitudes are critical for radio signal propagation for frequencies between 3kHz to 300 MHz (VLF, LF, MF, HF). BIWXM is be built on the foundation of existing models with improvements and extensions that will enable computational efficiency and increased fidelity through the whole altitude range of the bottom-side ionosphere. The development of the BIWXM address these key drivers of ionospheric structure:

1) Updated solar ionization physics for quiet and flare conditions,
2) D region chemistry and physics necessary for the accurate determination of quiet and disturbed D region profiles,
3) Accounting for secondary electron ionization,
4) Ion chemistry and transport with sufficient chemistry for E region, F1 region, F2 region, and topside ionosphere to provide good HF ray-tracing modeling,
5) Dynamics to include wind-altered profiles and metal ion layers throughout the bottomside ionosphere,
6) Including transport of all ion species from 95 km up to through the F region topside. The E region transport will include rigorous high-collisional calculations for transport.

The setup of the BIWXM code uses setup files to define the species of the system to be solved as well as the chemistry to be solved. The basic ion set that is required is H+, N+, O+, N2+, NO+, O2+, and O2-. These provide an excellent representation of the 30 to 3000km altitude range. Metal ions as well and a complex zoo of positive and negative ions can be included. Care must be taken to generate a suitable reaction set to ensure the proper source and loss of all species in the system. The species setup file also requires some definitions for each species that relates to mass, degrees of freedom (atomic, diatomic, or complex molecule), collision parameters to properly define the momentum, thermal, and collisional aspects of each species in the system. A more complete description of the species and reaction setup file are provided below.

The model numerical design is suitable for massively-parallel computer systems to enable high-resolution solutions of the ionosphere as well as very high-resolution regional specifications. The ionosphere model is developed for coupling with any Whole Atmosphere Model and other Electric Field Models through a suitable modeling framework. This document presence the physics, chemistry, and numerical methods within the BIWXM model.

The model is able to be released with MIT licensing to enable broad use and potential user improvement of the methods and modules. The Office of Naval Research and the U.S. government has full government right of use and distribution.

2 BIWXM – Five-Moment Fluid Equation Model

2.1 Fluid Equations

The **Bottomside Ionosphere: Winds, X-rays, and Metals** (BIWXM) is a new ionosphere model with the full array of physics and chemistry necessary for the modeling the ionosphere from 30 to 3000 km. The numerical methods provide (1) a robust solution of the stiff chemistry conditions in the D and E region, (2) a transport algorithm for mass and momentum to provide an accurate response for waves and non-linear motions, (3) complex ionization physics for severe solar flare and particle precipitation responses, (4) metal ion chemistry and transport to support more accurate modeling of ion layers of sporadic E and descending layers, (5) ion and electron temperature calculations according to that respond to the above processes. The development of BIWXM accommodates transport through collision-dominated altitudes for properly modeling of metal ion layers [Cai et al., 2017; 2018; 2019], but also extends transport correctly into the F region and the collisionless topside altitudes (z>1200km) as the formulation includes time-dependent ion momentum terms in the velocity solution. Each species is solved without discrimination using the conservative mass and momentum equations. The reactive mass equation is:

$$\frac{\partial n_i}{\partial t} + \nabla \cdot n_i \bar{v}_i = Q_i + \sum_k P_{ik} - \sum_l L_{il}$$

where t is time, n_i is the density of the i^{th} ion, $\bar{v}_i$ is the 3D velocity, q_i is the total solar ionization source term, P_{ik} and L_{il} are the production and losses of the ion. The momentum equation is

$$\frac{D\bar{v}_i}{Dt} + \frac{\nabla \mathrm{k} n_i T_i}{m_i n_i} = \bar{G} + \frac{e}{m_i}[\bar{E} + \bar{v}_i \times \bar{B}] + \sum_t \nu_{it}(\bar{u}_t - \bar{v}_i) + \frac{Q_i}{n_i}\bar{u}_n + \sum_k \frac{P_{ik}}{n_i}(\bar{u}_{ik} - \bar{v}_i)$$

The new variables are the following: m_i is species mass, k is the Boltzmann constant T_i is ion temperature, G is the gravity vector, E is the electric field vector, B is the magnetic field vector, e is electron charge, ν_{it} is the collision frequency with the t species, u_t is the t species velocity, u_n is the average neutral velocity (ionization of neutrals via photoelectrons), u_{ik} is the creation velocity of species i from the k^{th} chemical production. All of these terms become important in some particular altitude range (resonant charge exchange in above the F region) or elevated ionization period (bottomside during solar flare). Loss of the i^{th} species is assumed to approximately remove momentum and mass at the same rate, thus, the loss reactions (L_i) are not used in the momentum equation.

The momentum equation is solved for parallel and perpendicular motions to the magnetic field using the vector equation:

$$\mathrm{A}_i \begin{bmatrix} v_l \\ v_q \\ v_s \end{bmatrix} - \mathrm{B}_i \begin{bmatrix} \hat{l} & \hat{q} & \hat{s} \\ v_l & v_q & v_s \\ 1 & 0 & 0 \end{bmatrix} = \begin{bmatrix} \mathbb{C}_{il} \\ \mathbb{C}_{iq} \\ \mathbb{C}_{is} \end{bmatrix}$$

where $\hat{l}$ is the unit vector in the direction of B, $\hat{s}$ is the zonal and horizontal direction perpendicular to B, and $\hat{q} = \hat{s} \times \hat{l}$ as a meridional-vertical vector. The $\hat{l}$, $\hat{q}$, $\hat{s}$ coordinates are approximately the same as the *Haerandel et al.* [1992] dipolar coordinate system, however, we have chosen to tie our definition to the IGRF magnetic field. We used time-splitting to solve for parallel and perpendicular motions. When we solve the mass and momentum equations in this non-dipolar $\hat{l}$, $\hat{q}$, $\hat{s}$ coordinate system we must accommodate a slightly non-orthogonal system when performing motion perpendicular to B. The A_i, $\mathcal{B}_i$, and $\bar{\mathbb{C}}_i$ are determined via much algebraic manipulation:

$$\mathrm{A}_i = \sum_t \nu_{it} + \frac{Q_i}{n_i} + \sum_k \frac{P_k}{n_i}$$

$$\mathcal{B}_i = \frac{eB}{m_i}$$

$$\mathbb{C}_l = \mathrm{A}_i u_l - g \sin I + \mathcal{B}_i \frac{E_l}{B} - \frac{1}{n_i m_i} \frac{\partial k n_i T_i}{\partial l} - \left(\frac{D\bar{v}_i}{Dt}\right)_l$$

$$\mathbb{C}_q = \mathrm{A}_i u_q - g \cos I + \mathcal{B}_i \frac{E_q}{B} - \frac{1}{n_i m_i} \frac{\partial k n_i T_i}{\partial q} - \left(\frac{D\bar{v}_i}{Dt}\right)_q$$

$$\mathbb{C}_s = \mathrm{A}_i u_s + \mathcal{B}_i \frac{E_s}{B} - \frac{1}{n_i m_i} \frac{\partial k n_i T_i}{\partial s} - \left(\frac{D\bar{v}_i}{Dt}\right)_s$$

Using these definitions we get ion velocities of

$$v_l = \frac{\mathbb{C}_l}{\mathrm{A}_i}$$

$$v_q = \frac{\mathrm{A}\mathbb{C}_q + \mathcal{B}\mathbb{C}_s}{\mathrm{A}^2 + \mathcal{B}^2}$$

$$v_s = \frac{\mathrm{A}\mathbb{C}_s - \mathcal{B}\mathbb{C}_q}{\mathrm{A}^2 + \mathcal{B}^2}$$

These formulae are appropriate from the collisional E region physics through to the F region topside eddy diffusion is incorporated below 100 km. We note that numerical method provides for a smooth stable solution through the entire altitude range even as the momentum terms begin

to dominate through the use of time-stepping of these equations in the higher altitudes. The electron gas is assumed to be in quasi-neutral charge situation with the total ion density.

The energy equation for electrons is solved locally at low altitudes using collisions only and solved with a steady-state transport-only formula at high altitudes. This works well for magnetic latitudes above 30°. The ion temperature is currently calculated using average ion mass and collisional coupling to the electron and neutral gases as a single ion temperature. The details are given in later sections.

2.2 Collisions

The BIWXM multi-species includes rigorous collisional calculations for the momentum and energy characteristics involving ion-neutral, ion-ion, and neutral-neutral collisions. For ion-ion collisions the Coulomb interaction formulae in chapter 4 of *Schunk and Nagy* [2009]

$$\nu_{st} = 1.27 \frac{Z_s^2 Z_t^2 \mu_{st}^{1/2}}{m_s} \frac{n_t}{T_{st}^{3/2}} \tag{2.2.1a}$$

where m_s is the s ion mass in atomic mass units, μ_{st} is the reduced mass in atomic mass units, Z_s and Z_t are the charge numbers, n_t is the density (cm^{-3}), and T_{st} is the reduced temperature.

$$\mu_{st} = \frac{m_s m_t}{m+m_t} \tag{2.2.1b}$$

$$T_{st} = \frac{m_s T_t + m_t T_s}{m_s + m_t} \tag{2.2.1c}$$

with m_s and m_t being the mass of the s and t species. Equation 2.2.1a can also be used for electron-electron and electron-ion interactions as well, giving:

$$\nu_{ei} = 54.5 \frac{n_i Z_i^2}{T_e^{3/2}} \tag{2.2.4}$$

$$\nu_{ee} = \frac{54.5}{\sqrt{2}} \frac{n_e}{T_e^{3/2}} \tag{2.2.5}$$

Collisions between ions and neutrals are best represented by Maxwell collisions [*Schunk and Nagy*, 2009]. The collision coefficients between an ion and neutral can be calculated from the molecular polarizability values of the neutral species (Table 1.2.1).

Table 2.2.1. Polarizability of key neutrals.

Species	Average Polarizability (Bohr Volume)
H	4.4
He	1.4
N	7.5
O	5.4

CO	13.2
N_2	11.8
NO	11.0
O_2	10.7
Ar	10.0
CO_2	17.7

Bohr volume = $(5.29177\times10^{-09}\text{cm})^3$

The collision integral, $\Omega_{in}^{(1,1)}$, for ion-neutral collisions (*in*) based on Maxwell molecules can be evaluated analytically giving

$$\Omega_{in}^{(1,1)} = \frac{3}{16}2.210\pi(\alpha_n e^2/\mu_{in})$$

α_n is the average polarizability (cm^{-3}), e is electron charge (stat-coulombs), μ_{in} reduced mass (gm):

$$\mu_{in} = \frac{m_i m_n}{m_i+m_n}$$

Collision frequency, ν_{in}, becomes

$$\nu_{in} = \frac{16}{3}\frac{\mu_{in}}{m_i}\Omega_{in}^{(1,1)}n_n \qquad \text{or} \qquad \nu_{in} = C_{in}n_n$$

Table 2.2.2 from *Schunk and Nagy* [2009] presents the calculated collision coefficients, C_{in}. for ion-neutral collisions. The red R indicates that a resonant collision is dominant and must be calculated using a temperature dependent formula. Within BIWXM, these resonant pairs of ions to neutrals are recognized and calculated as needed. Not all resonant situations are calculated. For example, minor ion species transport terms will be dominated by non-resonant collisions and the resonant calculation can be ignored, (e.g., CO+ on CO or NO+ on NO).

Table 2.2.2. Collision frequency coefficients, C_{st} x 10^{10} for non-resonant i-n collisions

	H	**He**	**N**	**O**	**CO**	**N_2**	**O_2**	**Ar**	**CO_2**
H^+	**R**	10.49	26.25	**R**	35.42	33.49	31.96	30.99	41.28
He^+	4.68	**R**	12.03	10.36	16.92	16.00	15.36	15.01	20.06
C^+	1.68	1.70	5.78	5.05	8.74	8.06	8.02	7.97	10.72
N^+	1.45	1.48	**R**	4.52	7.90	7.47	7.26	7.24	9.75
O^+	**R**	1.32	4.66	**R**	7.22	6.83	6.65	6.65	8.97
CO^+	0.74	0.79	2.98	2.64	**R**	4.57	4.50	4.56	6.19
N_2^+	0.74	0.79	2.31	2.64	4.84	**R**	4.50	4.56	6.19
NO^+	0.69	0.74	2.81	2.49	4.59	4.34	4.27	4.35	5.90
O_2^+	0.65	0.69	2.66	2.36	4.37	4.13	**R**	4.15	5.64
Ar^+	0.52	0.69	2.20	1.96	3.68	3.42	3.44	**R**	4.80
CO_2^+	0.47	0.51	2.02	1.80	3.40	3.22	3.19	3.28	**R**

R indicates a resonant collision.

The ion-neutral resonant formula used within BIWXM are:

$$\upsilon_{H^+H} = 2.65 \times 10^{-16}\sqrt{T_r}\left(1 - 0.083 \cdot log_{10}(T_r)\right)^2$$
$$\upsilon_{O^+-O} = 3.67 \times 10^{-17}\sqrt{T_r}\left(1 - 0.064 \cdot log_{10}(T_r)\right)^2$$
$$\upsilon_{N_2^+-N_2} = 5.14 \times 10^{-17}\sqrt{T_r}\left(1 - 0.069 \cdot log_{10}(T_r)\right)^2$$
$$\upsilon_{O_2^+-O_2} = 2.59 \times 10^{-17}\sqrt{T_r}\left(1 - 0.073 \cdot log_{10}(T_r)\right)^2$$

The neutral-neutral collisional interactions are best defined by hard sphere collisions with polarization modifications. Kinetic diameter is used to define the scattering affect leading to the calculation of the mean free path of molecules in a gas. The mean free path, l, is given by

$$l = n\pi d^2$$

where n is the density of the gas and d is the kinetic diameter.

Table 2.2.3. Kinetic diameter for neutral gases.

Atoms (#p ,atomic mass)	**Diameter (nm)**	**Cross-Section (nm^2)**
H (1 ,1.008)	2.19	0.15*
He (2 ,4.003)	2.59	0.21
C (6 ,12.011)	2.65	0.22*
N (7 ,14.006)	2.71	0.23*
O (8 ,15.999)	2.76	0.24*
Na (11 ,22.990)	3.09	0.30*
Mg (12 ,24.305)	3.14	0.31*
S (16 ,32.065)	3.19	0.32*
Cl (17 ,35.453)	3.24	0.33*
Ar (18 ,39.948)	3.39	0.36
K (19 ,39.098)	3.43	0.37*
Ca (20 ,40.078)	3.48	0.38*
Fe (26 ,55.845)	3.52	0.39*
H_2 (2.016)	2.93	0.27
CH_4 (14.027)	3.83	0.46
H_2O (18.015)	3.43	0.37*
C_2H_4 (26.038)	4.51	0.64
CO (28.010)	3.43	0.37
N_2 (28.012)	3.70	0.43
NO (30.005)	3.52	0.39*
O_2 (32.000)	3.57	0.40
CO_2 (44.011)	4.07	0.52
Cl_2 (70.906)	5.44	0.93
SO_2 (74.065)	4.30	0.58
C_6H_6 (78.114)	5.29	0.88

*Estimated.

Electron important collisions for the determination of the electron temperature include elastic and inelastic collisions with neutrals and ions. The electron-ion elastic collisions are presented above. Electron energy loss to N_2 and O_2 vibrational and rotation states are complex calculations. These collisional processes are best embedded in energy loss terms since we are not calculating electron momentum. Rotational inelastic cooling terms of the electron gas are:

$$L_e(\mathrm{N_2}) = 3.5 \times 10^{-14} n_e n(\mathrm{N_2})(T_e - T_n)/T_e^{1/2}$$
$$L_e(\mathrm{O_2}) = 5.2{\times}10^{-15} n_e n(\mathrm{O_2})(T_e - T_i)/T_e^{1/2}$$

Notice: All collisional terms are presented in CGS as is commonly presented in ionospheric literature [Schunk and Nagy, 2009]. The BIWXM model uses all inputs and outputs to be in SI units. There is a program that translates a database of reaction rates from CGS to SI suitable for the setup files in BIWXM.

There are additional electron cooling calculations suitable for the middle atmosphere (z<100km) however, BIWXM assumes that electron temperature is quickly cool to the neutral temperature in this high collisional situation. This is not precisely true for the region below the auroral region or during the Solar Proton Events within the polar cap. These processes are complex and are currently embedded within parameterizations of these processes. Vibrational cooling terms are:

$$\begin{aligned} L_e = {} & n_e n(\mathrm{N_2})[1 - \exp(-E_1/T_{vib})] \\ & \times \sum_{v=1}^{10} Q_{0v}\left[1 - \exp[vE_1(T_e^{-1} - T_{vib}^{-1})]\right] \\ & + n_e n(\mathrm{N_2})[1 - \exp(-E_1/T_{vib})]\exp(-E_1/T_{vib}) \\ & \times \sum_{v=2}^{9} Q_{1v}\left[1 - exp[(v-1)E_1(T_e^{-1} - T_{vib}^{-1})]\right] \end{aligned}$$

where E_1=3353K and the Q_{0v}, and Q_{1v} coefficients are temperature dependent formulae:

$$\log Q_{0v} = A_{0v} + B_{0v}T_e + C_{0v}T_e^2 + D_{0v}T_e^3 + F_{0v}T_e^4 - 16$$
$$\log Q_{1v} = A_{1v} + B_{1v}T_e + C_{1v}T_e^2 + D_{1v}T_e^3 + F_{1v}T_e^4 - 16$$

with these polynomial coefficients presented in Tables 9.3, 9.4, and 9.5 on page 279 of [Schunk and Nagy, 2009]. Within BIWXM it is assumed that $T_{vib} = T_n$. The vibrational cooling formula for e-O_2 collisions is similar:

$$L_e(\mathrm{O_2}) = n_e n(\mathrm{O_2}) Q(T_e)\{1 - exp[2239(T_e^{-1} - T_n^{-1})]\}$$

with

$$\log_{10}[Q(T_e)] = -19.9171 + 0.0267T_e - 3.9960 \times 10^{-5}T_e^2$$

$$+3.5187 \times 10^{-8} T_e^3 - 1.9228 \times 10^{-11} T_e^4$$
$$+6.6865 \times 10^{-15} T_e^5 - 1.4791 \times 10^{-18} T_e^6$$
$$+2.0127 \times 10^{-22} T_e^7 - 1.5346 \times 10^{-26} T_e^8$$
$$+5.0148 \times 10^{-31} T_e^9$$

2.3 Ionizing Solar Spectrum

The BIWXM solar spectrum must cover solar ionization down through the lower D region which spans X-rays(1 to 50-10 nm) and extreme ultraviolent (10-121 nm). The EUVAC model [*Richards et al.*, 1994*ab*] is used for the EUV spectral range of of 5 nm to 105 nm. This model still provides the fastest, most accurate, code directly available for model ionospheres. More recent models (FISM) have yet to be placed in FORTRAN or C subroutines to embed directly in model ionospheres.

The Lyman Alpha (121.4 nm) line is not included in the EUVAC model. This is a particularly important line for the D region and is not that influential in the ionosphere above 100 km. The Data-Driven D-Region (DDDR) [Eccles et al., 2005] populated this line using a formula with F10.7 and F10.7a:

$$L_\alpha = 0.5839 + 0.3554\sqrt{F10.7} + 0.1730\left(\sqrt{F10.7} - \sqrt{F10.7a}\right) \text{ photos/cm/cm/s}$$

from *Woods et al.* [2000]. This formula was developed using data prior to 1999. The TIMED SEE database has been used to create an updated formula for Lyman α. This is a very suitable formula. However, for this effort we examined refinements to this formula using TIMED SEE data. Figure 2.2.1 plots various linear formulae against (a) F10.7, (b) F10.7a, (c) (F10.7+F10.7a)/2, and (d) Woods et al. The smallest standard error is the formula using (F10.7+F10.7a)/2 as the best predictor of Lyman for the TIMED data 2002 to 2019. There was a small downward offset in the Woods et al. formula. Tests of the BIWXM model electron density profiles suggested that the altitude range of 80 to 100 was improved over the DDDR results by a factor of 2 based on the quiet period profiles of the rocket measurement database.

The absorption and ionization cross sections for the EUVAC and Lyman α spectral range (EUVAC+) are listed in Tables in Appendix A as are the Tables of branching ratios of the products of ionization.

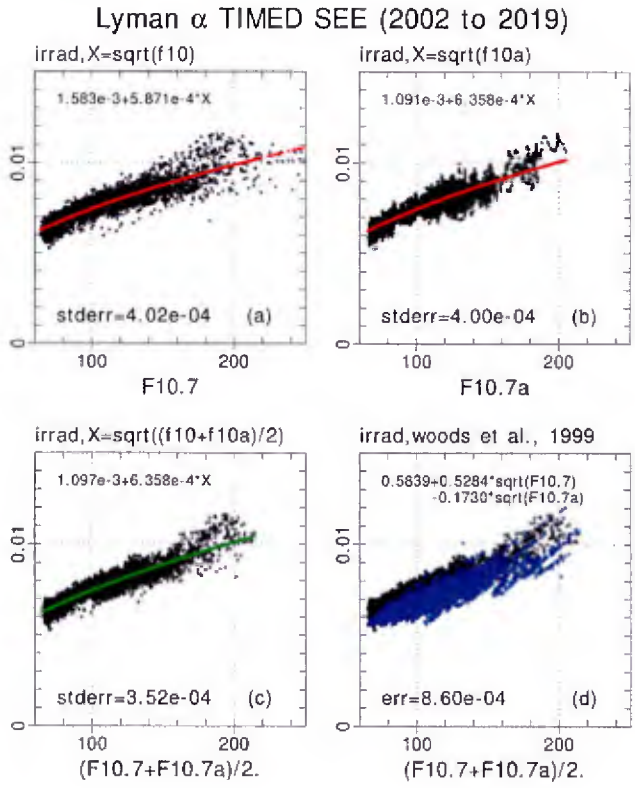

Figure 2.3.1. TIMED SEE data of Lyman α irradiance is plotted with black symbols in each plot. Four formula for are plotted on each graph (a) Linear form with F10.7, (b) linear form with F10.7a, (c) linear form with (F10.7+F10.7a)/2, (d) Woods et al formula. Standard error calculated against the data is listed in each plot.

The daytime X-ray spectrum is problematic for an ionosphere model that responses to real time solar measurements. The D region's response times to disturbance situations is very rapid. The GOES satellites have two overlapping bins of solar X-ray flux: 0.05 to 0.4 nm and 0.1 to 0.8 nm. The GOES X-ray flux measurements are at a 1-minute cadence which is useful for accommodating the rapid D region response to the abrupt solar flare occurrences. The energy per photon varies dramatically through the GOES X-ray ranges. The energy determines the depth of penetration into the atmosphere. Thus, there is an advantage to partition the GOES X-ray fluxes into several bins across this range. The X-ray bins are defined using the cross-section tables within from *Banks and Kocharts* [1973] with updates from *Pavlov* [2013] on the Lyman α bin (Appendix A). The separation of the GOES X-ray bins into the Banks and Kockarts bins from 0.05 to 0.8 nm is done by assuming a factor of 2 increase of flux from the shorter bins to the larger bins across both GOES bins and averaged in the overlapping portion of the GOES bins. This weights the energy towards the longer wavelengths and provides reasonable results in the BIWXM model results in the 40 to 60 km altitude range. *This needs to be improved for variation from quiet to disturbed situations, but this works better than a flat distribution.*

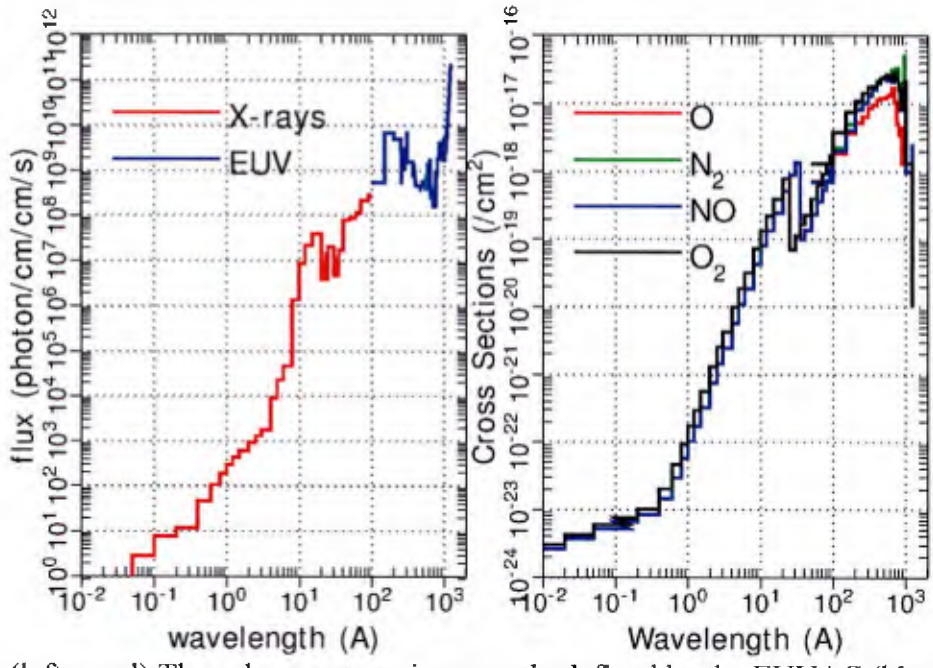

Figure 2.3.2 (left panel) The solar spectrum is currently defined by the EUVAC (blue lines) and an averaged TIMED-SEE spectrum (red lines). (right panel) The absorption cross sections for the major atmospheric species.

GOES defines 0.05 to 0.8 nm and TIMED-SEE X-ray data define the spectrum from 0.8 nm to 100 nm range. The TIMED-SEE x-ray database is used to generate a historical database for a spectrum is proportional to the daily F10.7 cm flux. Figure 2.3.2 presents the current definition of the solar flux in a number of wavelength ranges, λ_i, and the accompanying absorption cross sections, σ_a, within the BIWXM model.

We note that the TIMED SEE averaged spectral range (0.5 to 195.5 nm) and the EUVAC spectral range (5 to 121.4 nm) with Lyman a added have overlapping ranges. We used EUVAC for the EUV solar spectrum and TIMED SEE averages up to the EUVAC range. First TIMED SEE bin is replaced by the GOES spectral definition. However, the EUVAC first bin of 5 to 10 nm is very important for defining the E region bottomside [*Sojka et al.*, 2013; 2014]. Figure 2.2.1 plots the variation in electron density profile if one places all the energy of the first bin of EUVAC (5 to 10 nm) into different energy sub-bins 5-6nm, 6-7nm, 7-8nm, 8-9nm, and 9-10nm. The EUVAC needs to be updated to address this XUV portion of the spectrum. We have replaced this first EUVAC bin using the TIMED Xray fluxes in this range with the TIMED smaller 1nm bins.

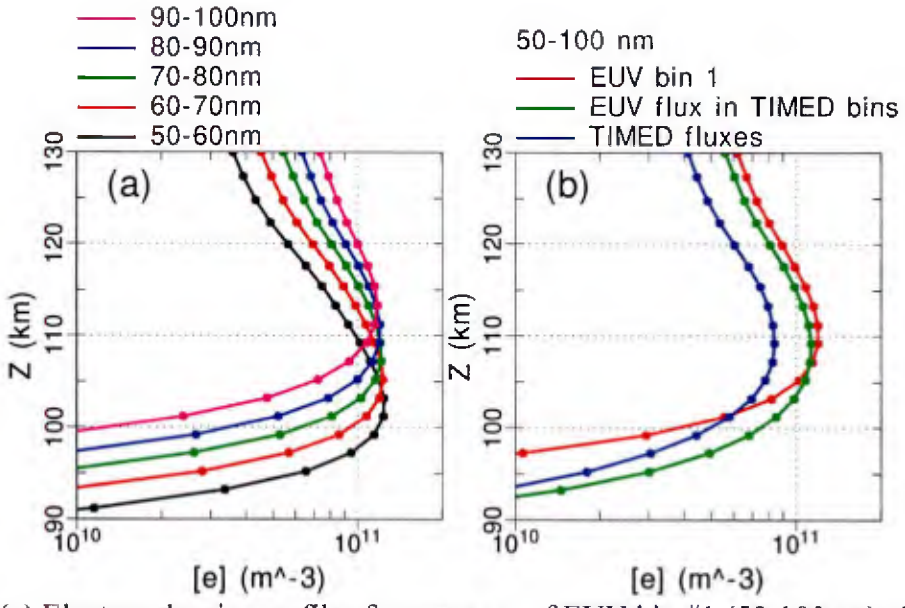

Figure 2.2.3. (a) Electron density profiles from energy of EUV bin #1 (50-100nm) placed in one of the 5 sub bins (50-60, 60-70, 70-80, 80-90, 90-100 nm). (b) Electron density profiles from EUV bin # 1 (red), from energy flux of EUV bin #1 distributed evening between the 5 TIMED bins, and from energy fluxes in the 5 TIMED bins based on TIMED data over the 50-100nm range (blue).

Thus, we ignore the EUVAC first bin. However, the TIMED SEE 50 to 100 nm range is known to disagree with the total energy flux of the EUVAC in this range by a factor of 2 to 4. Through various comparisons to electron densities from Incoherent scatter data and rocket flights, we have settled on multiplying the TIMED SEE bins in this range by a factor of 2.

The testing of the BIWXM D region altitude range is done primarily through comparisons with a database of rocket flights from 1950 to 2001. There are no X-ray data to generate a spectrum for many of these dates. We have examined the non-flare GOES data to generate the GOES X-ray range through a formula using F10.7. Figure 2.2.4 presents this empirical model of non-flare X-rays for the GOES X-ray bins A (0.05-0.4nm) and B (0.1-0.8nm). The small light green symbols plot the non-flare daily flux values for the B bin and the light red symbols for the A bin against F10.7. The large dark green and red symbols are the averages of the daily non-flare values for integer values of F10.7. The F10.7 averaging organizes the data very well. F10.7a does not improve these averages. The small black symbols are the empirical model that generates the average fluxes versus F10.7. It is a curiosity that the quietest sun conditions show increasing hard X-ray fluxes!

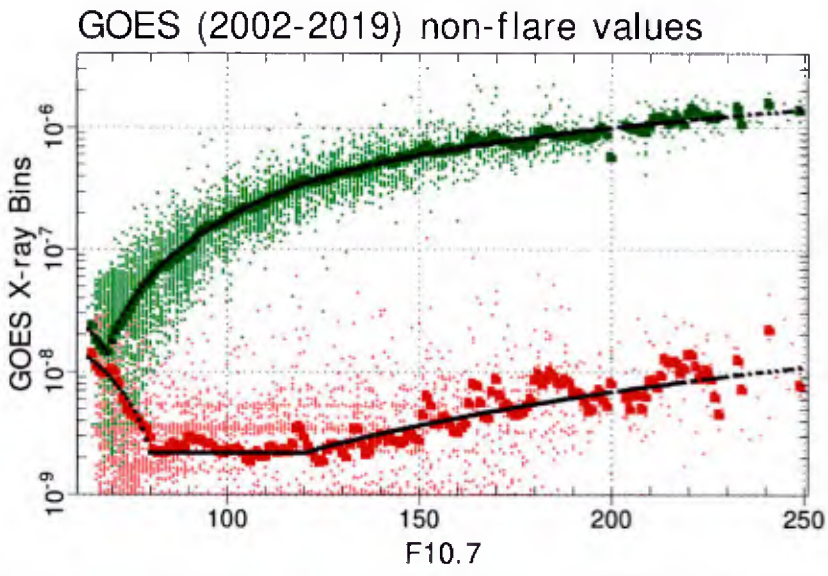

Figure 2.3.4. The light color symbols are the non-flare data of GOES from years 2002 through 2019. The larger darker symbols are averages of the data in each integer F10.7 bin. The black lines are the model relating daytime non-flare values and F10.7. A bin in red. B bin in green.

The empirical model for non-flare flux values of the GOES X-ray bins is:

A bin flux (W/m/m):

$\Phi_A = 2.012 \times 10^{-7} - 6.656 \times 10^{-8} F10.7^{0.25}$ F10.7<80

$\Phi_A = 2.2 \times 10^{-9}$ 80<=F10.7<=120

$\Phi_A = -4.345 \times 10^{-10} + 1.83 \times 10^{-13} F10.7^2$ F10.7>120

B bin flux (W/m/m):

$\Phi_B = 1.244 \times 10^{-7} - 1.6 \times 10^{-9} F10.7$ F10.7<69

$\Phi_B = -6.721 \times 10^{-8} + 2.472 \times 10^{-13} F10.7^3$ 69<=F10.7<100

$\Phi_B = -6.6 \times 10^{-7} + 8.4 \times 10^{-9} F10.7$ 100<=F10.7<150

$\Phi_B = -6 \times 10^{-7} + 8 \times 10^{-9} F10.7$ F10.7>=150

These formulae for the A and B GOES flux bins are very useful when running models in the early years of the rocket flights database of the D region electron density. These formulae were necessary to improve BIWXM model results below 80 km altitude in the pre-2002 rocket flight database particularly during very quiet solar conditions.

The nighttime spectrum is based on *Strobel et al.* [1974; 1980] and *Titheridge* [2001]. There are fluxes for interplanetary gas scatter, starlight, scattered sunlight from the earth's geocorona and radiative recombination of the F region.

The definition of the ionization spectra above is sensitive to F10.7, F10.7a, and GOES X-ray bins. The EUVAC range does not change dramatically during solar flares except for the first bin 5-10nm, which we replace with TIMED SEE spectral model based on F10.7 and F10.7a. However, there is no sensitivity of the TIMED SEE spectral range 0.8-10nm to flares. This leaves the BIWXM model insensitive to flares in the altitude range of 95 to 130 km. This is addressed by producing a TIMED SEE X-ray range (0.8-190nm) flare model unique to BIWXM based on SDO EVE flare studies (FLARE_EUVAC) . Figure 2.3.5 plots a non-flare daytime spectrum generated by the GOES X-ray model (0.05-0.8nm) , the TIMEDSEE X-ray model (0.8-10nm), and EUVAC+ (10-121.4nm) in bins defined by *Banks and Kocharts* [1973] bins for X-rays and the EUVAC model for EUV bins. The flare condition is plotted in Figure 2.3.6. The GOES X-ray range is elevated and well as the FLARE_EUVAC range which is proportional to the GOES B flux bin. Only the first bin used (10 of the EUVAC model is altered much during the flare.

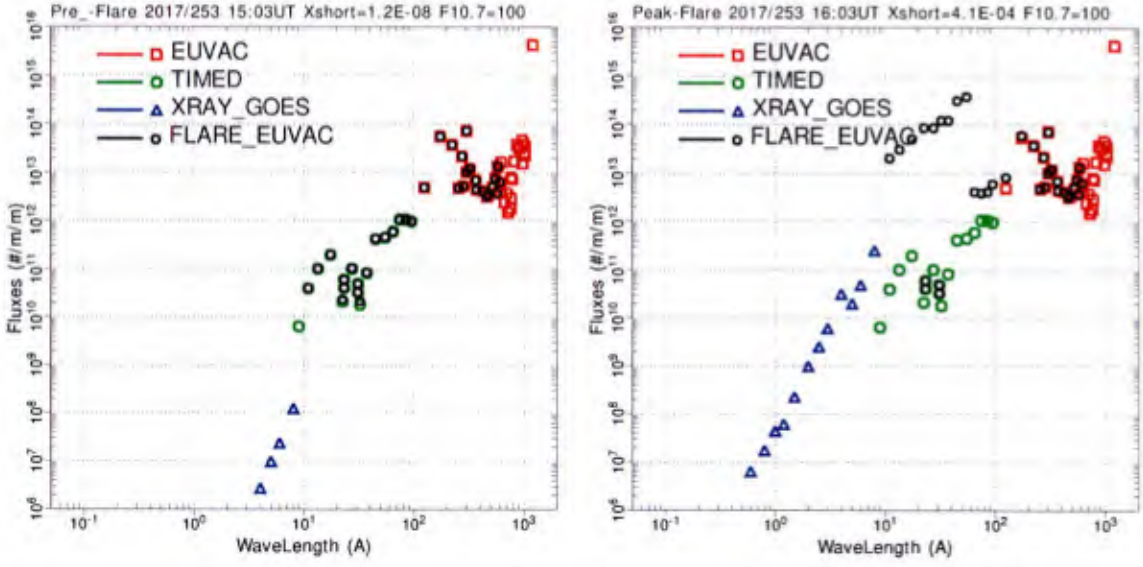

Figure 2.3.5. (Left panel) Non-Flare fluxes for each model within BIWXM. FLARE_EUVAC model (black circles) is currently set to background values. (Right panel) Flare fluxes for each model within BIWXM. FLARE_EUVAC model (black circles).

2.4 Ionization Profiles

2.4.1 Photoionization

The solar spectrum defines the flux at the top of the atmosphere. The intensity of the solar radiation decays exponential with altitude according to optical thickness, τ, and used to produce Chapman production function profiles [Schunk and Nagy, 2009]:

$$P_c(z) = I(z,\chi)\eta\sigma^a \mathrm{n(z)}{=}I_\infty exp[-Hn(z)\sigma^a sec\chi]\eta\sigma^a n(z)$$

Where the production profile ($P_c(z)$ is calculated for each wavelength bin, λ_i, using the absorption cross sections of the atmospheric species, σ^a, η is the probably of photon absorption resulting in an i-e pair, H is the scale height of the major neutral species, $n(z)$ is the density of the neutral species at the altitude z, based on the spectral flux at the top of the ionosphere, I_∞, which is diminished through the atmosphere ($I(z,\chi)$) calculated using $n_s(z)$, the density at altitude, z, of the species s; $\sigma^a{}_s(\sigma_i)$, is the absorption (ionization) cross section of species s for a wavelength range, which all depends on the solar angle, χ. This formula is used directly for solar angles greater than 60 degrees and grazing angles of the solar incidence are calculated using the formula in *Smith and Smith* [1972]. The EUV and X-ray fluxes in altitude and the resulting ionization profiles for the main ions produced in air are plotted in Figure 2.4.1. Secondary electrons are accounted for through the method of Rasmussen et al [1988] by considering electron mean-free-paths in the atmosphere are shorter than the atmosphere scale-height up to 180 kilometers. This permits a local determination of secondary electron ionization by producing an i-e pair for each 35eV energy of the photon. This is used throughout the X-ray spectral bins and for the first 3 EUVAC energy bins. This assumption produces a small amount of error in the ionization profile above 180km, but this is reduced because all major ion species are solved with full transport at all altitudes, i.e. energy going into ionization above 170km easily suffers transport away from that local calculation of ionization. All photon energy capable of ionization is used to produce i-e pairs.

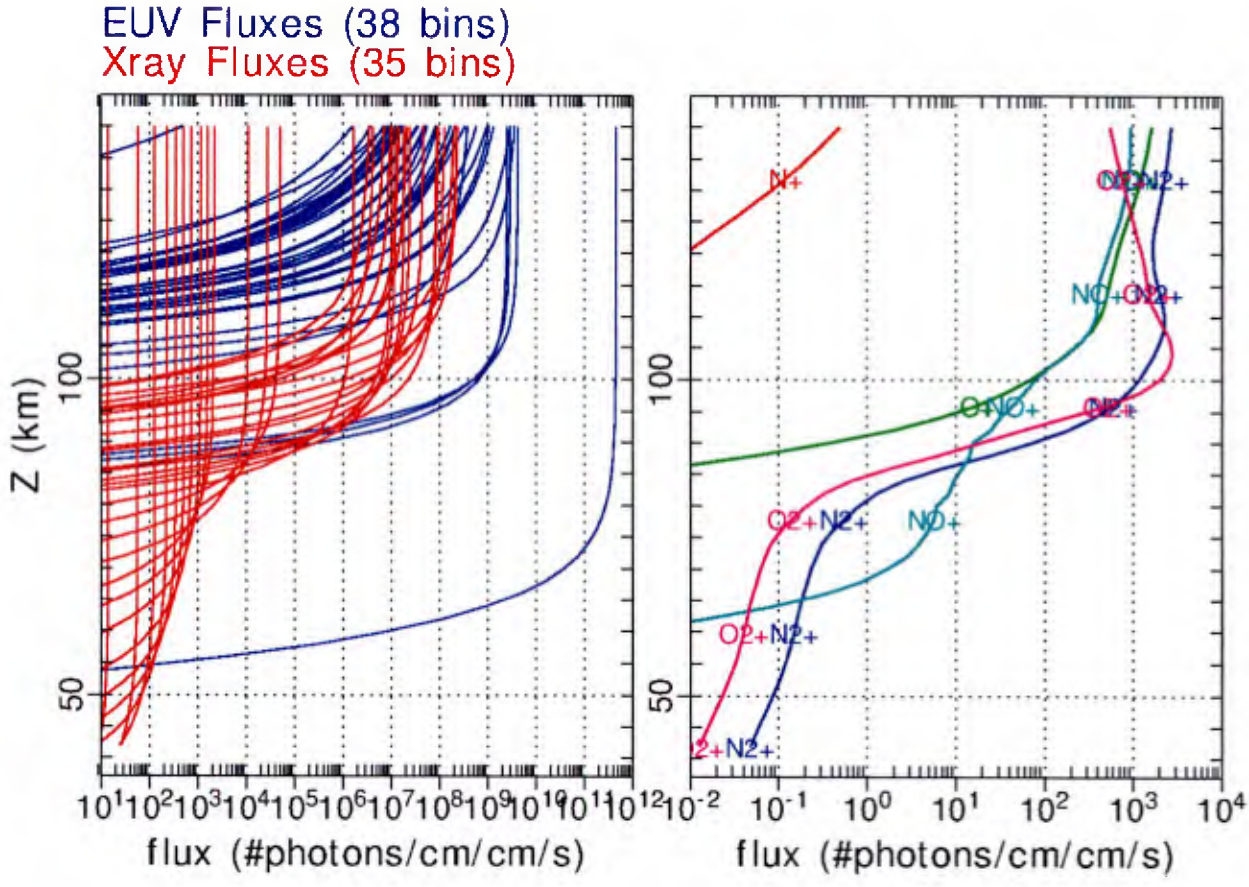

Figure 2.4.1 A noon time solar flux (left panel) and ionization profiles (right panel) for noon with no D region chemistry included.

2.4.2 Auroral Particle Precipitation

BIWXM has a module to generate the ionization profiles from auroral electron precipitation. The methods are based on *Rees* [1989] as accomplished by *Rasmussen et al.* [1988]. In an atmosphere of atmospheric number density, $n_a(z)$ in #/cm^3 at altitude z, on produces ionization of the atmosphere $P_a(\varepsilon,\Phi_e)$ in i-e pairs/cm^3/s, for a monoenergetic (ε in keV) beam of electron flux (Φ_e) in #/cm^2/s.

$$P_a(z,\varepsilon,\Phi_e) = \frac{\Phi_e}{r_o}\Gamma(d/D)\frac{\varepsilon n_a(z)}{\Delta\epsilon n_a(Z)}$$

where each i-e pair is generated for every $\Delta\varepsilon$=35eV. d is atmospheric depth at altitude z (g/cm^2).

$$d(z) = \int_z^\infty \rho_n(z)dz$$

Z is altitude of maximum penetration of the monoenergetic at atmospheric depth, D (g/cm^2), which is calculated for each beam energy.

$$D = 4.57 \times 10^{-6} \varepsilon^{1.75}$$

This formula is from Rees [1963]. In Rees [1989] a new formula for depth of penetration into the atmosphere is provided.

$$D = 4.30 \times 10^{-7} + 5.36 \times 10^{-6}\ \varepsilon^{1.67}$$

:r_o is the ratio of D and the mass density ρ_n at z

$$r_o = {}^{D}/_{\rho_n}$$

Finally, $\Gamma(d/D)$ is the fractional energy-dissipation function as described in *Rees* [1989]. Figure 2.4.2 plots the ionization profiles for monoenergetic electron precipitation with a number flux of 10^8 electrons/cm^2/s at several energies in keV using the new formula for depth of penetration. Figure 2.4.3 plots comparisons of ionization profiles calculated from Maxwellian distributions of electron precipitation of an energy flux of 1 erg/cm/cm/s and different characteristic energies of the distributions. The red curves are calculated using the GLOW model. The green curves use the old penetration formula from Rees [1963]. The blue curves use the new penetration formula from [1989]. Improvements of the $\Gamma(d/D)$ function in BIWXM can still be made as only one curve is used for all energies (2 keV curve). The curves change dramatically for lower electron energies (<1 keV). Exploration of measured Hall and Pedersen conductivities is required to demonstrate a preference for which model is to be used within BIWXM.

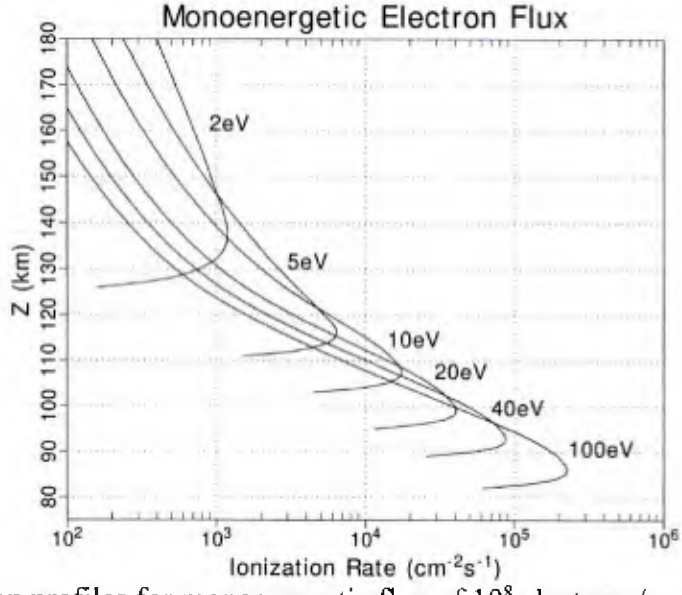

Figure 2.4.2. Ionization profiles for monoenergetic flux of 10^8 electrons/cm^2/s.

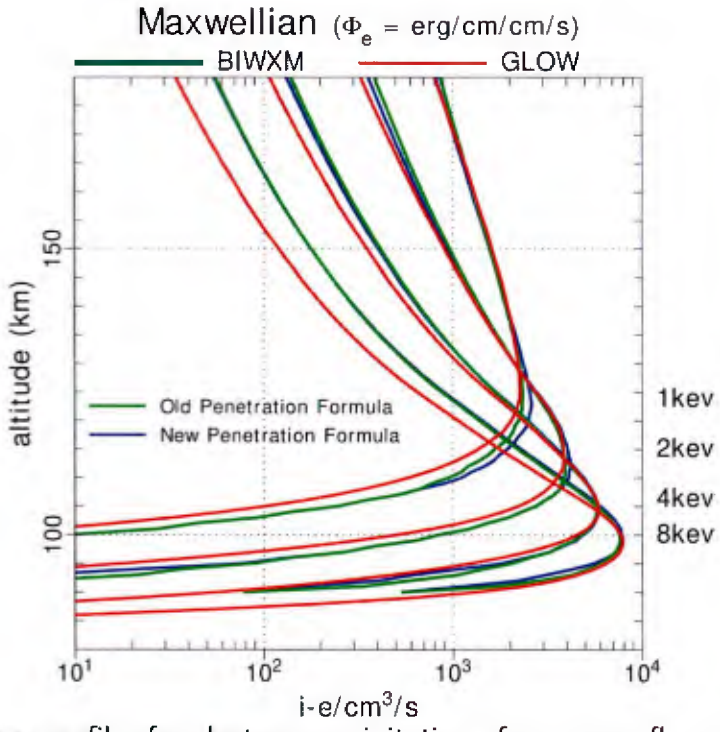

Figure 2.4.3. Ionization profiles for electron precipitation of an energy flux of 1 erg/cm/cm/s and 4 different characteristic energies of the Maxwellian electron distributions. The red curves are calculated using the GLOW model. The green curves use the old penetration formula from Rees [1963]. The blue curves use the new penetration formula from [1989].

The electron densities profiles produced by the GLOW model and BIWXM for strong auroral conditions with varying characteristic energies of the precipitating electrons are approximately the same through the altitude range that determines the values of integrated conductance. The BIWXM profiles are affected by transport parallel to B in these comparisons and GLOW is a chemical equilibrium calculation so some differences are expected. However, under strong precipitation conditions, then the profiles should be approximately the same from 90 to 150 km. Figure 2.4.4 presents electron density profiles from GLOW (red) and BIWXIM (blue) for precipitation energy flux of 10 ergs/cm/cm/s and characteristic energies of 1, 2, 4, and 8 keV for Maxwellian distributions of the precipitating electrons.

It is noted that we have currently chosen the energy bins that span the DMSP SSJ energy bins. The BIWXM has twice the resolution to ensure smoother ionization profiles. These energy bins were chosen to enable putting DMSP SSJ observations directly into the BIWXM model. There is code already embedded to do this. However, the SSJ bins below 500 eV energies are NOT used, since these are absorbed at very high altitudes (>200km) and do not seem to alter conductivities. These energies also require a different Γ profile, so for simplicity of the algorithm these energies are ignored. Finally, for large characteristics energies (>8 keV), the high energy tail of the Maxwellian is not well represented (is missing). Thus, the deepest penetration of the electron precipitation is sometimes sharply cut off at 90 kilometers. These issues should be addressed with further study.

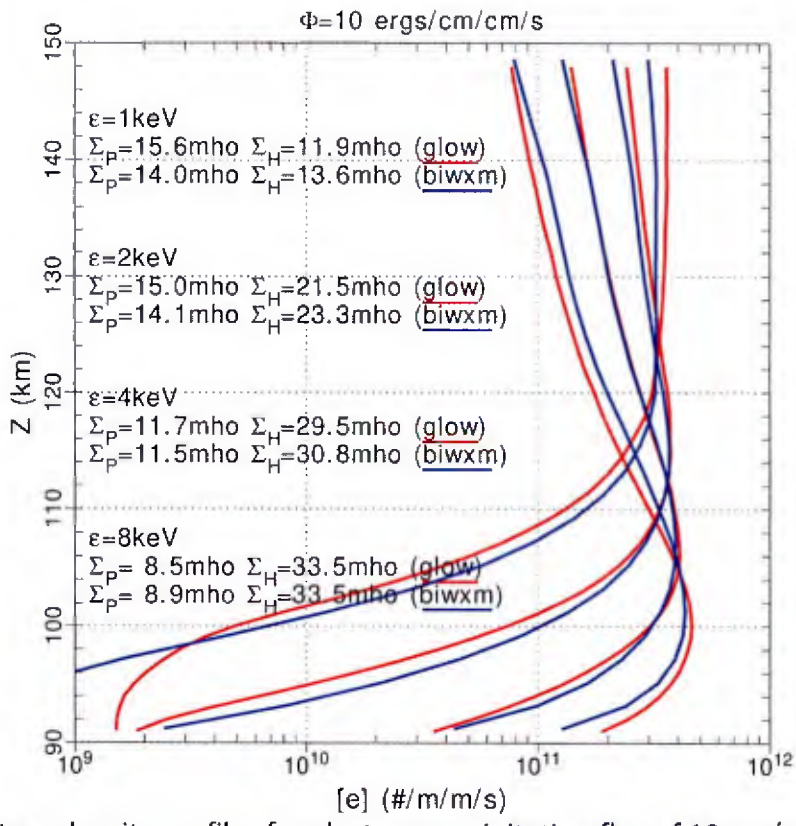

Figure 2.4.4. Electron density profiles for electron precipitation flux of 10 erg/cm/cm/s and 4 different characteristic energies of the Maxwellian electron distributions. The red curves are calculated using the GLOW model. The blue curves use the new penetration formula and the BWIXM model to determine the density profiles.

2.4.3 Ion Particle Ionization

The SPE ionization profiles calculated in BIWXM are based on the bins of proton fluxes measured on GOES satellites beginning at 1MeV. The bins measure fluxes of protons above the energy value of the bin. Thus, 1MeV bin measures all protons above that energy, so forth with 5MeV, 10MeV, 30MeV, 50MeV, and 100MeV bins. These bins are reduced to isolated energy bins through subtraction and used to generate ionization profiles per energy bin. These are calculated similarly as electron particle ionization with an energy deposition shape for each energy bin combined with a depth of penetration calculation. The algorithm aims at reproducing the ionization profiles based on the GOES ion flux bins cited above. Energetic ions ionization similarly to electrons in that i-e pairs are produced for every 35eV of ion energy. The ion penetration into the atmosphere can be similarly calculated as electron precipitation. For SPE energies, the energetic proton maximum depth of penetration is:

$$R(E) = 2.71 \times 10^{-3}\, E^{1.72} \quad E \text{ in } MeV$$

This formula for SPE protons penetration is based on numerical experiments to reproduce the SOLARISHEPPA SPE ionization profiles (https://solarisheppa.geomar.de/solarprotonfluxes) with 35eV producing each i-e pair [Matthess et al., 2017).

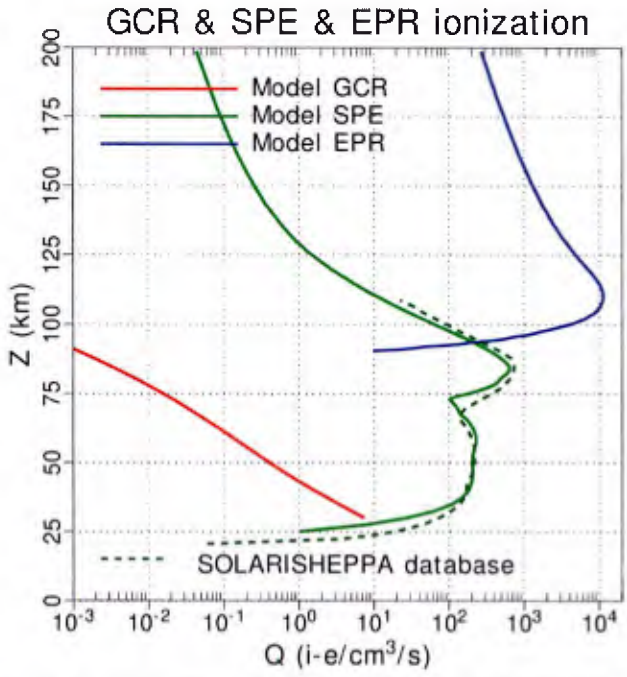

Figure 2.4.5. BIWXM calculated ionization profile for the Solar Proton Event for 2017 253 (green solid line) compared to the profile for the same event from the SOLARIS HEPPA database of SPEs (green dashed line). The electron precipitation profile (blue) and the galactic-cosmic ray profile (red) are also plotted for comparison.

The latitude cutoff formula used within BIWXM limits the SPE ionization appropriately. The current formula is proton energy and Kp dependent (Figure 2.4.6)

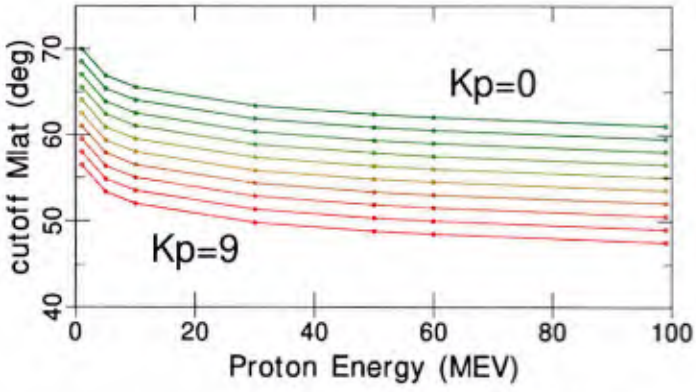

Figure 2.4.6 Magnetic Latitude cutoff values for various proton energies and for Kp=0 through 9. The energy dependent cutoff causes variations in the ionization rates with altitude.

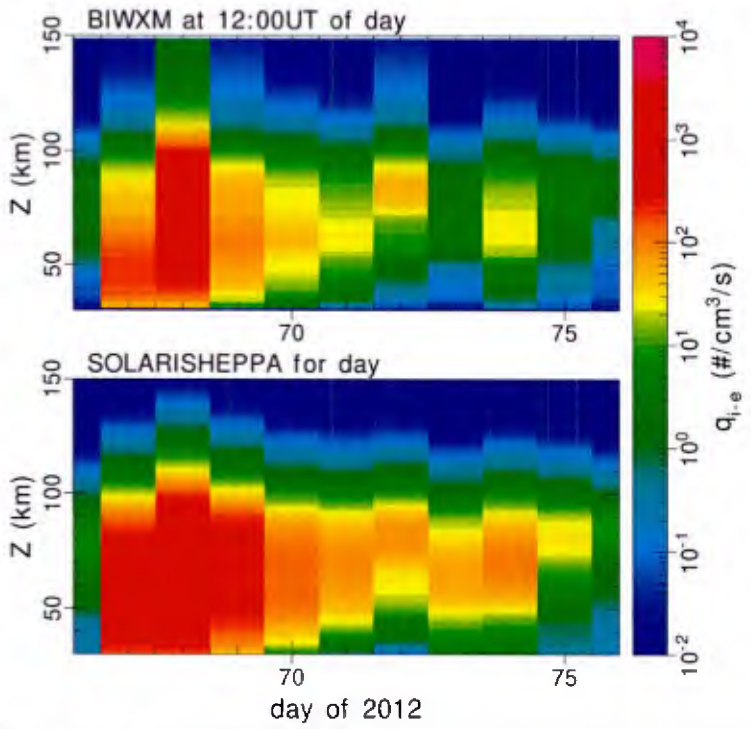

Figure 2.4 6. BIWXM calculation at 12:00UT of each day is compared with the SOLARIS HEPPA ionization profiles for each day from 66 to 76 of 2012.

The BIWXM ionization profiles from energetic solar protons are presented in Figure 2.4.6. These profiles are for the 12:00UT time on a series of days from 2012. The BIWXM location chosen for this calculation is 19E and 69N geographic. These profiles are not expected to be identical since SOLARIS HEPPA is developed from an average value of energetic protons over each day. However, the profiles reflect the altitude ranges of the SOLARIS HEPPA model ionization.

2.4.4 Galactic Cosmic Rays

The lowest altitudes of the BIWXM model that can be modeled is probably 30 kms. There may be significant errors given the simplicity of the chemical system used. However, it was observed in DDDR studies that during large X-ray flares the electron density profile below 40 km altitude affected VLF propagation. The Heaps model of i-e pair production is used [Heaps, 1978]. The formula requires magnetic latitude, λ_M for latitudes up to the polar region and F10.7a.

$$Q = (A + B\sin^4\lambda_M)N \ (\mathrm{cm^{-3}s^{-1}})$$

N is the neutral density in molecules/cm^3. A equals $1.74\text{x}10^{-18}$ and B equals $1.93\text{x}10^{-17}$ for solar maximum and 2.84x10-17 for solar minimum, B is calculated linearly between these two values based on F10.7a. It would be better to use a yearly average of F10.7, but F10.7a is used for simplicity. The above formula works down to 30 km altitude. An additional factor is necessary to model the role off of ionization in the lowest altitudes. In the polar region the Q levels off by

using a solar condition sensitive boundary to define this polar region level off:

$$\lambda_M = \min(\lambda, 63 + f * (56 - 63))$$
$$f = \max\left(0, \min\left(1, \frac{(F10.7a - 65)}{(265 - 65)}\right)\right)$$

These formulae give approximately what the Heaps [1978] calculations give for the year-to-year observations presented within.

ADDITIONAL NOTE: Using these formulae within BIWXM tends to give electron density profiles that are too dense in the low altitudes below 50 km at night. Exploring detailed chemistries that include increased nighttime 3-body recombination rates, the electron densities are still too high by an order of magnitude based on testing VLF propagation codes with these profiles. We speculate that galactic cosmic rays are sporadic ionization events that are unevenly spaced. These ionization events are spaced approximately like lightning events we observed in thunderstorms. The columns of these spatial sporadic ionization events probably accelerate recombination within the columns as the ionization spreads under slow diffusion transport. As a result, the resulting electron density profiles create a 'leaky' spatial distribution and a more rapid recombination than a smooth distribution of this ionization rate can provide. Thus, we divide the Heaps [1978] model by 5000 to remove the excessively high electron density below 50 km during nighttime conditions. It is possible that smoke particle or additional chemistry is required to calculate nighttime removal of electrons below 50 km, but the sporadic spatial ionization should also reduce the effectiveness of this ionization source in producing an evenly distributed electron density profile.

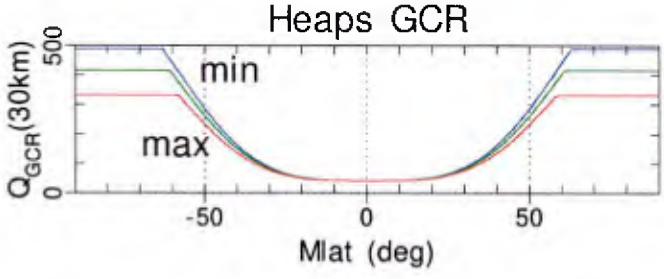

Figure 2.6.1. The ionization rates at 30 km due to galactic cosmic ray for minimum and maximum solar conditions.

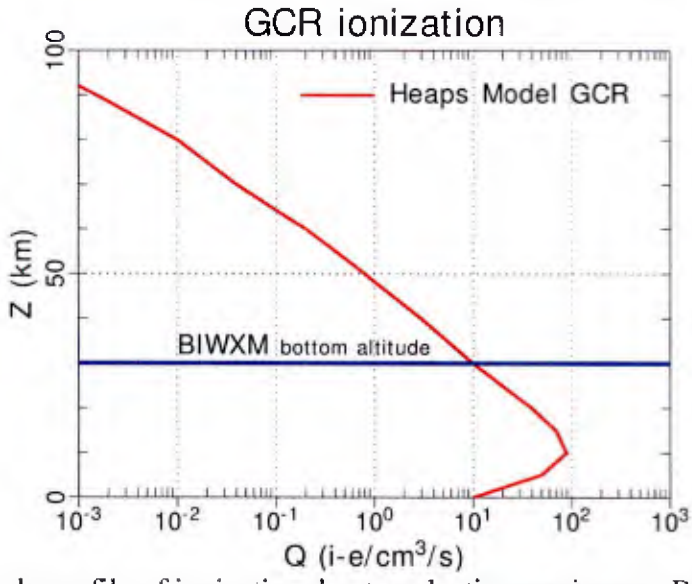

Figure 2.6.2. An altitude profile of ionization due to galactic cosmic rays. BIWXM is (sort of) valid down to 30 km. This is the Heaps profile which is divided by 5000 within BIWXM. See text above.

3 Chemical System in BIWXM

BIWXM's chemistry is define by two setup files: species.set and reaction.set. The species.set file presents the fundamental species to be included within the ionosphere-atmosphere system. There are a number required species for the neutral atmosphere and ionosphere associated with the fundamental requirements for D, E and F region modeling. Additional species can be included for specialty situation such as an active chemical release of H_2O or SF_6, or additional metal layer modeling of Mg^+, Na^+, etc. The reactions must reflect the full chemistry of the introduced species.

3.1 Species Input.

Numerical equations are set up once the species and reaction lists define the system. The BIWXM model is designed to be defined by setup files containing the species and reactions necessary for the upper atmosphere from 50 to 500 km. The species setup file, species.txt, contains information on each species for collisions, for thermal properties, and for solution decisions. This file may be changed to suit the further development of BIWXM, but the current species.set text file is currently used in BIWXM V0.1. Table 3.1.1 provides a short example of a species field.

Table 3.1.1 Species file for initializing the BIWXM D region chemistry.

#Species	AMN	Q	DEG_FREE	HSCOL_NN	MMCOL_IN	CHEM	TRAN
h+	1	1	3	1.00	0.00	1	1
o+	16	1	3	1.20	0.00	1	1
n2+	28	1	5	3.80	0.00	1	1
no+	30	1	5	3.70	0.00	1	1
o2+	32	1	5	3.60	0.00	1	1
fe+	56	1	3	3.70	0.00	1	1
feo+	72	1	5	3.80	0.00	1	1
fen2+	84	1	5	3.80	0.00	1	1
feo2+	88	1	5	3.80	0.00	1	1
o2-	32	-1	5	3.60	0.00	1	1
&							
h	1	0	3	1.20	0.64	0	0
n	14	0	3	1.20	1.13	0	0
o	16	0	3	1.20	0.77	0	0
n2	28	0	5	3.80	1.76	0	0
no	30	0	5	3.70	1.74	0	0
o2	32	0	5	3.60	1.60	0	0
o2(1d)	32	0	5	3.60	1.60	0	0
fe	56	0	3	1.50	0.86	0	0
m	29	0	5	3.80	1.74	0	0
e	0	-1	3	0.00	0.00	0	0
$							

The species.set file defines the species with 8 columns of information. The columns must be separated by white space but do not require a particular format definition. The setup file can have comment lines with '#' in the first position of the line. The last two species are necessary at the end of the species list. First, M is the total particle density for 3-body reactions. M is defined approximately by N_2 specifications. Second, e is the electron species, which is massless.

The 8 columns are defined as:

SPECIES	- species chemical formula in Hill Notation (up to 10 characters)
AMN	- atomic mass number (number of nucleons)
Q	- charge in units of *e* (-1,0,1,2 …)
DEG_FREE	- degrees freedom of the atom (3) and diatomic molecule (5)
HSCOL_NN	- hard-sphere collision coefficients for neutrals (A_mx10^{-8}cm^2)
MMCOL_IN	- Maxwell molecule collision coefficients (C_mx10^{-10})
CHEM	0 Do not change species density with the chemistry.
	1 Change species with chemistry.
TRANS	0 Do not solve for transport.
	1 Solve for transport of this species.

The species name can hold +, -, parentheses, and underscores to enable the inclusion of metastable species $(O(2D)^+$, $O(3P)^+$, …) , vibrational modes (N2(0), N2(1), N2(2), …), etc. The AMN defines the mass of the species through the nucleon count. This is used to define the mass of the species. Commonly an integer is sufficient to define the AMN, but a decimal number can be used to more accurately describe the mass when multiplied by the atomic mass unit (1.6600539040x10-24 gm). Q defines the number of charge units, which permits multiply ionized species (O++, O+++, etc.).

The CHEM and TRANS flags permit species to exist within the model without transport and/or chemistry altering their density or temperature profiles. This is used to provide external model definition of neutral atmosphere species. The & within the species.set file indicates where external models will provide specifications. After the & the transport and chemistry flags are not used. For simplicity of the model, we have used the MSIS model empirical atmosphere model [*Picone et al.*, 2002] to define the major neutral species H, He, N, O, N_2, and O_2 as well as the neutral temperature. We also use another empirical model of minor neutral species to simplify our initial studies of the D-region chemistry. The MODTRAN Atmosphere mixing ratios [*Anderson et al.*, 1986] provide densities for the following species as needed: H_2O, CO_2, O_3, N_2O, CO, CH_4, NO, SO_2, NO_2, NH_3, HNO_3, OH, HCl, ClO, OCS, H_2CO, HOCl, HCN, CH_3Cl, H_2O_2, C_2H_2, C_2H_6, PH_3. All of these species could be provided to BIWXM through coupling to the large physic-based models of the atmosphere.

HSCOL_NN provides the hard sphere radius to define neutral on neutral collisions. This is the kinetic radius defined in nanometers. MMCOL_NN is the Maxwell molecule collision parameter for ion-neutral collisions. Ion-ion, electron-ion, and electron-neutral collisions are defined separately. These will be defined for a number of species during subsequent quarters of effort.

3.2 Reactions Input.

A second text input file, reactions. Set, is used to define the chemical reactions to be used in the BIWXM model. Blank lines are permitted, and comment lines must have '#' in the first column of the line. Each reaction line is read using a 256-character variable. This is the limit of the reaction line definition. Table1.1.2 presents a short example of a reaction setup file for a minimal ionospheric chemistry. These reactions have no specific format except for the white space between each token on the line (species, +, --->, numbers).

There can be 1 to 3 reactants and 1 to 5 products in each reaction.

r1 + r2 + r3 ---> p1 + p2 + p3 + p4 + p5 a b c d e

where r's are the reactants and p's are the products. The reaction rate is defined by the coefficients a, b, c, d, and e. There can be 1 to 5 numbers used to define the rate. If a is positive then

$$k = a$$

or

$$k = a\left(\frac{T}{300}\right)^b$$

or

$$k = a\left(\frac{T}{300}\right)^b e^{-1000*c/T}$$

or

$$k = \min\left(a\left(\frac{T}{300}\right)^{b} e^{-1000*c/T}, d\right)$$

with d representing a 3-body reaction saturation limit. If a>0, then the e (5th coefficient) is not currently used. If a is negative, then the polynomial form is used:

$$k = -a + b\frac{T}{300} + c\left(\frac{T}{300}\right)^{2} + d\left(\frac{T}{300}\right)^{3} + e\left(\frac{T}{300}\right)^{4}$$

The rate subroutine can handle 1 through 5 coefficients for either form of the rate equation. Note that all reactions use the normalized temperature ratio of T/300K. Some published rates for the D region use different ratios. These must be reformed into the expected T/300 ratio for use in the BIWXM program.

Solar ionization processes are not explicitly included in reaction.set. These are created within BIWXM by recognition of the dominant neutral species to be ionized.

There is a consistency preprocessor program for BIWXM that examines the reaction.set file to discover whether there are reactants or products not in the species.set file. Additionally, a set of log files are written in the directory ./log/. Each species within species.set has a log file, which contains all the reactions associated with the species. This enables the BIWXM user to examine the consistency of the reaction list. APPENDIX B lists the most complete set of reactions for the D, E and F region chemistry based mostly on the work of Pavlov [2013] with all citations listed in the comments at the end of APPENDIX B.

Modeling neutral species necessary for neutral metal layers were explored with Titus Yuan of USU and a second version of the BIWXM model focused on neutral metal layers. This version of BIWXM is focused on the ionosphere results. A metal neutral layer must be generated by an embedded layer model which can be a coupled neutral layer model or an empirical neutral layer model. As a result we present the ion chemistry within the Space Environment Corporation effort.

The simplest reaction set that still provides excellent electron density profiles from 30 to 3,000 km is presented in Table 3.2.1. Note that the three-body recombination of the electron profile below 85 km has `| recom` identifier at the end of each 3-body reaction. This is an identifier to the BIWXM program to use a subroutine to calculate an altitude dependent value of the formula. This formula is different for sunlit and nighttime conditions. The daytime values can be approximated by using a more direct 3-body formula in the reaction commented out (#). The higher 3-body reaction rate at night helps remove electrons in the 85 to 50 km altitude range after sunset. This seems to better agree with VLF propagation calculates. These elevated 3-body rates were not needed in the DDDR since it calculated an approximately steady-state profile. BIWXM is fully time-dependent and the dusk decay of the D region requires the elevated nighttime 3-body recombination rates.

Table 3.2.1. Simple ionosphere reaction set.

```
#######################################################################
#
#     k = a (T/300)**b exp(-1000*c/T)
#     k = -a + b*(T/300) + c*(T/300)**2 + d*(T/300)**3 + e*(T/300)**4
#
#######################################################################
#
#  Standard E and F region chemistry
#
#  i-e recombination
#
 n2+        + e          ---> n          + n          1.80D-13  -0.39
 no+        + e          ---> n          + o          4.20D-13  -0.85
 o2+        + e          ---> o          + o          1.90D-13  -0.50
#
#  3-body i-e recombination (recom3 is faster at night but it is an
artificial formula)
#
#h+         + e   + m    ---> h          + m          2.50D-33  -0.5
#n+         + e   + m    ---> n          + m          2.50D-33  -0.5
#o+         + e   + m    ---> o          + m          2.50D-33  -0.5
#n2+        + e   + m    ---> n2         + m          2.50D-33  -0.5
#no+        + e   + m    ---> no         + m          2.50D-33  -0.5
#o2+        + e   + m    ---> o2         + m          2.50D-33  -0.5
 h+         + e          ---> h                       |recom3
 n+         + e          ---> n                       |recom3
 o+         + e          ---> o                       |recom3
 n2+        + e          ---> n2                      |recom3
 no+        + e          ---> no                      |recom3
 o2+        + e          ---> o2                      |recom3

#  charge exchange
#
 h+         + o          ---> o+         + h          3.75D-16
 o+         + h          ---> h+         + o          3.00D-16
 o+    + o2   ---> o2+  + o  -2.01D-17 -5.53D-18 7.640D-19 -3.69D-20 6.89D-22
 n+         + o2         ---> o2+        + n          3.10D-16
 n+         + o          ---> o+         + n          1.00D-18
 n2+        + o          ---> o+         + n2         1.00D-17  -0.23
 n2+        + o2         ---> o2+        + n2         5.00D-17   0.80
 o2+        + no         ---> no+        + o2         4.50D-16
#
#  charge interchange
#
 n2+        + o          ---> no+        + n          1.40D-16  -0.44
 n+         + o2         ---> o+         + no         3.60D-17
 o+      + n2      ---> no+        + n        -1.533d-18 -5.920e-19 8.600e-20
 o2+        + n          ---> no+        + o          1.00D-17
 o2+        + n2         ---> no+        + no         5.00d-22
#
#######################################################################
#
# D Region Negative chemistry
#
 e          + o2         ---> o2-                     1.00d-25
```

```
 e          + o2  + n2    ---> o2-        + n2       1.00d-43
 e          + o2  + o2    ---> o2-        + o2       1.40d-41 -1.0 0.6
#
 o2-        + o2(1d)      ---> o2         + o2  + e  2.00d-16
 o2-        + n           ---> no         + o   + e  3.00d-16
 o2-        + o           ---> o2         + o   + e  1.50d-16
#
#  detachment
#
 o2-                      ---> o2         + e        0.33    !day
#
#  ion ion recombination
#
 h+         + o2-         ---> h          + o2       6.00d-14
 n+         + o2-         ---> n          + o2       6.00d-14
 o+         + o2-         ---> o          + o2       6.00d-14
 n2+        + o2-         ---> n2         + o2       6.00d-14
 no+        + o2-         ---> no         + o2       6.00d-14
 o2+        + o2-         ---> o2         + o2       6.00d-14
#
#  3-body ion ion recombination (doesn't make a difference.)
#
 h+         + o2- + m     ---> h          + o2 + m   3.00D-37 -2.5
 n+         + o2- + m     ---> n          + o2 + m   3.00D-37 -2.5
 o+         + o2- + m     ---> o          + o2 + m   3.00D-37 -2.5
 n2+        + o2- + m     ---> n2         + o2 + m   3.00D-37 -2.5
 no+        + o2- + m     ---> no         + o2 + m   3.00D-37 -2.5
 o2+        + o2- + m     ---> o2         + o2 + m   3.00D-37 -2.5
#
###############################################################################
#
```

If metal layers are to be included in the BIWXM results, this is most simply done using Fe as the main metal species. It is the densest neutral and ion metal with Mg being a close second. However, their chemistries are nearly identical so modeling one metal species to represent all metals will provide a proper metal ion layer response in the total electron density. Table 3.2.2 presents a simple ionosphere and Fe+ layer model reaction set. Note that O_3 density must be prescribe in this data set. BIWXM can use the MODTRAN mixing ratios to generate O_3 profiles. Studies have not been performed to determine if the O_3 influence changes the electron density results.

Table 3.2.1. Simple ionosphere and metal ion reaction set.

```
#     k = a (T/300)**b exp(-1000*c/T)
#     k = -a + b*(T/300) + c*(T/300)**2 + d*(T/300)**3 + e*(T/300)**4
#
#########################################################################
#
#  Standard E and F region chemistry
#
#  i-e recombination
#
 n2+        + e          ---> n          + n          1.00D-13  -0.390
 no+        + e          ---> n          + o          4.20D-13  -0.850
 o2+        + e          ---> o          + o          1.90D-13  -0.500
#
# 3-body i-e recombination
#
#h+         + e    + m    ---> h          + m          2.50D-33  -0.5
#n+         + e    + m    ---> n          + m          2.50D-33  -0.5
#o+         + e    + m    ---> o          + m          2.50D-33  -0.5
#n2+        + e    + m    ---> n2         + m          2.50D-33  -0.5
#no+        + e    + m    ---> no         + m          2.50D-33  -0.5
#o2+        + e    + m    ---> o2         + m          2.50D-33  -0.5
 h+         + e           ---> h                       |recom3
 n+         + e           ---> n                       |recom3
 o+         + e           ---> o                       |recom3
 n2+        + e           ---> n2                      |recom3
 no+        + e           ---> no                      |recom3
 o2+        + e           ---> o2                      |recom3
#
#  charge exchange
#
 h+         + o           ---> o+         + h          3.75D-16
 o+         + h           ---> h+         + o          3.00D-16
 o+    + o2  ---> o2+    + o   -2.01D-17 -5.53D-18 7.64D-19 -3.69D-20  6.89D-22
 n+         + o2          ---> o2+        + n          3.10D-16
 n+         + o           ---> o+         + n          1.00D-18
 n2+        + o2          ---> o2+        + n2         5.00D-17   0.800
 o2+        + no          ---> no+        + o2         4.40D-16
#
#  charge interchange
#
 n2+        + o           ---> no+        + n          1.40D-16  -0.440
 n+         + o2          ---> o+         + no         3.60D-17
 o2+        + n           ---> no+        + o          1.20D-16
 o+      + n2          ---> no+        + n         -1.533d-18 -5.92e-19 8.6e-20
 o2+        + n           ---> no+        + o          1.00D-17
#
#########################################################################
#
#  Fe chemistry
#     Feng et al. A Global Meteoric Iron Model, JGR, 2013
#
# Fe ion Chemistry
#
 fe+        + e           ---> fe                    6.50d-18 -0.51
```

```
 feo+       + e          ---> fe         + o        3.00d-13 -0.50
 feo2+      + e          ---> fe         + o2       3.00d-13 -0.50
 fen2+      + e          ---> fe         + n2       3.00d-13 -0.50
#fe+                     ---> fePMC                 requires heterogeneous
chemistry subroutine

 fe+        + e   + m    ---> fe                 + m  2.00D-33
 feo+       + e   + m    ---> fe         + o     + m  2.00D-33
 feo2+      + e   + m    ---> fe         + o2    + m  2.00D-33
 fen2+      + e   + m    ---> fe         + n2    + m  2.00D-33

 o+         + fe         ---> fe+        + o        2.00d-15
 o2+        + fe         ---> fe+        + o2       1.10d-15
 no+        + fe         ---> fe+        + no       9.20d-16

 fe+        + n2 + m     ---> fen2+      + m        4.00d-36 -1.52
 fe+        + o2 + m     ---> feo2+      + m        8.30d-36 -1.86
 fe+        + o  + m     ---> feo+       + m        2.50d-36

 fe+        + o3         ---> feo+       + o2       7.60d-16 0.0  0.2405
 feo+       + o          ---> fe+        + o2       3.00d-17
 fen2+      + o          ---> feo+       + n2       5.00d-17
 feo2+      + o          ---> feo+       + o2       5.00d-17
#
#########################################################################
#
# D Region Negative chemistry
#
 e          + o2  + n2   ---> o2-        + n2       1.00d-43
 e          + o2  + o2   ---> o2-        + o2       1.40d-41 1.0  0.6
#
 o2-        + o2(1d)     ---> o2         + o2  + e  1.50d-16
 o2-        + n          ---> no         + o   + e  3.00d-16
#
 o2-                     ---> o2         + e        0.33    |day
#
 h+         + o2-        ---> h          + o2       6.00d-14
 n+         + o2-        ---> n          + o2       6.00d-14
 o+         + o2-        ---> o          + o2       6.00d-14
 n2+        + o2-        ---> n2         + o2       6.00d-14
 no+        + o2-        ---> no         + o2       6.00d-14
 o2+        + o2-        ---> o2         + o2       6.00d-14
 fe+        + o2-        ---> fe         + o2       6.00d-14
 feo+       + o2-        ---> fe         + o   + o2 6.00d-14
 feo2+      + o2-        ---> fe         + o2  + o2 6.00d-14
 fen2+      + o2-        ---> fe         + n2  + o2 6.00d-14

 h+         + o2-  + m   ---> h          + o2  + m  3.00d-37 -2.5
 n+         + o2-  + m   ---> n          + o2  + m  3.00d-37 -2.5
 o+         + o2-  + m   ---> o          + o2  + m  3.00d-37 -2.5
 n2+        + o2-  + m   ---> n2         + o2  + m  3.00d-37 -2.5
 no+        + o2-  + m   ---> no         + o2  + m  3.00d-37 -2.5
 o2+        + o2-  + m   ---> o2         + o2  + m  3.00d-37 -2.5
 fe+        + o2-  + m   ---> fe         + o2  + m  3.00d-37 -2.5
 feo+       + o2-  + m   ---> fe   + o   + o2  + m  3.00d-37 -2.5
 feo2+      + o2-  + m   ---> fe   + o2  + o2  + m  3.00d-37 -2.5
 fen2+      + o2-  + m   ---> fe   + n2  + o2  + m  3.00d-37 -2.5
```

3.3 Rigorous Chemical Solution for D and E Region

The BIWXM model can accommodate up to 99 species and any number of reactions. The numerical method that is used to solve the complex chemical system is the Livermore Solver for Ordinary Differential Equations (LSODE) [Radhakrishnan and Hindmarsh, 1993]. The current BIWXM model has been tested using D-Region chemistry of 57 species and 384 reactions has been run successfully. Figure 3.3.1 shows an instance in time for the run. The neutral species produced by MSIS and the MODTRAN mixing ratios are plotted in the left panel. The metastable neutral O2(1D) is calculated by a formula provided by *Swider and Foley* [1978]. It is plotted in red in the left panel. The right panel plots the normal ionosphere ion species in blue, the D-region positive ions in green, and the D-region negative ions in red. The electron density is plotted in black.

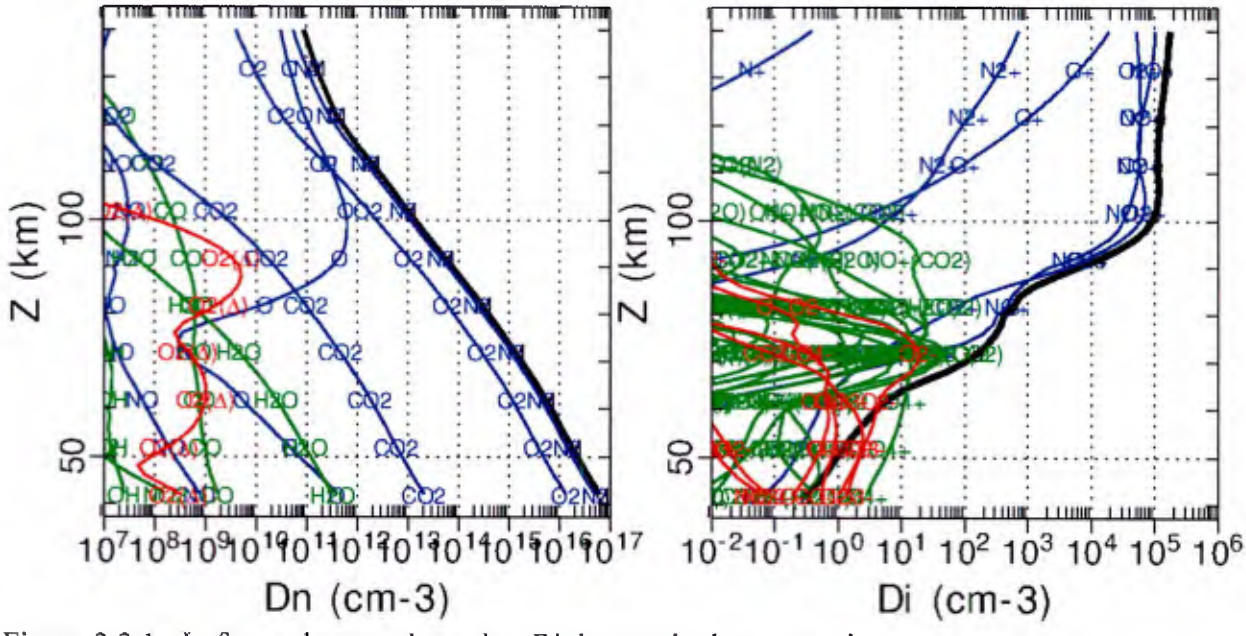

Figure 3.3.1. Left panel: neutral species. Right panel: charge species.

The BIWXM D-region capability will be adaptable to the very complex chemistry of the middle atmosphere, but also have a simplified chemistry that still obtains the same electron density profile. The complex positive and negative ion species partitioning need not be solved in enormous detail if one is only pursuing the electron density profile used in RF propagation and absorption codes. The adaptability is based on the species.set and reaction.set files that define the chemical system. There are other setup files for simple design and updating of the physics within BIWXM. The BIWXM group has decided upon text files containing collimated data and self-describing header comments. The tables included in the discussion below are taken directly from these BIWXM txt files.

Metal ions are particularly important in the E region due to the presence of metal ion chemistry. The long-lived metal ions permit very large densities within thin layers. A vertical gradient in the

horizontal neutral winds will move ions up and down the field line and potentially can pinch the ions towards a null in the parallel neutral wind component. SEC will produce a model of metal ion layers with chemistry and transport prior to this BSION effort. Figure 3.3.2 presents results of this preliminary model using a 2nd-order explicit finite-difference method for the transport and chemistry. The BIWXM will have high-order transport numerical capability to better model the sharp ionospheric features within the E and F region ionosphere. The top panel plots the total electron density over a 24-hour period above the Bear Lake Observatory in Garden City, Utah (41.93N,111.42W). The middle panel plots the Na^+ density and the bottom panel plots the neutral wind component parallel to the magnetic field. The Na^+ ion layer forms at the altitude of the null in the parallel neutral wind.

The BIWXM code was developed over three years. The first year will create a 1D model of the ionosphere with all the necessary chemistry and physics for the ionosphere including TID propagation, metal ion layers, and D region space weather. The second year included improvements in the solar spectrum required for the full range of altitudes and solar conditions and worked towards studying metal ion chemistry and transport under tides and waves. Figure 3.3.2 gives results of the metal ion chemistry and transport of BIWXM to generate descending ion layers under the tidal forcing of the HWM wind model. This solution was obtain using explicit transport and chemistry solution which requires very short timesteps to accommodate the chemistry of the E region. To combine F, E, and D region transport and chemistry into a single BIWXM model, more sophisticated numerical methods were required.

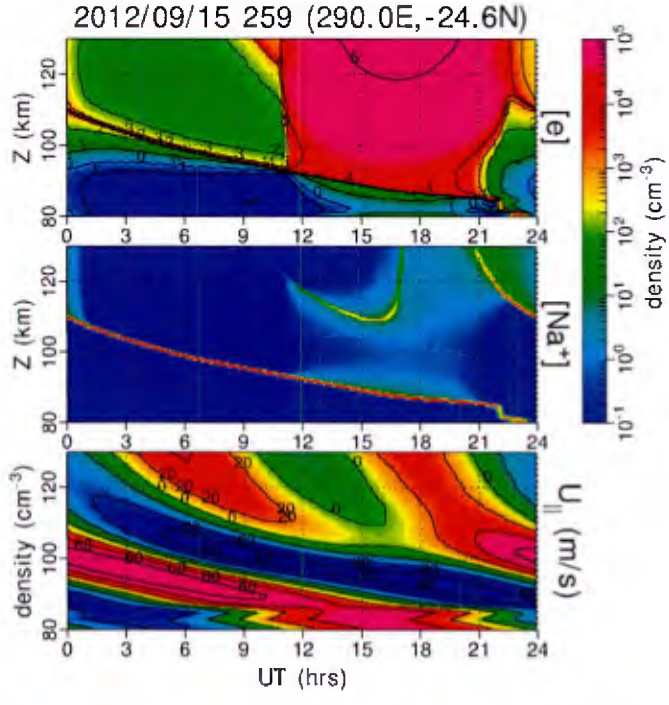

Figure 3.3.2. The simple metal layer model solved for the standard ionospheric chemistry, but also included chemistry for metal ions (Fe^+, FeO^+, FeO_2^+, FeN_2^+, Na^+, NaO^+, NaO_2^+, NaN_2^+). Electron density (top panel), Na+ density (middle panel), and parallel component of neutral wind (bottom panel).

4 BIWXM Numerics

4.1 Transport Algorithm Tests

There have been significant advances made in transport numerics for the conservation equations of mass, momentum, and energy. The Flux Corrected Transport of Boris and Book [1979] was a significant leap forward. However, Flux Corrected Transport suffers from artifacts when shocks and step structures are present within advecting gases. The MUSCL Transport method and variants have solved this defect. MUSCL stands for *Monotonic Upwind Scheme for Conservation Laws* [van Leer, 1979]. The method uses a total variation diminishing (TVD) scheme that is second-order in spatial accuracy.
In addition, the method can be implemented in a manner suitable for our chemical-transport system of ordinary differential equations. This allows us to explore the efficiencies of advance matrix inversions. FCT algorithms were not suitable because Jacobians could not be accurately determined in exact difference formulae. The MUSCL transport adds a small diffusive term using the speed of sound and the second derivative of the conserved quantities, *U*:

$$\frac{\partial U}{\partial t} + \frac{dF}{dx} = 0$$

where F is the flux of the conserved quantity where

$$U = \begin{pmatrix} \rho \\ \rho u \\ E \end{pmatrix} \quad F = \begin{pmatrix} \rho u \\ p + \rho u^2 \\ (E + p)u \end{pmatrix},$$

for mass density (ρ), momentum (ρu), and total energy (E). Energy is given by

$$E = \rho e + \frac{1}{2}\rho u^2$$

where e is the specific internal energy under an equation of state:

$$p = \rho(\gamma - 1)e$$

with γ as the ratio of specific heats (c_p/c_v) for the gas. The difference equation is defined for the cell point i with fluxes at the boundaries of i+1/2 and i-1/2.

$$U_i^{t+1} = U_i^t - \frac{\Delta t}{\Delta x}\left[F_{i+\frac{1}{2}} - F_{i-\frac{1}{2}}\right]$$

A second-order determination of the fluxes at the cell boundaries is calculated from cell boundaries of conserved quantities and velocities

$$F_{i+\frac{1}{2}} = \rho_{i+\frac{1}{2}} u_{i+\frac{1}{2}} - c_s(u_{k+1} - u_k)/\Delta x$$

with $c_s = \gamma \frac{kT_s}{m_s}$.

The FCT algorithm uses a very large diffusive term that is only employed near a steepened structure within the conserved quantity. The MUSCL algorithm uses the small diffusive term throughout the solution and, thus avoids the FCT artifacts. Figure 2.8 shows the time history of the mass, momentum, and energy of a gas beginning from an initial step density function. The severe initial condition does produce small instabilities in the gas, which are smoothed out by the small diffusive term placed within the MUSCL algorithm:

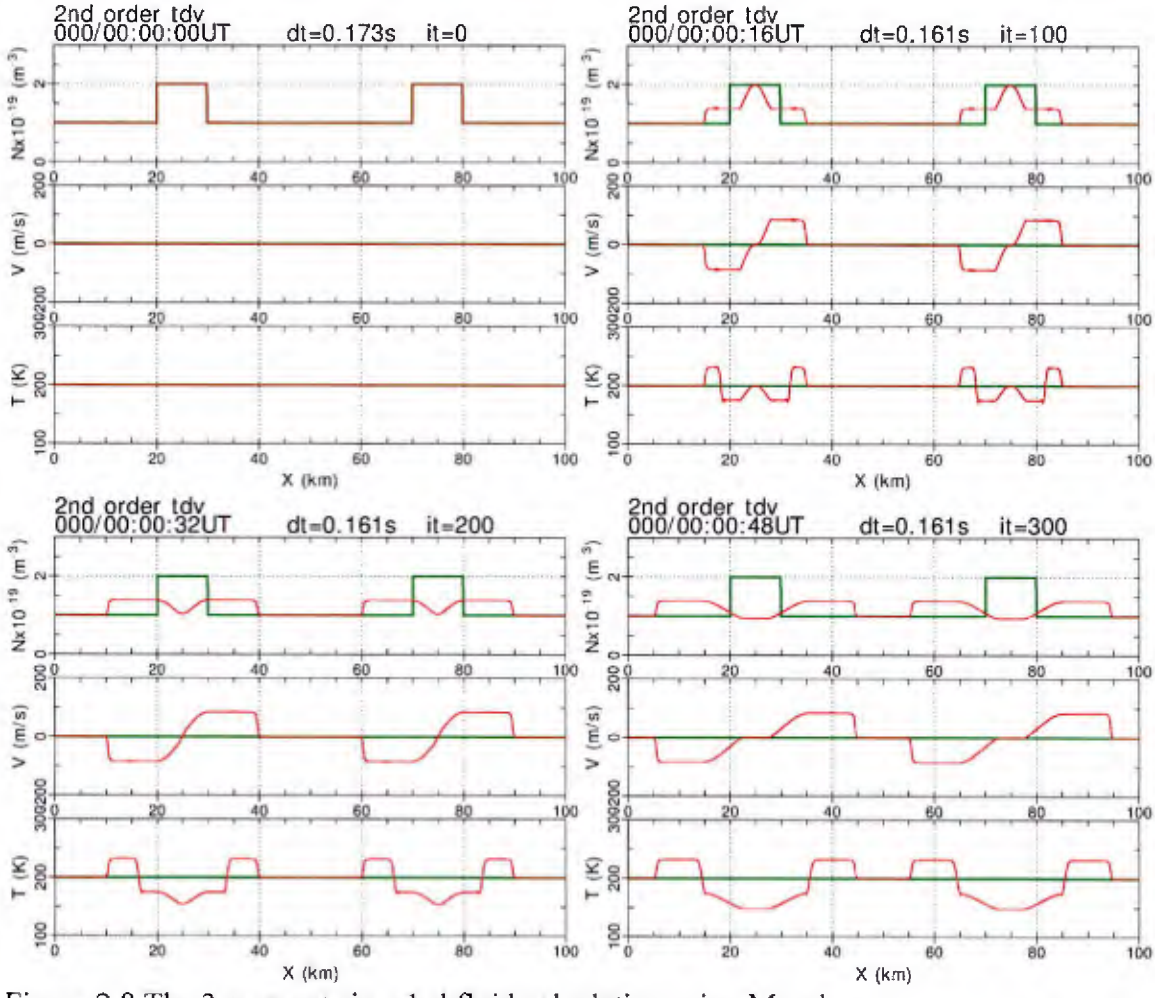

Figure 2.8 The 3 moments in a 1-d fluid calculation using Muscl.

A version of the MUSCL algorithm for irregularly spaced grids is to be used for 3D versions of BIWXM to model irregularity structures and artificial perturbation of ionospheric chemistry. However, this is a will be a future effort.

The MUSCL algorithm seems to be stable for single gas dynamics but is unstable for multi-species dynamics of the BIWXM for transport along the field line. The MUSCL algorithm will continue to be explored, but the BIWXM currently uses a version of the Lax-Wendroff Flux

Corrected Transport (FCT) for 2nd order in both time and space for transport parallel to B. Instead, the MUSCL algorithm can be used for perpendicular transport in 3D model calculations in the future. The current 1D transport code is efficient numerically and stable under the diffusive transport of the ion transport parallel for many species. Examples of time-dependent solutions for BIWXM will be provided below.

4.2 Numerical Methods for Complex Chemical Systems with Transport

The difficulty with a multispecies chemically actives system in the ionosphere is that the time-scales of the various competing processes varies dramatically through the altitude range of 30 to 3000 km and through day-night and quiet-disturbed conditions. The difficulty is developing a method that accommodates the full range of conditions. The approach used within BIWXM is time-splitting of chemical terms and the transport terms in the mass equations with variable timesteps to accommodate the large variability of ion velocities occurring through the day. The minimum courant condition for all ion species transport is used to determine to be the fundamental time step of the full mass, momentum, and energy equations of the multi-ion system. Actually, it is 1/3 the minimum courant condition step to properly integrate the time-splitting method with the chemistry terms. Shorter time steps do not alter the solutions obtained within BIWXM. The chemical systems are solved on much shorter time scales as needed using the 1D LSODE solver for the transport limiting time step at every altitude. If the chemical system is not a strong driver of the mass equations (such as at high altitudes), then the LSODE solution does not alter the local ion densities within that time step. However, if the chemical system is dominant (at low altitudes), then the transport changes to ion densities is quickly erased by the LSODE time-split step, which occurs after the transport step. This time-splitting on the mass equation of the ion species remains stable and is a single numerical method for all altitudes from 30 to 3000 km. This method allows transport to alter the D region profiles during undisturbed times in the 85 to 100 km range, where transport is often expected to not influence the electron density profiles. The nighttime D region electron density profiles are extremely variable. Figure 4.2.1 shows four rocket profile observations with the DDDR and BIWXM calculations. The BIWXM profiles with transport show strong departure from the chemical steady state represented by DDDR above 85 km. Both fail to match the rocket measurements, but they do manage a decent average profile when compared to all night time rocket flights.
i

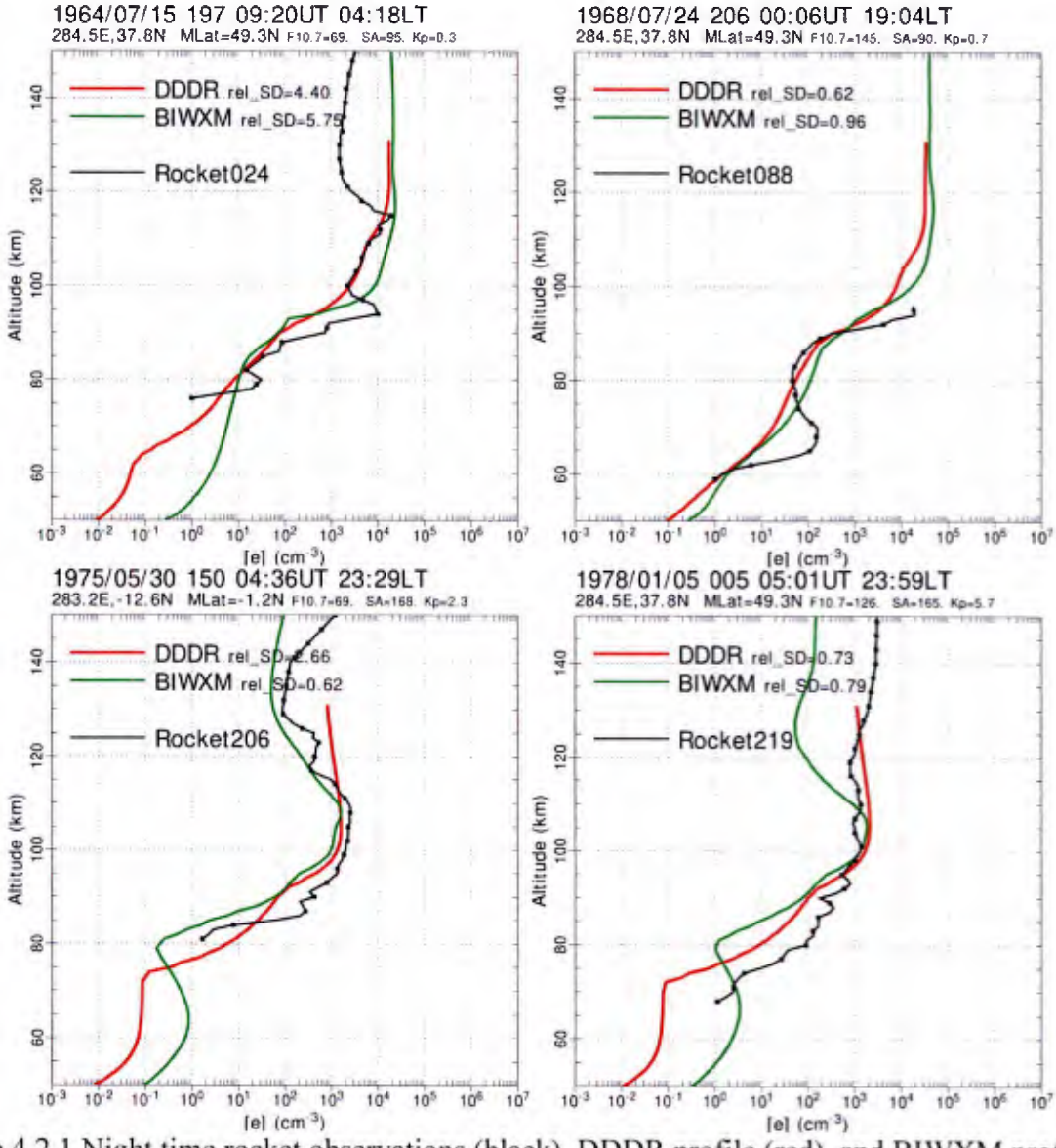

Figure 4.2.1 Night time rocket observations (black), DDDR profile (red), and BIWXM profile (green).

The time dependent velocity (momentum) equation for each ion is solved using the equations presented in section 2. This velocity equation is ordered to represent the collision dominated altitudes. However, the methods used in the transition and collisionless regions permit a stable solution through all altitudes. The ion velocities are solved for every transport time step of the stable mass equation. Neutral atmosphere conditions, solar spectrum, auroral precipitation, SPE ionization, ExB convection velocities, and other drivers are updated every 60 seconds to present a reasonably smooth set of conditions to drive the multi-species reactive transport system.

5 BIWXM Temperature Calculations

BIWXM calculates the ion and electron temperatures giving the ionization conditions and the neutral temperature generated by the MSIS model. A steady-state electron temperature profile is calculated, then the ion temperature profile is calculated for the average ion profile characteristics. All ions are assigned this average ion temperature. This is done to optimize speed of the solution. Figure 5.1 plots the various cooling rates of various processes using the temperatures of the IRI model and MSIS atmosphere model. These cooling collisions were calculated using the equations detailed in the collision section 2.2 above.

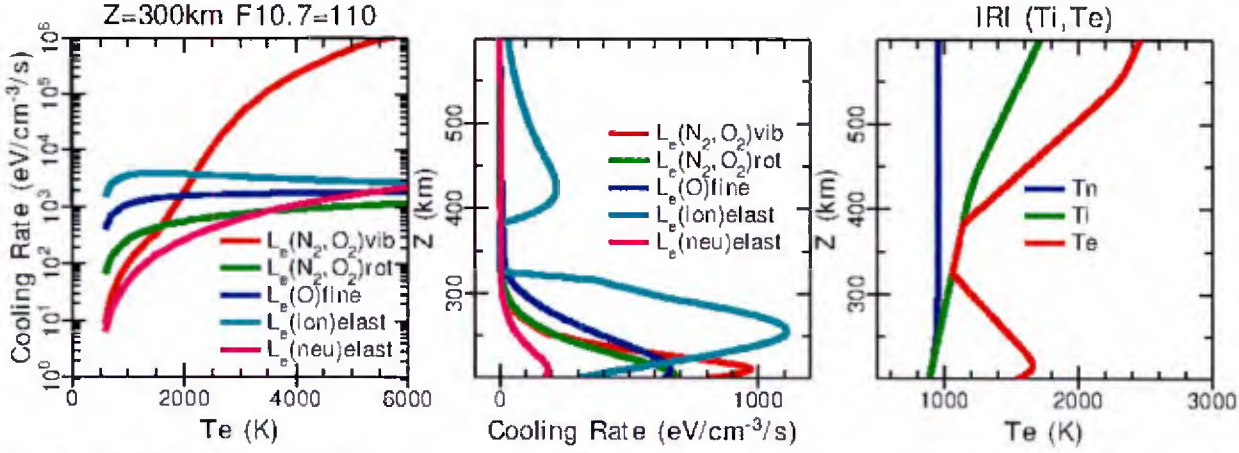

Figure 5.1 Electron cooling rates through the full temperature range of the ionosphere (left panel), for an IRI noontime ionosphere profile (middle panel) for the temperature profiles (right panel).

The lower altitude calculation of the electron temperature profile depends on the balance of local energy deposition and collisional cooling processes, which are temperature dependent.

$$0 = \sum Q_e - \sum L_e - \sum_i \frac{\rho_e \nu_{ei}}{m_i} 3k(T_e - T_i) - \sum_n \frac{\rho_e \nu_{en}}{m_n} 3k(T_e - T_n)$$

The energy deposition, Q_e, is proportional to the ionization rate at each altitude. The loss terms, L_e, are the electron collisional losses rotational and vibrational states of the molecular neutral constituents and to atomic fine-structure excitation and emission processes described in the section 2 above. The T_i term from the previous step could be used for this equation above, but it is assumed at these altitudes below 300 km that the other terms dominate in the cooling of the electron gas. The solution of the balance equation is obtained using an advanced Newton's method of obtaining zeros of equations. The upper altitude solution is obtained using a steady-state energy transport solution of a dominantly ionization atmosphere (F region topside) that is dominated by thermal conduction. This is presented in Schunk and Nagy [2010] on page 362 (2nd edition)

$$\frac{d}{dz}\left(7.7 \times 10^5 T_e^{5/2} \frac{dT_e}{dz}\right) = 0$$

which reduces to

$$T_e = \left[T_{eb}^{7/2} - \frac{7}{2}\left(\frac{q_{et}}{7.7 \times 10^5}\right)(z - z_b)\right]^{2/7}$$

where T_{eb} is the electron temperature at the bottom boundary, z_b, of the thermal conduction region and q_{et}. as the heat flow through the top boundary. A positive gradient in altitude means that there is a downward heat flow through the electron gas (negative q_{et}). This is used to generate the F region and topside Te profile where the downward q_{et} is proportional to the energy being deposited in the lower altitudes only meaning that the ionospheric electron gas has been heated through the processes of ionization. This heat is transported upward along field lines until a steady-state situation is reach and the steady-state heat flow is downward due to the positive gradient in T_e with z. These two solutions are combined in an altitude range around 300 km, but this altitude range moves with solar conditions. This has been tested for solar ionization and auroral ionization conditions for magnetic latitudes above 30° and the solutions compare favorably IRI T_e profiles.

The ion temperature is similarly calculated using a Newton's method to obtain a zero residual in the ion energy equation. The ion energy equation retains the time-dependent and simple spatial gradient term along the magnetic field, l, in the calculation with the strong collisional terms with the atmospheric neutrals and the electron gas.

$$\frac{3}{2}\mathrm{k}\frac{dT_i}{dt} + \frac{5}{2}\mathrm{k}T_i\left(\frac{dv_{li}}{dl}\right) = \frac{m_i v_{in}}{m_i + m_n}[3k(T_n - T_i) + m_n(\vec{u}_n - \vec{u}_i)^2] + v_{ie}3k(T_e - T_i)$$

Figure 5.2 provides a comparison of the BIWXM temperature solver with the IRI temperatures and the Millstone Hill ISR near noon. The BIWXM temperatures generally are close to the IRI temperature profiles, but the BIWXM temperature solver permits elevation of Te and Ti under

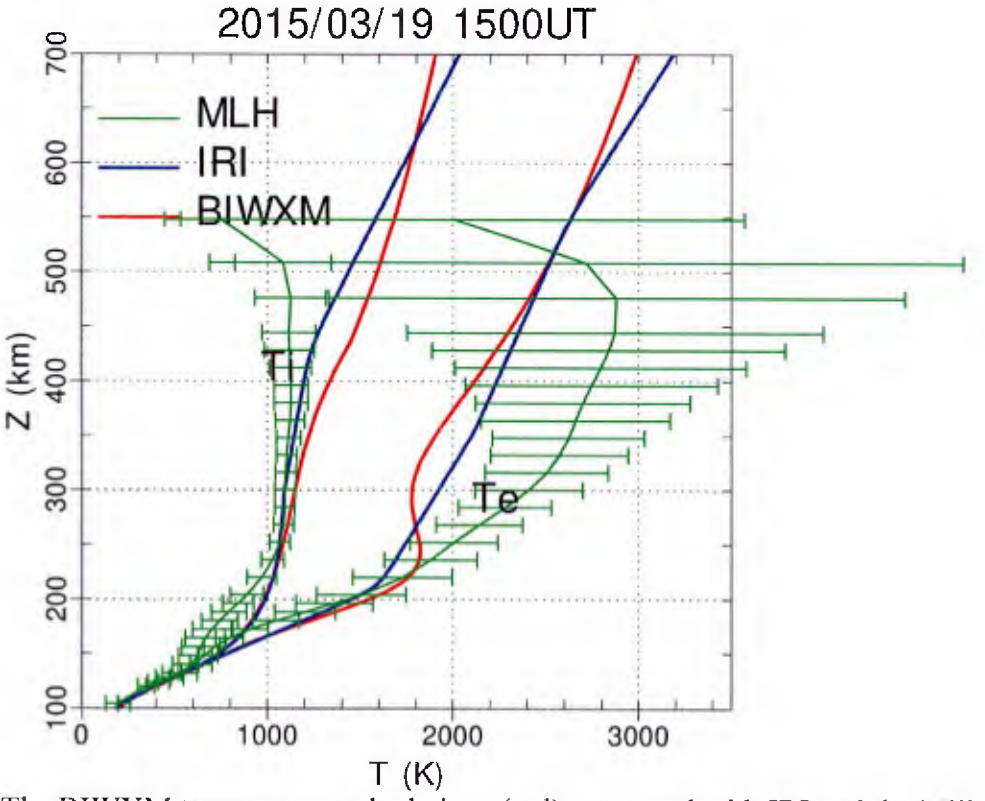

Figure 5.2 The BIWXM temperature calculations (red) compared with IRI and the Millstone Hill ISR measurement.

6 Full Profile Solution of BIWXM

The BIWXM 1D profile physics and numerics is complete. The full profile solutions are presented in Figure 6.1 for near noon and near midnight profiles at the Millstone Hill ISR. The tests for conditions of the BIWXM model are fairly close to the IRI ionosphere representation. However, the first benchmarking tests of the F region peak density and TEC values demonstrated that the BIWXM was producing too much plasma by nearly a factor of 2. After much testing of the chemistry, the ionization model, the solar spectral model, the Burnside factor, etc., there seemed to be no solution to this very dense F region result. However, it was mentioned at a BSION annual meeting that the NRLMSIS2000e model was providing an oxygen density profile that was too dense by nearly a factor of 2. Multiplying a the MSIS [O] values by 0.55 brought BSION into line with the IRI NMF2 and TEC values. We anticipate this factor to be eliminated when using the MSIS 2020 model release. Figure 6.1 presents the full model solution for a run at the Millstone Hill Radar site near noon and midnight. The MSIS neutral temperature is added to show the comparison with Te and Ti produced by BIWXM.

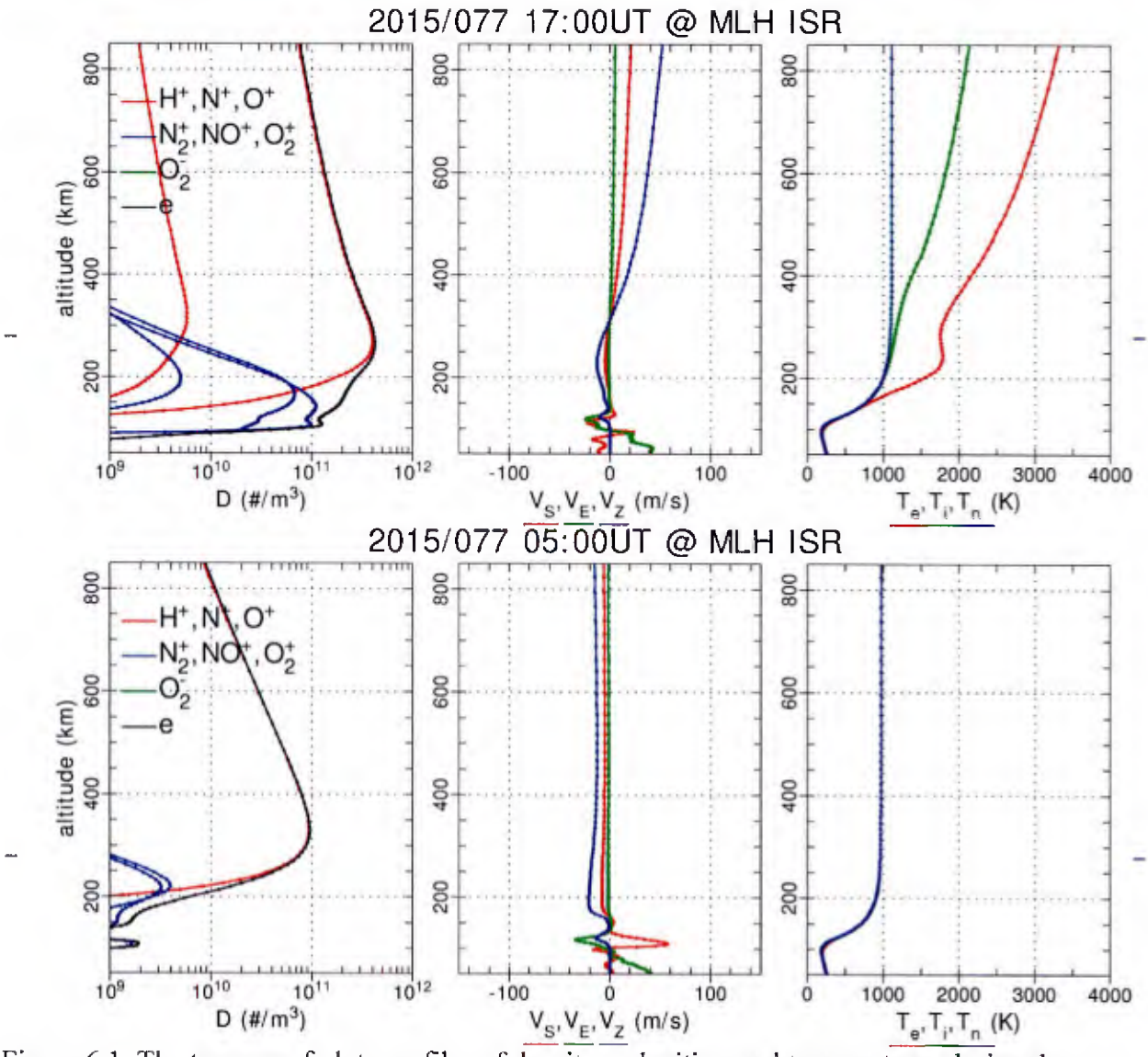

Figure 6.1. The top row of plots profiles of density, velocities, and temperatures during the daytime near noon at the Millstone Hill Radar site. The bottom row plots the profiles near midnight.

7 High Latitude Convection

The Weimer Potential model is currently used to provide high latitude convection of the 1D BIWXM model. The convection pattern is changed every 5 minutes using 5-minute average solar wind and IMF inputs. The convecting field-line is convected to a new position every minute. The ExB electric field in a part of the velocity calculation and provides substantial changes to the low altitude horizontal and vertical velocity within those regions of high collisions (100 to 150 km).

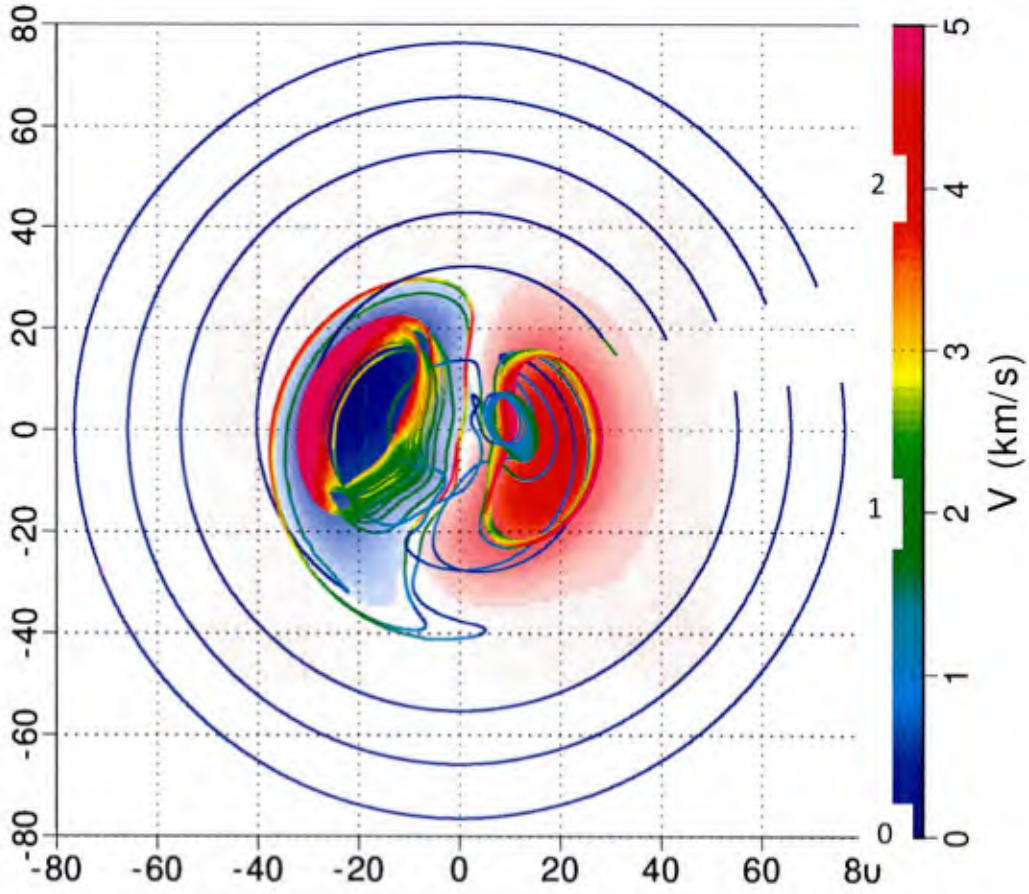

Figure 7.1 Convection of 7 BIWXM 1D calculations at increasing magnetic latitude start positions. The blue circles are the paths of co-rotating field lines within the solar magnetic time plot. The light pink, red, blue contour plot is the Weimer potential pattern at one time. The rainbow-colored lines are the convecting field lines present the time history of a day of time varying convection. The color scale shows velocity magnitude of the convecting lines.

The convection field is used to move the BIWXM along the convecting trajectories with the ExB motion. Or the user can request that the model solution does not convect but all velocity components within the transport solution still use the E and B fields in the determination of velocities. Figure 7.2 is a solution where the convection field is present, but the model solution is not convected. This shows the influence of the potential electric field on the plasma velocity above an incoherent scatter radar position. This is not the true representation of reality for the F peak but is does provide a good time history solution for the more chemically dominated altitudes (z< 150km).

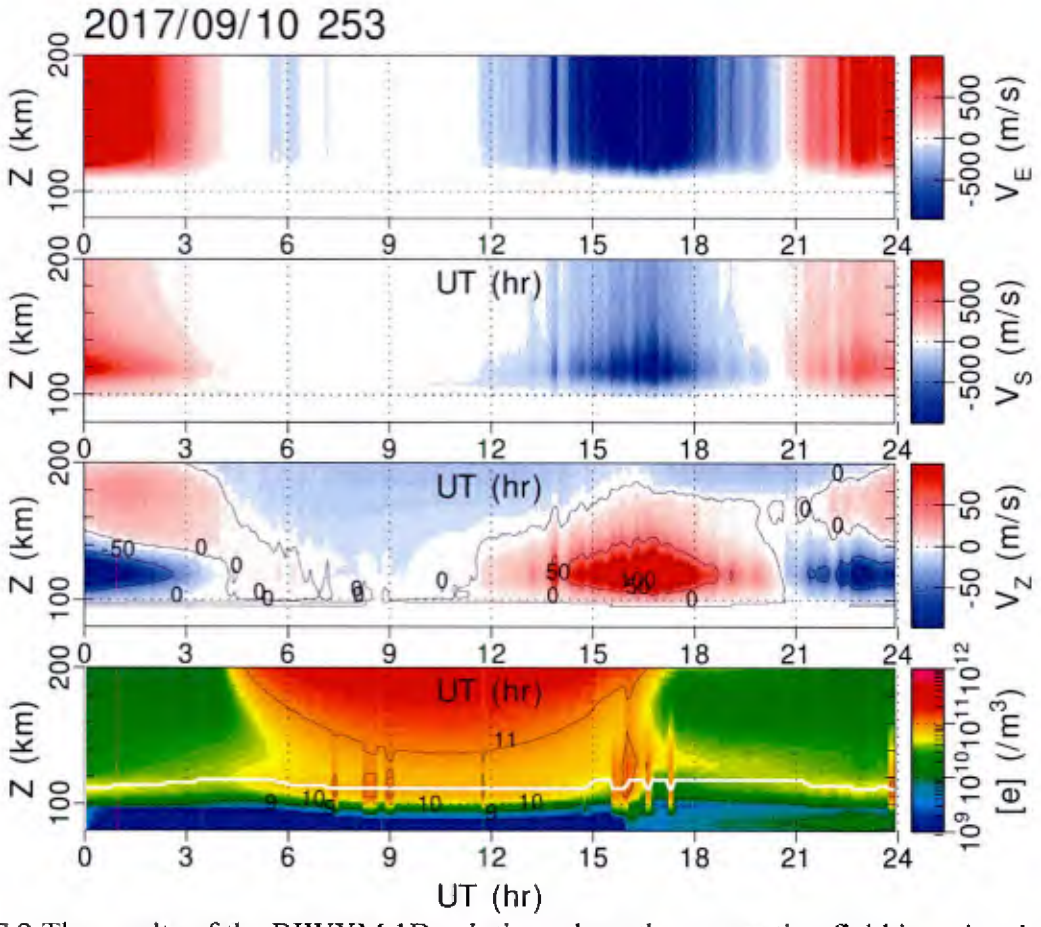

Figure 7.2 The results of the BIWXM 1D solution where the convection field is active, but the BIWXM model is not permitted to convect. The bottom panel is electron density. The three upper panels are the velocities plotted in time and altitude. The color scales on the left indicate which component is plotted: vertical (V_Z), southward (V_S), and eastward (V_E).

8 BIWXM 3D Solution

The time creating the physics within the BIWXM model to accommodate multiple ionization sources of the aurora, SPEs, solar EUV, solar X-ray, and convection and a stable numerical method to accommodate the full range of altitudes for a multi-species ionosphere cause the development of the 3D BIWXM model to be delayed to the end of the BSION effort. This work was done to provide for a 3D solution of the northern and southern latitudes above +/-30° magnetic latitude. The equatorial BIWXM was developed early, but the direction of the development proved to be a stillborn effort. We redirected toward a robust mid and high latitude 3D model instead. The current 3D ionosphere results can be run at a requested resolution and is probably valid down to 20 kilometers horizontally. The current resolution in the E region in altitude is 1 km, but the altitude resolution is a user selected option. Horizontal features down to 1 km are still within the physics of the model, but it would require a different method of generating the 3D ionosphere region. The current method is delightfully parallel and scales with the number of trajectories used.

Under the BSION contract a BIWXM_TR program was created to run the 1D BIWXM many times using a selected number of CPUs available for the calculation. The BIWXM_TR steps through all trajectories in time to produce ionospheric description above 40° magnetic latitude. A 1.0° resolution is currently aimed for but one run with 25,433 trajectories produced a 0.5° resolution result. In this 3D model, the convecting trajectories do clump or evacuate some regions. The convection subroutine is very accurate, so the clumping/evacuation is not too troubling after a 24-hour run. To avoid empty regions, a second program, TR_TO_XY, examines the distribution of trajectories every hour of model time and removes a few trajectories in regions of clumping and creates new trajectories in rarified regions by averaging nearby trajectories around the rarified region. The 3D BIWXM_TR programs generates a mid and high latitude ionosphere representation that is an irregular pattern of trajectories. This part of the 3D ionosphere model was completed under this BSION effort. An AFRL contract provided an opportunity to create the TR_TO_XY program, which performs the 'unclumping' task mentioned above , but it also generates a regular grid of the ionosphere at the resolution of the trajectory run for every timestep of BIWXM output (Figure 8.1). The full BIWXM model for 1D and 3D solutions and 3D regular gridded solutions is made available to ONR with full government rights.

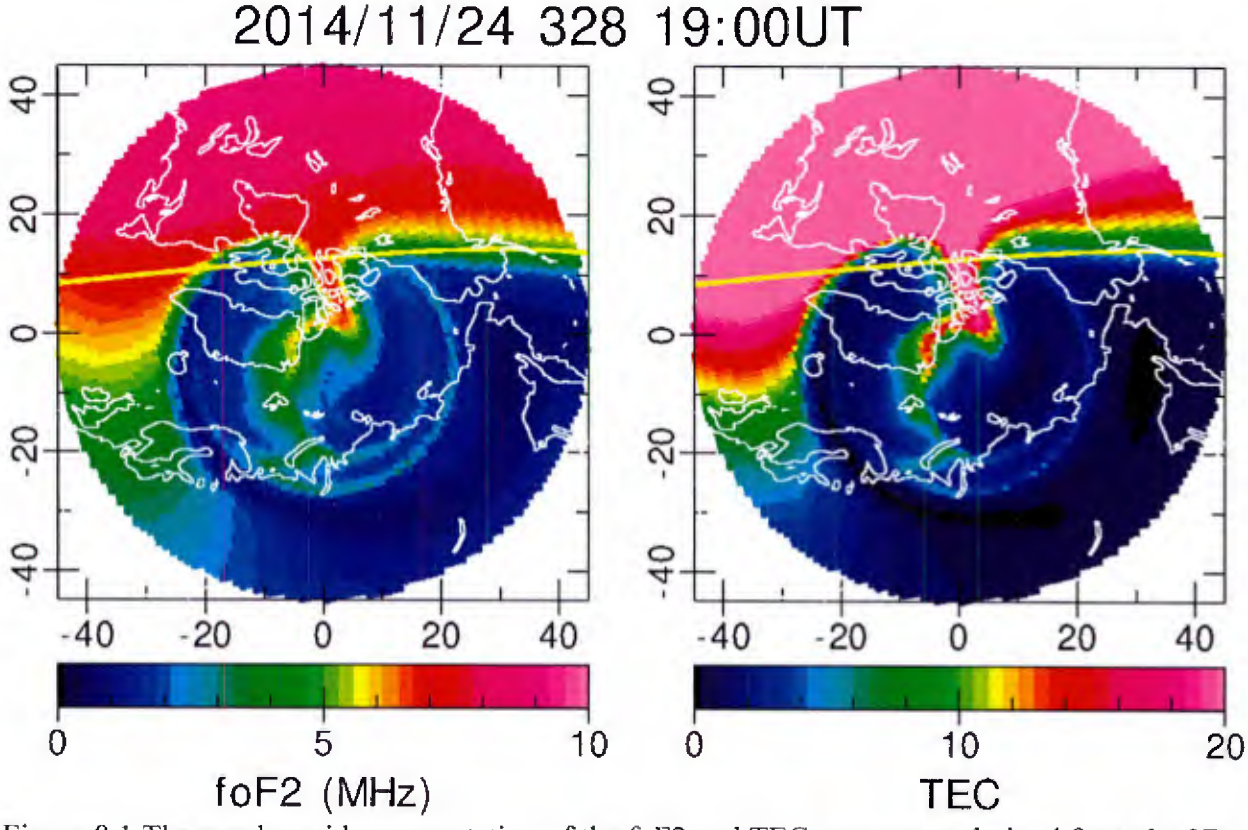

Figure 8.1 The regular grid representation of the foF2 and TEC parameters derived from the 3D ionosphere produced by BIWXM. The presentation is in magnetic solar time with noon at the top of the graph.

9 References

Anderson, G.P., S. A. Clough, F. X. Kneizys, J. H. Chetwynd, and E. P. Shettle (1986), AFGL Atmospheric Constituent Profiles (0-120km), AFGL-TR-86-0110, Air Force Geophysical Laboratory, Hanscom AFB, MA.

Baggaley, W. J. (1975), The excitation of the oxygen metastable OI(1S) state in meteors

Baulch, D., R. Cox, P. Crutzen, R. Hampson, J. Kerr, J. Troe, R. J. Watson (1982), Phys. Chem. Ref. Data, 11, 327.

Banks, P., and G. Kockart (1973), Aeronomy Parts A and B, Academic Press.

Boris, J. P., and D. L. Book (1971), Flux-corrected transport. I. SHASTA, A fluid transport algorithm that works, J. Comp. Phys., 11, 38-69.

Böhringer H., F. Arnold (1982), Temperature dependence of three-body associative reactions from 45 to 400 K. The reactions N2+ + 2N2 ---> N4+ + N2 and O2+ + 2O2 ---> O4+ + O2, J. Chem. Phys., 77, 5534-5541.

Böhringer H, Durup-Ferguson M, Ferguson EE, Fahey DW (1983) Collisional relaxation of vibrationally excited O2+ ions. J Chem Phys 79(9):4201,Äi4213

Cai, X., Yuan, T., & Eccles, J. V. (2017). A numerical investigation on tidal and gravity wave contributions to the summertime Na variations in the midlatitude E region. *Journal of Geophysical Research: Space Physics*, 122. https://doi. org/10.1002/2016JA02376.

Cao, Y. S. and R. Johnsen (1991), Recombination of N4+ ions with electrons, J. Chem. Phys., 95(10), 7356-7359.

Cohen, N., K. J. Westerberg (1983), Phys. Chem. Ref. Data, 12, 531.

Dheandhanoo, S., R. Johnsen (1983) Laboratory measurements of the association rate coefficients of NO+, O2+, N+, and N2+ ion with N2 and CO2 at temperatures between 100 K and 400 K. Plan. Space Sci., 31, 933-938.

Duleancy, J. L., M. A. Biondi, R. Johnsen (1988), Electron-temperature dependence of the recombination of electrons with O4+ ions, Phys. Rev. A., 37(7), 2539-2542.

Eccles, J. V. (2004). Eccles, J. V., The effect of gravity and pressure in the electrodynamics of the low-latitude ionosphere, J Geophys. Res., 109, A05304, doi:10.1029/2003JA010023.

Eliasson, B., U. Kogelschatz (1986), Basic Data for Modeling of Electrical Discharges in Gases: Oxygen, Asea Brown Boveri, Baden, Switzerland.

Eyet, N. et al (2011) The importance of NO+(H2O)4 in the conversion of NO+(H2O)N to H2O+(H2O)n: I. Kinetics measurements and statistical rate modeling, J. Phys. Chem. A 115, 7582-7590.

Fehsenfeld FC, Ferguson EE (1972) Thermal energy reaction rate constants for H and CO with O and NO. J Chem Phys 56(3), 3066-3070.

Ferguson EE, Bohme DK, Fehsenfeld FC, Dunkin DB (1969) Temperature dependence of slow ion-atom interchange reactions. J Chem Phys 50(11):5039,Äi5040

Gallagher, J., E. Beaty, J. Dutton, L. J. Pitchford (1983), Phys. Chem. Ref. Data, 12, 109.

Gledhill, J. A. (1986) The effective recombination coefficient of electrons in the ionosphere between 50 and 150 km, Radio Sci., 3, p399-408.

Haerendel, G., J. V. Eccles, and S. Cakir (1992), Theory for modeling the equatorial evening ionosphere and the origin of the shear in the horizontal plasma flow, *J. Geophys. Res.*, 97, 1209.

Hampson, R. F., D. Garvin (1978), Reaction Rate and Photochemical Data for Atmospheric Chemistry, NBS Special Publication 513; U.S. Government Printing Office, Washington, DC.

Heaps, M. G. (1978) Parameterization of the cosmic ray ion-pair production rate above 18 km, Planet. Space Sci, 26, pp. 513-517.

Heicklen, J. (1976), Atmospheric Chemistry, Academic Press, New York.

Henry, R. J. W. (1970), Photoionization cross-sections for atoms and ions of carbon, nitrogen, oxygen, and neon, Astrophys J., 161, 1153-1155.

Hunton, D. M., M. B. McElroy (1966), Quenching of metastable states of atomic and molecular oxygen and nitrogen, Rev. Geophys., 4, 303-328.

Kopp E (1997) On the abundance of metal ions in the lower ionosphere. J Geophys Res 102(5):9667,Äi9674

Matthes, K., Funke, B., Anderson, M. E., Barnard, L., Beer, J., Charbonneau, P., Clilverd, M. A., Dudok de Wit, T., Haberreiter, M., Hendry, A., Jackman, C. H., Kretschmar, M., Kruschke, T., Kunze, M., Langematz, U., Marsh, D. R., Maycock, A., Misios, S., Rodger, C. J., Scaife, A. A., Seppälä, A., Shangguan, M., Sinnhuber, M., Tourpali, K., Usoskin, I., van de Kamp, M., Verronen, P. T., and S. Versick, 2017: Solar Forcing for CMIP6 (v3.2). Geosci. Model Dev., 10, doi:10.5194/gmd-10-2247-2017.

McFarland, M., D. L. Albritton, F. C. Fehsenfeld, E. E. Ferguson, A. L. Schmeltekopf (1973) Flow-drift technique for ion mobility and ion-molecule reaction rate constant measurements. II. Positive ion reactions of N+, O+, and H2+ with O2 and O+ with N2 from thermal to ~2 eV. J. Chem. Phys., 59, 6620-6628.

McFarland, M., D. L. Albritton, F. C. Fehsenfeld, E. E. Ferguson, A. L. Schmeltekopf (1977) Energy dependence and branching ratio of the N2+ + O reaction, J. Geophys. Res., 79, 2925-2926.

Midey AJ, A. A. Viggiano (1999) Rate constants for the reaction of O2+ with NO from 300 to 1400 K. J Chem Phys 110(22):10746-10748.

Midey AJ, I. Dotan, A. A. Viggiano (2004) Reactions of N+, N2+, and N3+ with NO from 300 to 1400 K, J. Chem. Phys., 112, 3040-3045, doi:10.1021jp710539s.

Neau, A., A. Al Khalili, et al. (2000), Dissociative recombination of D3O+ and H3O+: absolute cross sections and branching ratios, J. Chem. Phys., 113(5), 1762-1770.

O'Keefe, A., G. Mauclaire, D. Parent, M. T. Bowers (1986), Product energy disposal in the reaction of N+(3P) and O2(3S), J. Chem. Phys., 81, 2442-2444.

Öjekull, J., P. U. Andersson, et al. (2007), Dissociative recombination of H+(H2O)3 and D+(D2O)3 water cluster ions with electrons: cross sections and branching ratios, *J. Chem. Phys.*, 127(19) 194301, doi:10.1063/1.2803901.

Öjekull, J., P. U. Andersson, et al. (2008), Dissociative recombination of water cluster ions with free electrons: Cross sections and branching ratios, *J. Chem. Phys.*, 128(4), 044311-044311. Doi:10.1063/1.2823062.

Pavlov, A. V. (2013), Photochemistry of ions at D-region altitudes of the ionosphere: A Review, *Surv. Geophys.*, doi:10.1007/s10712-013-9253.

Picone, J. M., A. E. Hedin, D. P. Drob, and A. C. Aikin (2002) NRLMSISE-00 empirical model of the atmosphere: Statistical comparisons and scientific issues, *J. Geophys. Res., 107(A12)*, 1468, doi:10.1029/2002JA009430.

Rasmussen, C. E., R. W. Schunk, and V. B. Wickwar (1988) A photochemical equilibrium model for ionospheric conductivity, J. Geophys. Res. Space Physics, 93, 9831-9840, doi.org/10.1029/ja093ia09.

Radhakrishnan, K., and A. C. Hindmarsh (1993), Description and Use of LSODE the Livermore Solver for Ordinary Differential Equations, NASA Reference Publication 1327, Lawrence Livermore National Laboratory Report, UCRL-ID-113855.

Rees, M. H. (1989) *Physics and Chemistry of the Upper Atmosphere*, Cambridge University Press.

Richards, P. G., J. A. Fennelly, D. G. Torr (1994a), EUVAC: A solar EUV flux model for aeronomic calculations, *J. Geophys. Res., 99*, 8981-8992.

Richards, P. G., J. A. Fennelly, D. G. Torr (1994b), Correction to "EUVAC: A solar EUV flux model for aeronomic calculations", *J. Geophys. Res., 99*, 13,283.

Sabadil, H., P. Bachmann, H. Kastelewicz (1985), Beitr. Plasma Phys., 20, 283. Frimer, A. Singlet O2, Vol. I, Physical-Chemical Aspects; CRC Press: Boca Raton, FL.

Schunk, R. S., and A. Nagy (2009), Ionospheres: Physics, Plasma Physics, and Chemistry, 2nd edition, Cambridge.

Scott, G. B. I., D. S. Fairley, C. G. Freeman, M. J. McEwan, V. G. Anicich (1998), Gas-phase reactions of some positive ions with atomic and molecular nitrogen, J. Chem. Phys., 109, 9010-9014.

Seaton, M. J., and D. E. Osterbrock (1957), Relative (OII) intensities in gaseous nebulae, Astrophys. J., 125, 66-83.

Sheehan, C. H., J-P St.-Maurice (2004), Dissociative recombination of N2+, O2+, and NO+: rate coefficients for ground state and vibrationally excited ions, *J. Geophys. Res., 109*, 3302, doi:10.1029/2003JA010132.

Shemansky, D. E. (1969), J. Chem. Phys., 51, 689.

Sheehan, C. H., J-P St.-Maurice (2004), Dissociative recombination of N2, O2, and NO rate coefficients for ground state and vibrationally excited ions, J. Geophys. Res., 109, 3302, doi:10.1029/2003JA010132.

Smith WH, Bromander J, Curtis LJ, Berry HG, Buchta R (1971) Lifetime measurements and absolute oscillator strengths for some vacuum-ultraviolet transitions in O I and O II. Astrophys J, 165(5),217-221.

Smith, F. L., and C. Smith, Numerical evaluation of Chapman's grazing incidence integral Ch(χ,x), *J. Geophys. Res.*, 77, 3592, 1972.

Sojka, J. J., J. Jensen, M. David, R. W. Schunk, T. Woods, and F. Eparvier (2013), Modeling the ionospheric *E* and *F1* regions: Using SDO-EVE observations as the solar irradiance driver, *J. Geophys. Res. Space Physics, 118*, 5379–5391, doi:10.1002jgra.50480.

Sojka, J. J., J. B. Jensen, M. David, R. W. Schunk, T. Woods, F. Eparvier, M. P. Sulzer, S. A. Gonzalez, and J. V. Eccles (2014), Ionospheric model-observation comparisons: *E* layer at Arecibo Incorporation of SDO-EVE solar irradiances, *J. Geophys. Res. Space Physics, 119*, 3844–3856, doi:10.1002/2013JA019528.

Solomon, S. (2017) Global modeling of thermospheric airglow in the far ultraviolet, J. Geophys. Res. Space Physics, 122, 7834-7848, doi:10.1002/207ja024314.

Swider, W., and C. L. Foley (1978), Steady-state multi-ion disturbed D-region model, AFGL-TR-78-0155, Air Force Geophysics Laboratory, Hanscom AFB, MA.

Tachiev, G. I., C. F. Fischer (2002), Astron. Astrophys. 385, 716.

Titheridge, J. E. (1998). Temperatures in the upper ionosphere and plasmasphere, J. Geophys. Res., 103, 2261-2277.

Viggiano AA, Knighton WB, Williams S, Arnold ST, Midey AJ, Dotan I (2003) A reexamination of the temperature dependence of the reaction of N? with O2. Int J Mass Spectrom 223, 397-402.

Van Leer, B. (1979), *Towards the ultimate conservative difference scheme, second order sequel to Godunov's method, J. Com. Phys.., 32*, 101–136.

Woods, T. N., W. K. Tobiska, G. J. Rottman, and J. R. Worden (2000) Improved solar Lyman a irradiance modeling from 1947 through 1999 based on UARS observations, J. Geophys. Res., 105, 27195, doi:10.1029/2000JA000041.

Zipf, E. C. (1969), Can. J. Chem, 47, 1863.

APPENDIX A

Table A.1 Absorption cross sections for EUV wavelength bins.

```
# euv_across.txt
# euv absorption cross sections from EUVAC Richards et al. [1994] w Lyman Alpha
#
# n    is bin number
# A    is Angstrom of bin's lower bound or line
# to_A is Angstrom of bin's upper bound
# a_n1 atomic nitrogen    absorption cross section in cm-2
# a_o1 atomic oxygen      absorption cross section in cm-2
# a_n2 molecular nitrogen absorption cross section in cm-2
# a_no nitric oxide       absorption cross section in cm-2
# a_o2 molecular oxygen   absorption cross section in cm-2
# a_ar atomic argon       absorption cross section in cm-2
#
# n       A    to_A       a_n1       a_o1       a_n2       a_no       a_o2       a_ar
#-------------------------------------------------------------------------------------
  1   50.00  100.00  3.310E-19  7.300E-19  7.200E-19  7.000E-19  1.316E-18  7.200E-19
  2  100.00  150.00  9.960E-19  1.839E-18  2.261E-18  2.000E-18  3.806E-18  2.261E-18
  3  150.00  200.00  2.490E-18  3.732E-18  4.958E-18  4.000E-18  7.509E-18  4.958E-18
  4  200.00  250.00  3.946E-18  5.202E-18  8.392E-18  8.000E-18  1.090E-17  8.392E-18
  5  256.30  256.30  4.874E-18  6.050E-18  1.021E-17  1.000E-17  1.337E-17  1.021E-17
  6  284.15  284.15  5.725E-18  7.080E-18  1.090E-17  1.000E-17  1.579E-17  1.090E-17
  7  250.00  300.00  5.244E-18  6.461E-18  1.049E-17  1.000E-17  1.439E-17  1.049E-17
  8  303.31  303.31  6.399E-18  7.680E-18  1.167E-17  1.100E-17  1.680E-17  1.167E-17
  9  303.78  303.78  6.413E-18  7.700E-18  1.170E-17  1.100E-17  1.681E-17  1.170E-17
 10  300.00  350.00  7.298E-18  8.693E-18  1.386E-17  1.300E-17  1.744E-17  1.386E-17
 11  368.07  368.07  8.302E-18  9.840E-18  1.691E-17  1.600E-17  1.832E-17  1.691E-17
 12  350.00  400.00  8.150E-18  9.687E-18  1.639E-17  1.600E-17  1.812E-17  1.639E-17
 13  400.00  450.00  9.556E-18  1.150E-17  2.167E-17  2.000E-17  2.031E-17  2.167E-17
 14  465.22  465.22  1.058E-17  1.193E-17  2.316E-17  2.100E-17  2.191E-17  2.316E-17
 15  450.00  500.00  1.102E-17  1.213E-17  2.347E-17  2.300E-17  2.310E-17  2.347E-17
 16  500.00  550.00  1.150E-17  1.206E-17  2.450E-17  2.400E-17  2.461E-17  2.450E-17
 17  554.37  554.37  1.177E-17  1.259E-17  2.413E-17  2.400E-17  2.604E-17  2.413E-17
 18  584.33  584.33  1.178E-17  1.309E-17  2.240E-17  2.200E-17  2.272E-17  2.240E-17
 19  550.00  600.00  1.176E-17  1.302E-17  2.279E-17  2.200E-17  2.661E-17  2.279E-17
 20  609.76  609.76  1.180E-17  1.340E-17  2.279E-17  2.200E-17  2.807E-17  2.279E-17
 21  629.73  629.73  1.121E-17  1.340E-17  2.337E-17  2.300E-17  3.206E-17  2.337E-17
 22  600.00  650.00  1.195E-17  1.336E-17  2.334E-17  2.300E-17  2.602E-17  2.334E-17
 23  650.00  700.00  1.242E-17  1.725E-17  3.175E-17  2.100E-17  2.192E-17  3.175E-17
 24  703.36  703.36  1.326E-17  1.146E-17  2.654E-17  2.600E-17  2.744E-17  2.654E-17
 25  700.00  750.00  1.210E-17  1.074E-17  2.466E-17  2.400E-17  2.853E-17  2.466E-17
 26  765.15  765.15  1.132E-17  4.000E-18  1.205E-16  2.000E-17  2.080E-17  1.205E-16
 27  770.41  770.41  1.124E-17  3.890E-18  1.418E-17  1.400E-17  1.891E-17  1.418E-17
 28  789.36  789.36  1.096E-17  3.749E-18  1.649E-17  1.600E-17  2.667E-17  1.649E-17
 29  750.00  800.00  1.117E-17  5.091E-18  3.358E-17  2.200E-17  2.215E-17  3.358E-17
 30  800.00  850.00  1.029E-17  3.498E-18  1.699E-17  1.600E-17  1.663E-17  1.699E-17
 31  850.00  900.00  2.110E-19  4.554E-18  2.025E-17  8.000E-18  8.562E-18  2.025E-17
 32  900.00  950.00  0.000E+00  1.315E-18  9.680E-18  9.000E-18  1.282E-17  9.680E-18
 33  977.62  977.62  0.000E+00  0.000E+00  2.240E-18  2.000E-18  1.873E-17  2.240E-18
 34  950.00 1000.00  0.000E+00  0.000E+00  5.099E-17  2.100E-17  2.111E-17  5.099E-17
 35 1025.72 1025.72  0.000E+00  0.000E+00  0.000E+00  1.000E-18  1.630E-18  0.000E+00
 36 1031.91 1031.91  0.000E+00  0.000E+00  0.000E+00  1.000E-18  1.050E-18  0.000E+00
 37 1000.00 1050.00  0.000E+00  0.000E+00  0.000E+00  1.000E-18  1.346E-18  0.000E+00
 38 1214.00 1214.00  0.000E+00  0.000E+00  0.000E+00  2.560E-18  1.000E-20  0.000E+00
```

Table A.2 Ionization cross sections for EUV wavelength bins.

```
# euv_icross.txt
# euv ionization cross sections from EUVAC Richards et al. [1994] & Lyman Alpha
#
# n    is bin number
# A    is Angstrom of bin's lower bound or line
# to_A is Angstrom of bin's upper bound
# i_n1 atomic nitrogen    ionization cross section in cm-2
# i_o1 atomic oxygen      ionization cross section in cm-2
# i_n2 molecular nitrogen ionization cross section in cm-2
# i_no nitric oxide       ionization cross section in cm-2
# i_o2 molecular oxygen   ionization cross section in cm-2
# i_ar atomic argon       ionization cross section in cm-2
#
```

# n	A	to_A	i_n1	i_o1	i_n2	i_no	i_o2	i_ar
1	50.00	100.00	3.310E-19	7.300E-19	7.200E-19	7.000E-19	1.316E-18	7.200E-19
2	100.00	150.00	9.960E-19	1.839E-18	2.261E-18	2.000E-18	3.806E-18	2.261E-18
3	150.00	200.00	2.490E-18	3.732E-18	4.958E-18	4.000E-18	7.509E-18	4.958E-18
4	200.00	250.00	3.946E-18	5.202E-18	8.392E-18	8.000E-18	1.090E-17	8.392E-18
5	256.30	256.30	4.874E-18	6.050E-18	1.021E-17	1.000E-17	1.337E-17	1.021E-17
6	284.15	284.15	5.725E-18	7.080E-18	1.090E-17	1.000E-17	1.579E-17	1.090E-17
7	250.00	300.00	5.244E-18	6.461E-18	1.049E-17	1.000E-17	1.439E-17	1.049E-17
8	303.31	303.31	6.399E-18	7.680E-18	1.167E-17	1.100E-17	1.680E-17	1.167E-17
9	303.78	303.78	6.413E-18	7.700E-18	1.170E-17	1.100E-17	1.681E-17	1.170E-17
10	300.00	350.00	7.298E-18	8.693E-18	1.386E-17	1.300E-17	1.744E-17	1.386E-17
11	368.07	368.07	8.302E-18	9.840E-18	1.691E-17	1.600E-17	1.832E-17	1.691E-17
12	350.00	400.00	8.150E-18	9.687E-18	1.639E-17	1.600E-17	1.812E-17	1.639E-17
13	400.00	450.00	9.556E-18	1.150E-17	2.167E-17	2.000E-17	2.031E-17	2.167E-17
14	465.22	465.22	1.058E-17	1.193E-17	2.316E-17	2.100E-17	2.191E-17	2.316E-17
15	450.00	500.00	1.102E-17	1.213E-17	2.347E-17	2.300E-17	2.310E-17	2.347E-17
16	500.00	550.00	1.150E-17	1.206E-17	2.450E-17	2.400E-17	2.461E-17	2.450E-17
17	554.37	554.37	1.177E-17	1.259E-17	2.413E-17	2.400E-17	2.604E-17	2.413E-17
18	584.33	584.33	1.178E-17	1.309E-17	2.240E-17	2.200E-17	2.272E-17	2.240E-17
19	550.00	600.00	1.176E-17	1.302E-17	2.279E-17	2.200E-17	2.661E-17	2.279E-17
20	609.76	609.76	1.180E-17	1.340E-17	2.279E-17	2.200E-17	2.639E-17	2.279E-17
21	629.73	629.73	1.121E-17	1.340E-17	2.337E-17	2.300E-17	3.110E-17	2.337E-17
22	600.00	650.00	1.195E-17	1.336E-17	2.334E-17	2.300E-17	2.494E-17	2.334E-17
23	650.00	700.00	1.242E-17	1.725E-17	2.924E-17	2.100E-17	2.131E-17	2.924E-17
24	703.36	703.36	1.326E-17	1.146E-17	2.548E-17	2.300E-17	2.375E-17	2.548E-17
25	700.00	750.00	1.210E-17	1.074E-17	1.506E-17	1.500E-17	2.380E-17	1.506E-17
26	765.15	765.15	1.132E-17	4.000E-18	6.580E-17	1.100E-17	1.172E-17	6.580E-17
27	770.41	770.41	1.124E-17	3.890E-18	8.500E-18	8.000E-18	8.470E-18	8.500E-18
28	789.36	789.36	1.096E-17	3.749E-18	8.860E-18	8.000E-18	1.019E-17	8.860E-18
29	750.00	800.00	1.117E-17	5.091E-18	1.427E-17	1.000E-17	1.060E-17	1.427E-17
30	800.00	850.00	1.029E-17	3.498E-18	0.000E+00	6.000E-18	6.413E-18	0.000E+00
31	850.00	900.00	2.110E-19	4.554E-18	0.000E+00	5.000E-18	5.494E-18	0.000E+00
32	900.00	950.00	0.000E+00	1.315E-18	0.000E+00	9.000E-18	9.374E-18	0.000E+00
33	977.62	977.62	0.000E+00	0.000E+00	0.000E+00	2.000E-18	1.554E-17	0.000E+00
34	950.00	1000.00	0.000E+00	0.000E+00	0.000E+00	1.300E-17	1.394E-17	0.000E+00
35	1025.72	1025.72	0.000E+00	0.000E+00	0.000E+00	1.000E-18	1.050E-18	0.000E+00
36	1031.91	1031.91	0.000E+00	0.000E+00	0.000E+00	5.000E-19	0.000E+00	0.000E+00
37	1000.00	1050.00	0.000E+00	0.000E+00	0.000E+00	2.000E-19	2.590E-19	0.000E+00
38	1214.00	1214.00	0.000E+00	0.000E+00	0.000E+00	2.000E-18	0.000E+00	0.000E+00

Table A.3 Atomic Branching ratios for EUV ionization in wavelength bins.

```
# euv_atomic_branch.txt
# euv ionization branching ratios from EUVAC Richard et al. [1994] & Lyman Alpha
#
# n      is bin number
# A      is Angstrom of bin's lower bound or line
# to_A   is Angstrom of bin's upper bound
# bo_4s  branching ratio from O ionization to O(4s)+
# bo_2d  branching ratio from O ionization to O(2d)+
# bo_2p  branching ratio from O ionization to O(2p)+
# bo_4p  branching ratio from O ionization to O(4p)+
# bo_2ps branching ratio from O ionization to O(2p)+*
# bo_opp branching ratio from O ionization to O++
# bo_opp branching ratio from N ionization to N+
# bo_opp branching ratio from N ionization to N++
#
```

# n	A	to_A	bo_4s	bo_2d	bo_2p	bo_4p	bo_2ps	bo_opp	bn_np	bn_npp
1	50.00	100.00	0.260	0.282	0.184	0.085	0.067	0.121	0.864	0.136
2	100.00	150.00	0.264	0.288	0.188	0.089	0.071	0.101	0.882	0.118
3	150.00	200.00	0.255	0.314	0.206	0.093	0.074	0.058	0.924	0.076
4	200.00	250.00	0.252	0.339	0.220	0.098	0.070	0.021	0.957	0.042
5	256.30	256.30	0.255	0.354	0.226	0.099	0.068	0.000	0.982	0.017
6	284.15	284.15	0.250	0.370	0.230	0.100	0.049	0.000	1.000	0.000
7	250.00	300.00	0.252	0.360	0.230	0.099	0.059	0.000	0.990	0.010
8	303.31	303.31	0.250	0.370	0.250	0.090	0.040	0.000	1.000	0.000
9	303.78	303.78	0.250	0.370	0.250	0.090	0.040	0.000	1.000	0.000
10	300.00	350.00	0.260	0.396	0.250	0.094	0.000	0.000	1.000	0.000
11	368.07	368.07	0.260	0.400	0.260	0.080	0.000	0.000	1.000	0.000
12	350.00	400.00	0.260	0.401	0.250	0.089	0.000	0.000	1.000	0.000
13	400.00	450.00	0.267	0.426	0.260	0.047	0.000	0.000	1.000	0.000
14	465.22	465.22	0.280	0.450	0.270	0.000	0.000	0.000	1.000	0.000
15	450.00	500.00	0.280	0.450	0.270	0.000	0.000	0.000	1.000	0.000
16	500.00	550.00	0.284	0.450	0.266	0.000	0.000	0.000	1.000	0.000
17	554.37	554.37	0.290	0.450	0.260	0.000	0.000	0.000	1.000	0.000
18	584.33	584.33	0.299	0.460	0.241	0.000	0.000	0.000	1.000	0.000
19	550.00	600.00	0.278	0.454	0.268	0.000	0.000	0.000	1.000	0.000
20	609.76	609.76	0.269	0.460	0.270	0.000	0.000	0.000	1.000	0.000
21	629.73	629.73	0.290	0.469	0.241	0.000	0.000	0.000	1.000	0.000
22	600.00	650.00	0.318	0.461	0.221	0.000	0.000	0.000	1.000	0.000
23	650.00	700.00	0.297	0.664	0.039	0.000	0.000	0.000	1.000	0.000
24	703.36	703.36	0.427	0.573	0.000	0.000	0.000	0.000	1.000	0.000
25	700.00	750.00	0.628	0.372	0.000	0.000	0.000	0.000	1.000	0.000
26	765.15	765.15	1.000	0.000	0.000	0.000	0.000	0.000	1.000	0.000
27	770.41	770.41	1.000	0.000	0.000	0.000	0.000	0.000	1.000	0.000
28	789.36	789.36	1.000	0.000	0.000	0.000	0.000	0.000	1.000	0.000
29	750.00	800.00	1.000	0.000	0.000	0.000	0.000	0.000	1.000	0.000
30	800.00	850.00	1.000	0.000	0.000	0.000	0.000	0.000	1.000	0.000
31	850.00	900.00	1.000	0.000	0.000	0.000	0.000	0.000	1.000	0.000
32	900.00	950.00	1.000	0.000	0.000	0.000	0.000	0.000	0.000	0.000
33	977.62	977.62	0.000	0.000	0.000	0.000	0.000	0.000	0.000	0.000
34	950.00	1000.00	0.000	0.000	0.000	0.000	0.000	0.000	0.000	0.000
35	1025.72	1025.72	0.000	0.000	0.000	0.000	0.000	0.000	0.000	0.000
36	1031.91	1031.91	0.000	0.000	0.000	0.000	0.000	0.000	0.000	0.000
37	1000.00	1050.00	0.000	0.000	0.000	0.000	0.000	0.000	0.000	0.000
38	1214.00	1214.00	0.000	0.000	0.000	0.000	0.000	0.000	0.000	0.000

Table A.3 Molecular Branching ratios for EUV ionization in wavelength bins.

```
# euv_molecular_branch.txt
# euv ionization branching ratios from EUVAC Richards et al. [1994] & Lyman Alpha
#
# n    is bin number
# A    is Angstrom of bin's lower bound or line
# to_A is Angstrom of bin's upper bound
# b_n2 branching from N2 ionization to N2+
# b_n1 branching from N2 ionization to N+
# b_o2 branching from O2 ionization to O2+
# b_o1 branching from O2 ionization to O+
# e_eff is the i-e pair production from photo e
# n       A     to_A bn2_n2p bn2_n1p bo2_o2p bo2_o1p   e_eff
#-------------------------------------------------------------
  1   50.00  100.00    0.62    0.38    1.00    0.00      3.
  2  100.00  150.00    0.65    0.35    0.62    0.38      2.
  3  150.00  200.00    0.64    0.36    0.55    0.45      1.
  4  200.00  250.00    0.62    0.38    0.61    0.39      1.
  5  256.30  256.30    0.66    0.34    0.63    0.37      1.
  6  284.15  284.15    0.74    0.26    0.63    0.37      1.
  7  250.00  300.00    0.70    0.30    0.63    0.37      1.
  8  303.31  303.31    0.79    0.21    0.65    0.35      1.
  9  303.78  303.78    0.79    0.21    0.65    0.35      1.
 10  300.00  350.00    0.84    0.16    0.70    0.30      1.
 11  368.07  368.07    0.91    0.09    0.75    0.25      1.
 12  350.00  400.00    0.89    0.11    0.74    0.26      1.
 13  400.00  450.00    0.95    0.05    0.76    0.24      1.
 14  465.22  465.22    0.95    0.05    0.77    0.23      1.
 15  450.00  500.00    0.97    0.03    0.77    0.23      1.
 16  500.00  550.00    1.00    0.00    0.79    0.21      1.
 17  554.37  554.37    1.00    0.00    0.83    0.17      1.
 18  584.33  584.33    1.00    0.00    0.83    0.17      1.
 19  550.00  600.00    1.00    0.00    0.86    0.14      1.
 20  609.76  609.76    1.00    0.00    0.93    0.07      1.
 21  629.73  629.73    1.00    0.00    0.97    0.03      1.
 22  600.00  650.00    1.00    0.00    0.96    0.04      1.
 23  650.00  700.00    1.00    0.00    0.99    0.01      1.
 24  703.36  703.36    1.00    0.00    1.00    0.00      1.
 25  700.00  750.00    1.00    0.00    1.00    0.00      1.
 26  765.15  765.15    1.00    0.00    1.00    0.00      1.
 27  770.41  770.41    1.00    0.00    1.00    0.00      1.
 28  789.36  789.36    1.00    0.00    1.00    0.00      1.
 29  750.00  800.00    1.00    0.00    1.00    0.00      1.
 30  800.00  850.00    0.00    0.00    1.00    0.00      1.
 31  850.00  900.00    0.00    0.00    1.00    0.00      1.
 32  900.00  950.00    0.00    0.00    1.00    0.00      1.
 33  977.62  977.62    0.00    0.00    1.00    0.00      1.
 34  950.00 1000.00    0.00    0.00    1.00    0.00      1.
 35 1025.72 1025.72    0.00    0.00    1.00    0.00      1.
 36 1031.91 1031.91    0.00    0.00    0.00    0.00      1.
 37 1000.00 1050.00    0.00    0.00    1.00    0.00      1.
 38 1214.00 1214.00    0.00    0.00    0.00    0.00      1.
```

Table A.4 Absorption and ionization cross sections for X-ray wavelength bins.

```
# xray_icross.txt
# xray cross sections from Banks & Kockarts and Pavlov [2013]
# Ionization and absorption cross sections are identical
# #    is bin number
# A    is Angstrom of bin's lower bound
# to_A is Angstrom of bin's upper bound
# i_o1 atomic oxygen      absorption & ionization cross section in cm-2
# i_n2 molecular nitrogen absorption & ionization cross section in cm-2
# i_no nitric oxide       absorption & ionization cross section in cm-2
# i_o2 molecular oxygen    absorption & ionization cross section in cm-2
# i_ar atomic argon       absorption & ionization cross section in cm-2
# e_eff is the i-e pair production from photo e
```

# n	A	to_A	i_o1	i_n2	i_no	i_o2	i_ar	e_eff
1	0.01	0.02	2.660E-24	2.660E-24	2.660E-24	3.030E-24	3.420E-24	17711.
2	0.02	0.05	3.690E-24	3.690E-24	3.690E-24	4.220E-24	4.770E-24	7084.
3	0.05	0.10	5.280E-24	5.280E-24	5.280E-24	6.050E-24	7.110E-24	3542.
4	0.10	0.20	6.640E-24	6.640E-24	6.640E-24	7.650E-24	1.090E-23	1771.
5	0.20	0.40	8.400E-24	8.400E-24	8.400E-24	1.010E-23	2.960E-23	885.
6	0.40	0.60	1.450E-23	1.450E-23	1.450E-23	2.030E-23	1.660E-22	590.
7	0.60	0.80	2.910E-23	2.910E-23	2.910E-23	4.590E-23	5.230E-22	442.
8	0.80	1.00	5.710E-23	5.710E-23	5.710E-23	9.510E-23	1.200E-21	354.
9	1.00	1.20	1.030E-22	1.030E-22	1.030E-22	1.760E-22	2.270E-21	295.
10	1.20	1.50	1.710E-22	1.710E-22	1.710E-22	2.950E-22	3.830E-21	236.
11	1.50	2.00	3.230E-22	3.230E-22	3.230E-22	5.630E-22	7.180E-21	177.
12	2.00	2.50	7.470E-22	7.470E-22	7.470E-22	1.310E-21	1.590E-20	141.
13	2.50	3.00	1.440E-21	1.440E-21	1.440E-21	2.570E-21	2.900E-20	118.
14	3.00	4.00	2.460E-21	2.460E-21	2.460E-21	4.290E-21	4.670E-20	88.
15	4.00	5.00	5.730E-21	5.730E-21	5.730E-21	9.930E-21	1.100E-20	70.
16	5.00	6.00	1.100E-20	1.100E-20	1.100E-20	1.900E-20	1.930E-20	59.
17	6.00	8.00	1.870E-20	1.870E-20	1.870E-20	3.200E-20	3.090E-20	44.
18	8.00	10.00	4.270E-20	4.270E-20	4.270E-20	7.220E-20	6.230E-20	35.
19	10.00	12.00	8.050E-20	8.050E-20	8.050E-20	1.340E-19	1.050E-19	29.
20	12.00	15.00	1.340E-19	1.340E-19	1.340E-19	2.200E-19	1.600E-19	23.
21	15.00	20.00	2.470E-19	2.470E-19	2.470E-19	3.940E-19	3.000E-19	17.
22	20.00	25.00	5.260E-19	5.260E-19	5.260E-19	7.950E-19	6.160E-19	14.
23	23.30	23.30	7.400E-19	7.400E-19	7.400E-19	1.300E-18	8.000E-19	15.
24	23.31	23.31	7.400E-19	7.400E-19	7.400E-19	5.600E-20	8.000E-19	15.
25	25.00	30.00	8.960E-19	8.960E-19	8.960E-19	7.000E-20	1.000E-18	11.
26	30.00	35.00	1.380E-18	1.380E-18	1.380E-18	1.120E-19	1.700E-18	10.
27	31.00	31.00	1.400E-18	1.400E-18	1.400E-18	1.210E-19	1.790E-18	11.
28	31.01	31.01	7.100E-20	7.100E-20	7.100E-20	1.210E-19	1.790E-18	11.
29	35.00	40.00	9.700E-20	9.700E-20	9.700E-20	1.640E-19	2.500E-18	8.
30	40.00	50.00	1.350E-19	1.350E-19	1.350E-19	2.290E-19	2.500E-18	7.
31	50.00	60.00	2.350E-19	2.350E-19	2.350E-19	4.000E-19	3.800E-18	5.
32	60.00	70.00	3.710E-19	3.710E-19	3.710E-19	6.310E-19	4.200E-19	5.
33	70.00	80.00	5.450E-19	5.450E-19	5.450E-19	9.280E-19	5.600E-19	4.
34	80.00	90.00	7.610E-19	7.610E-19	7.610E-19	1.300E-18	7.100E-19	3.
35	90.00	100.00	1.120E-18	1.120E-18	1.120E-18	1.740E-18	8.500E-19	3.

APPENDIX B

The most complete set of reactions for the BIWXM reaction.set file for D, E, and F region chemistry. These reaction rates are in CGS. There is an interpreter that changes the reaction rates into SI for the BIWXM model.

```
#############################################################################################
#
# if a>0 then
#      k = a * (t/300)^b * exp(-c*1000/te)
# else
#      k = -a + b*(t/300) + c*(t/300)^2 + d*(t/300)^3 + e*(t/300)^4
# endif
#
#  There is also the ability to request a subroutine rate using | symbol. The only
#  subroutine created to date is |DAY, which requests a solar angle dependence on
#  the rate.
#
######################### E & F CHEMISTRY ###########################################################
#
# i-e recombination
#
  o(2p)+ + e   ---> o              1.89d-07  -0.5  #Henry etal 1969
  n2+    + e   ---> n     + n      2.20d-07 -0.39  #Sheehan&St-Maurice 2004
  no+    + e   ---> n     + o      3.50d-07 -0.69  #Sheehan&St-Maurice 2004 (T<1200K)
# no+    + e   ---> n     + o      2.95d-07 -0.56  #Sheehan&St-Maurice 2004 (T>1200K)
(betterJVE)
  o2+    + e   ---> o     + o(1d)  1.95d-07 -0.70  #Sheehan&St-Maurice 2004 (T<1200K)
  o2+    + e   ---> o     + o(1s)  4.00d-08 -0.70  #Sheehan&St-Maurice 2004 (T<1200K)
# o2+    + e   ---> o     + o(1d)  1.75d-07 -0.61  #Sheehan&St-Maurice 2004 (T>1200K)
(betterJVE)
# o2+    + e   ---> o     + o(1s)  3.59d-08 -0.61  #Sheehan&St-Maurice 2004 (T>1200K)
(betterJVE)
#
# charge exchange
#
  o+     + o2  ---> o2+   + o    -2.01E-11 -5.53E-12 7.64E-13 -3.69E-14 6.89E-16 #Hierl etal 1997
  n+     + o2  ---> o2+   + n      1.92d-10          #Viggiano etal 2003
  n+     + o2  ---> o2+   + n(2D)  8.25d-11          #Viggiano etal 2003
  n2+    + o   ---> o+    + n2     7.00d-12 -0.23d0  #Scott etal 1998
  n2+    + o2  ---> o2+   + n2     5.00d-11  0.80d0  #Ferguson etal 1969
  o2+    + no  ---> no+   + o2     4.10d-10          #Midey&Viggiano 1999
#
# ion-neutral interchange
#
  o+  + n2 ---> no+   + n  -1.72d-12 -7.20d-13 1.33d-13 -9.28d-15 6.40d-16 #St-Maurice&Laneville
1992
  n2+   + o    ---> no+   + n       1.40d-10 -0.47    #Scott etal 1998
  n+    + o2   ---> o+    + no      2.75d-11          #Viggiano etal 2003
  o2+   + n    ---> no+   + o       1.00d-10          #Scott etal 1998
  o2+   + n    ---> no+   + o(1s)   1.00d-11          #Torr etal 1982
#
# metastable quenching
#
  o(2p)+ + o   ---> o     + o       2.00d-10          #NACE  etal 1969
  o(2p)+ + n2  ---> o     + n2      5.00d-11          #NACE  etal 1969
#
# metastable emission rate
#
  o(2p)+       ---> o     + hv      0.2188            # 4.57s  #Seaton&Osterbrock 1957
#
################### Neutral Atmosphere Chemistry ############################################
#
  o    + o   + m   ---> o2(1d) + m         4.70e-33 -2.0  0.000   #Campbell&Gray 1973
  o    + o2  + m   ---> o3     + m         1.85e-35 0.00  1.057   #Sabadil etal 1980
  o    + o3        ---> o2     + o2        1.50e-11 0.00 -2.250   #Hampson& Garvin 1978
  o3   + m         ---> o      + o2  + m   7.26e-10 0.00 -11.40   #Hampson&Garvin 1978
#
# metastable excitation
```

```
#
  n(2d)   + o2       ---> o(1d)   + no         4.80e-12                #Torr etal 1981

# o2(1d) + o2(1d)   ---> o2(1s) + o2         1.81e-19 0.00  0.700   #Cohen&Westerberg 1983
#
# metastable quenching
#
  o(1d)   + o        ---> o       + o          1.60e-13                #Hunton&McElroy 1966
  o(1d)   + n2       ---> o       + n2         2.30e-11                #Torr etal 1982
  o(1d)   + o2       ---> o       + o2         4.00e-11                #Streit etal 1976
  o(1d)   + o3       ---> o       + o3         1.00e-10                #Hunton&McElroy 1966
  o(1s)   + o        ---> o(1d)   + o          7.50e-12                #Felder&Young 1972
  o(1s)   + n2       ---> o       + n2         1.00e-17                #Hunton&McElroy 1966
# o(5s)   + n2       ---> o       + n2         1.40e-10                #Hunton&McElroy 1966

  n2(a)   + o        ---> n2      + o          5.00e-11                #Zipf 1969
  n2(a)   + o        ---> n2      + o(1d)      1.00e-13                #Baggaley 1975
  n2(a)   + o        ---> n2      + o(1s)      4.00e-11                #Sharp&Torr 1979
  n2(a)   + n2       ---> n2      + n2         3.00e-19                #Hunton&McElroy 1966
  n2(a)   + o2       ---> n2      + o2         1.00e-13                #Zipf 1969

# o2(1d) + he       ---> o2      + he         8.00e-21                #Frimer 1985
  o2(1d) + o        ---> o2      + o          1.65e-16                #Eliasson&Kogelschatz 1986
  o2(1d) + n2       ---> o2      + n2         2.00e-19                #Hunton&McElroy 1966
  o2(1d) + o2       ---> o2      + o2         5.00e-18 0.00 -0.280   #Eliasson&Kogelschatz 1986
  o2(1d) + o3       ---> o2      + o2  + o    5.00e-18 0.00 -0.280   #Gallagher etal 1983
  o2(1d) + o        ---> o2      + o(1s)      1.81e-19 0.00  0.700   #
  o2(1d) + o(1s)    ---> o2      + o          1.70e-10                #Slanger&Black 1981

# o2(1s) + he       ---> o2      + he         1.00e-17                #Frimer 1985
# o2(1s) + o        ---> o2      + o          8.00e-14                #Baulch etal 1982
# o2(1s) + o        ---> o2      + o(1s)      8.00e-14                #Baulch etal 1982
# o2(1s) + n2       ---> o2      + n2         2.00e-16                #Hunton&McElroy 1966
# o2(1s) + o2       ---> o2      + o2         1.00e-16                #Heicklen 1976
# o2(1s) + o3       ---> o2      + o2  + o    1.50e-11                #Baulch etal 1982
#
# metastable emission
#
  o(1d)             ---> o       + hv         8.77e-03   #t=114.s, 6300A       #Tachiev 2002
  o(1d)             ---> o       + hv         1.64e-03   #t=610.s, 6363A       #Baggaley 1975
  o(1s)             ---> o       + hv         4.50e-02   #t=22.0s, 2972A       #Kernahan&Pang 1975
  o(1s)             ---> o(1d)   + hv         1.06e-00   #t=0.94s, 5577A       #Kernahan&Pang 1975
# o(5s)             ---> o       + hv         1.30e+03   #t=7.7(-4)s, 1355.6A  #Baggaley 1975
# o(5s)             ---> o       + hv         4.00e+02   #t=2.5(-3)s, 1358.5A  #Baggaley 1975

  n2(a)             ---> n2      + hv         5.00e-01   #t=2.0s               #Shemansky 1996

  o2(1d)            ---> o2      + hv         3.70e-04                         #Heicklen 1976
# o2(1s)            ---> o2      + hv         1.40e-01                         #Heicklen 1976
#
########################## D Region Chemistry ######################################################
#
# photodetachment & photodissociation
#
  n4+             + hv   ---> n2+    + n2              0.49 |day
  o4+             + hv   ---> o2+    + o2              0.63 |day
  o4+             + hv   ---> o2+    + o2              0.63 |day
  no+(h2o)        + hv   ---> no+    + h2o             0.50 |day
  no+(h2o)(h)     + hv   ---> no+    + h2o + h         0.50 |day
  no+(h2o)(n2)    + hv   ---> no+    + h2o + n2        0.50 |day
  no+(h2o)(co2)   + hv   ---> no+    + h2o + co2       0.50 |day
  no+(h2o)2       + hv   ---> no+    + h2o + h2o       0.50 |day
  no+(h2o)2(n2)   + hv   ---> no+    + h2o + h2o + n2  0.50 |day
  no+(h2o)2(co2)  + hv   ---> no+    + h2o + h2o + co2 0.50 |day
  no+(h2o)3       + hv   ---> no+    + h2o + h2o + h2o 0.50 |day
  no+(n2)         + hv   ---> no+    + n2              0.50 |day
  no+(co2)        + hv   ---> no+    + co2             0.50 |day
  o2+(h2o)        + hv   ---> o2+    + h2o             0.50 |day
  h3o+(oh)        + hv   ---> h3o+   + oh              0.50 |day
  h3o+(n2)        + hv   ---> h3o+   + n2              0.50 |day
  h3o+(co2)       + hv   ---> h3o+   + co2             0.50 |day
```

```
  h+(h2o)2        + hv   ---> h3o+   + h2o              0.50 |day
  h+(h2o)3        + hv   ---> h3o+   + h2o + h2o        0.50 |day
  h+(h2o)4        + hv   ---> h3o+   + h2o + h2o + h2o  0.50 |day
  h+(h2o)2(co2)   + hv   ---> h3o+   + h2o + co2        0.50 |day
#
  co3-            + hv   ---> co2    + o-               0.40 |day
  no3-            + hv   ---> no2-   + o                0.60 |day
#
  o-              + hv   ---> o      + e                2.80 |day
  o2-             + hv   ---> o2     + e                0.46 |day
  co4-            + hv   ---> co2    + o2 + e           0.60 |day
  no2-            + hv   ---> no2    + e                0.60 |day
  no3-            + hv   ---> no     + o2 + e           0.44 |day
#
# positive ion chemistry
#
  n4+             + o2   ---> o2+           + n2 + n2  3.00e-10           #Fehsenfeld&Ferguson
1972
  n4+             + co2  ---> co2+          + n2 + n2  7.00e-10           #Smith etal 1978
  o4+             + o    ---> o2+           + o3       3.00e-10           #Fehsenfeld&Ferguson
1972
  o2+(h2o)        + h2o  ---> h3o+(oh)      + o2       1.00e-09           #Swider&Foley 1978
  o2+(h2o)        + h2o  ---> h3o+          + oh + o2  2.00e-10           #Swider&Foley 1978
  h3o+(n2)        + co2  ---> h3o+(co2)     + n2       1.00e-09           #Swider&Foley 1978
  h3o+(co2)       + h2o  ---> h+(h2o)2      + co2      1.00e-10           #Swider&Foley 1978
  h+(h2o)2(co2)   + h2o  ---> h+(h2o)3      + co2      1.00e-10           #Swider&Foley 1978
  h3o+(oh)        + h2o  ---> h+(h2o)2      + oh       1.40e-09           #Swider&Foley 1978
  no+(co2)        + h2o  ---> no+(h2o)      + co2      5.00e-10           #Swider&Foley 1978
  no+(h2o)3       + h2o  ---> h+(h2o)3      + h + no2  7.00e-11           #Swider&Foley 1978
  no+(n2)         + co2  ---> no+(co2)      + n2       2.00e-09           #Swider&Foley 1978
  no+(n2)         + n2   ---> no+           + n2 + n2  1.00e-08 -4.4 2.1  #Swider&Foley 1978
  no+(h2o)(n2)    + co2  ---> no+(h2o)(co2) + n2       2.00e-09           #Swider&Foley 1978
  no+(h2o)(co2)   + h2o  ---> no+(h2o)2     + co2      2.00e-09           #Swider&Foley 1978
  no+(h2o)2(n2)   + co2  ---> no+(h2o)2(co2)+ n2       2.00e-09           #Swider&Foley 1978
  no+(h2o)2(co2)  + h2o  ---> no+(h2o)3     + co2      2.00e-09           #Swider&Foley 1978
  h+(h2o)4        + m    ---> h+(h2o)3      + h2o + m  1.20e-01 -4.0 8.8  #Swider&Foley 1978
(error in rate?)
#
# 3-body positive ion chemistry
#
  n2+       + n2   + m   ---> n4+           + m   6.80e-29 -2.93  #Troe 2005
  o2+       + o2   + m   ---> o4+           + m   4.00e-30 -2.93  #Bohringer&Arnold 1982
  no+       + n2   + m   ---> no+(n2)       + m   3.00e-31 -4.30  #Dheandhanoo & Johnsen 1983
  no+       + co2  + m   ---> no+(co2)      + m   1.40e-29 -4.00  #Dheandhanoo & Johnsen 1983
  no+       + h2o  + m   ---> no+(h2o)      + m   1.00d-28 -2.84  #Eyet et al 2011 (O2 + N2)
  no+(h2o)  + h2o  + m   ---> no+(h2o)2     + m   1.00d-27 -4.70  #Swider & Foley 1978
  no+(h2o)2 + h2o  + m   ---> no+(h2o)3     + m   1.00d-27 -4.70  #Swider & Foley 1978
  no+(h2o)  + n2   + m   ---> no+(h2o)(n2)  + m   2.00d-31 -4.40  #Swider & Foley 1978
  no+(h2o)2 + n2   + m   ---> no+(h2o)2(n2) + m   2.00d-31 -4.40  #Swider & Foley 1978
  h3o+      + n2   + m   ---> h3o+(n2)      + m   1.40d-30 -2.00  #Swider & Foley 1978
  h3o+      + h2o  + m   ---> h+(h2o)2      + m   3.50d-27 -3.00  #Swider & Foley 1978
  h+(h2o)2  + h2o  + m   ---> h+(h2o)3      + m   2.20d-27 -3.00  #Swider & Foley 1978
  h+(h2o)3  + h2o  + m   ---> h+(h2o)4      + m   2.30d-27 -3.00  #Swider & Foley 1978
  h+(h2o)2  + co2  + m   ---> h+(h2o)2(co2) + m   3.00d-30        #Swider & Foley 1978
#
# 3-body attachment
#
  e         + o2  + n2   ---> o2-           + n2  1.00d-31           #Swider & Foley 1978
  e         + o2  + o2   ---> o2-           + o2  1.40d-29  1.0  0.6 #Swider & Foley 1978
  o-        + o2  + o2   ---> o3-           + o2  1.00e-30  1.0      #Swider & Foley 1978
  o2-       + o2  + o2   ---> o4-           + o2  2.00e-31  1.0      #Swider & Foley 1978
#
# negative ion chemistry
#
  o-        + o          ---> o2       + e          2.00d-10   #Swider & Coley 1978
  o-        + o          ---> o2       + e          2.00d-10   #Swider & Coley 1978
  o-        + o3         ---> o3-      + o          4.40d-10   #Swider & Coley 1978
  o-        + o3         ---> o2-      + o2         4.40d-10   #Swider & Coley 1978
  o2-       + o          ---> o3       + e          1.50d-10   #Swider & Coley 1978
  o2-       + o          ---> o-       + o2         1.50d-10   #Swider & Coley 1978
  o2-       + o2(1d)     ---> o2       + o2  + e    2.00d-10   #Swider & Coley 1978
```

```
  o2-       + o3          ---> o3-       + o2          5.00d-10   #Swider & Coley 1978
  o3-       + o           ---> o2-       + o2          3.20d-10   #Swider & Coley 1978
  o3-       + co2         ---> co3-      + o2          5.50d-10   #Swider & Coley 1978
  o4-       + co2         ---> co4-      + o2          4.30d-10   #Swider & Coley 1978
  co3-      + o           ---> o2-       + co2         1.10d-10   #Swider & Coley 1978
  co3-      + no          ---> no2-      + co2         1.10d-11   #Swider & Coley 1978
  co3-      + no2         ---> no3-      + co2         2.00d-10   #Swider & Coley 1978
  no2-      + o3          ---> no3-      + o2          9.00d-11   #Swider & Coley 1978
  co4-      + o3          ---> o3-       + co2 + o2    1.30d-10   #Swider & Coley 1978
  co4-      + no          ---> no3-      + co2         4.80d-11   #Swider & Coley 1978
  co4-      + o           ---> co3-      + o2          1.50d-10   #Swider & Coley 1978
#
# negative ion detachment chemistry
#
  o-        + o2(1d)      ---> o3        + e           3.00d-10   #Swider & Coley 1978
#
# i-e recombination
#
  n4+    + e          ---> n2  + n2                    2.60d-06         #Kopp 1984
  o4+    + e          ---> o2  + o2                    4.20e-06 -0.48   #Cao and Johnsen 1991
  h3o+   + e          ---> h2o + h                     7.60d-07 -0.83   #Neau etal 2000
  h3o+(oh) + e        ---> h2o + h2o                   5.00d-06         #Pavlov 2013
  h3o+(n2) + e        ---> h2o + n2 + h                5.00d-06         #Pavlov 2013
  h3o+(co2) + e       ---> h2o + co2 + h               5.00d-06         #Pavlov 2013
  h+(h2o)2 + e        ---> h2o + h2o + h               1.40d-06 -0.66   #Ojekull etal 2007
  h+(h2o)3 + e        ---> h2o + h2o + h2o + h         2.48d-06 -0.76   #Ojekull etal 2007
  h+(h2o)4 + e        ---> h2o + h2o + h2o + h2o + h   5.50d-07 -0.78   #Ojekull etal 2007
  h+(h2o)2(co2) + e   ---> h2o + h2o + co2 + h         3.20d-06         #Pavlov 2013
  co2+   + e          ---> co  + o                     2.00d-06         #Pavlov 2013
  no+(h2o) + e        ---> no  + h2o                   1.50d-06 -0.90   #Pavlov 2013
  no+(h2o)(h) + e     ---> no  + h2o + h               2.80d-06         #Pavlov 2013
  no+(h2o)(n2) + e    ---> no  + h2o + n2              5.00d-06         #Pavlov 2013
  no+(h2o)(co2) + e   ---> no  + h2o + co2             5.00d-06         #Pavlov 2013
  no+(h2o)2     + e   ---> no  + h2o + h2o             2.80d-06         #Pavlov 2013
  no+(h2o)2(n2) + e   ---> no  + h2o + h2o + n2        5.00d-06         #Pavlov 2013
  no+(h2o)2(co2) + e  ---> no  + h2o + h2o + co2       5.00d-06         #Pavlov 2013
  no+(h2o)3     + e   ---> no  + h2o + h2o + h2o       2.80d-06         #Pavlov 2013
  no+(n2)   + e       ---> no  + n2                    1.50d-06 -0.90   #Pavlov 2013
  no+(co2) + e        ---> no  + co2                   1.50d-06 -0.90   #Pavlov 2013
  o2+(h2o) + e        ---> o2  + h2o                   4.20d-06 -0.48   #Pavlov 2013
#
# i-i recombination
#
  n+             + o2- ---> n   + o2                                 6.00d-08  #Pavlov 2013
  o+             + o2- ---> o   + o2                                 6.00d-08  #Pavlov 2013
  o(2p)+         + o2- ---> o   + o2                                 6.00d-08  #Pavlov 2013
  o(2d)+         + o2- ---> o   + o2                                 6.00d-08  #Pavlov 2013
  n2+            + o2- ---> n2  + o2                                 6.00d-08  #Pavlov 2013
  no+            + o2- ---> no  + o2                                 6.00d-08  #Pavlov 2013
  o2+            + o2- ---> o2  + o2                                 6.00d-08  #Pavlov 2013
  co2+           + o2- ---> co2 + o2                                 6.00d-08  #Pavlov 2013
  n4+            + o2- ---> n2  + n2 + o2                            6.00d-08  #Pavlov 2013
  o4+            + o2- ---> o2  + o2 + o2                            6.00d-08  #Pavlov 2013
  no+(h2o)       + o2- ---> no  + h2o                    + o2        6.00d-08  #Pavlov 2013
  no+(h2o)(h)    + o2- ---> no  + h2o + h                + o2        6.00d-08  #Pavlov 2013
  no+(h2o)(n2)   + o2- ---> no  + h2o + n2               + o2        6.00d-08  #Pavlov 2013
  no+(h2o)(co2)  + o2- ---> no  + h2o + co2              + o2        6.00d-08  #Pavlov 2013
  no+(h2o)2      + o2- ---> no  + h2o + h2o              + o2        6.00d-08  #Pavlov 2013
  no+(h2o)2(n2)  + o2- ---> no  + h2o + h2o + n2         + o2        6.00d-08  #Pavlov 2013
  no+(h2o)2(co2) + o2- ---> no  + h2o + h2o + co2        + o2        6.00d-08  #Pavlov 2013
  no+(h2o)3      + o2- ---> no  + h2o + h2o + h2o        + o2        6.00d-08  #Pavlov 2013
  no+(n2)        + o2- ---> no  + n2                     + o2        6.00d-08  #Pavlov 2013
  no+(co2)       + o2- ---> no  + co2                    + o2        6.00d-08  #Pavlov 2013
  o2+(h2o)       + o2- ---> o2  + h2o                    + o2        6.00d-08  #Pavlov 2013
  h3o+           + o2- ---> h2o + h                      + o2        6.00d-08  #Pavlov 2013
  h3o+(oh)       + o2- ---> h2o + h2o                    + o2        6.00d-08  #Pavlov 2013
  h3o+(n2)       + o2- ---> h   + h2o + n2               + o2        6.00d-08  #Pavlov 2013
  h3o+(co2)      + o2- ---> h   + h2o + co2              + o2        6.00d-08  #Pavlov 2013
  h+(h2o)2       + o2- ---> h   + h2o + h2o              + o2        6.00d-08  #Pavlov 2013
  h+(h2o)3       + o2- ---> h   + h2o + h2o + h2o        + o2        6.00d-08  #Pavlov 2013
  h+(h2o)4       + o2- ---> h   + h2o + h2o + h2o + h2o  + o2        6.00d-08  #Pavlov 2013
```

```
  h+(h2o)2(co2)  + o2- ---> h   + h2o + h2o + co2          + o2  6.00d-08  #Pavlov 2013
#
  n+             + o-  ---> n   + o                              1.00d-07  #Pavlov 2013
  o+             + o-  ---> o   + o                              1.00d-07  #Pavlov 2013
  o(2p)+         + o-  ---> o   + o                              1.00d-07  #Pavlov 2013
  o(2d)+         + o-  ---> o   + o                              6.00d-08  #Pavlov 2013
  n2+            + o-  ---> n2  + o                              1.00d-07  #Pavlov 2013
  no+            + o-  ---> no  + o                              1.00d-07  #Pavlov 2013
  o2+            + o-  ---> o2  + o                              1.00d-07  #Pavlov 2013
  co2+           + o-  ---> co2 + o                              1.00d-07  #Pavlov 2013
  n4+            + o-  ---> n2  + n2 + o                         1.00d-07  #Pavlov 2013
  o4+            + o-  ---> o2  + o2 + o                         1.00d-07  #Pavlov 2013
  no+(h2o)       + o-  ---> no  + h2o                      + o   6.00d-08  #Pavlov 2013
  no+(h2o)(h)    + o-  ---> no  + h2o + h                  + o   6.00d-08  #Pavlov 2013
  no+(h2o)(n2)   + o-  ---> no  + h2o + n2                 + o   6.00d-08  #Pavlov 2013
  no+(h2o)(co2)  + o-  ---> no  + h2o + co2                + o   6.00d-08  #Pavlov 2013
  no+(h2o)2      + o-  ---> no  + h2o + h2o                + o   6.00d-08  #Pavlov 2013
  no+(h2o)2(n2)  + o-  ---> no  + h2o + h2o + n2           + o   6.00d-08  #Pavlov 2013
  no+(h2o)2(co2) + o-  ---> no  + h2o + h2o + co2          + o   6.00d-08  #Pavlov 2013
  no+(h2o)3      + o-  ---> no  + h2o + h2o + h2o          + o   6.00d-08  #Pavlov 2013
  no+(n2)        + o-  ---> no  + n2                       + o   6.00d-08  #Pavlov 2013
  no+(co2)       + o-  ---> no  + co2                      + o   6.00d-08  #Pavlov 2013
  o2+(h2o)       + o-  ---> o2  + h2o                      + o   6.00d-08  #Pavlov 2013
  h3o+           + o-  ---> h2o + h                        + o   6.00d-08  #Pavlov 2013
  h3o+(oh)       + o-  ---> h2o + h2o                      + o   6.00d-08  #Pavlov 2013
  h3o+(n2)       + o-  ---> h   + h2o + n2                 + o   6.00d-08  #Pavlov 2013
  h3o+(co2)      + o-  ---> h   + h2o + co2                + o   6.00d-08  #Pavlov 2013
  h+(h2o)2       + o-  ---> h   + h2o + h2o                + o   6.00d-08  #Pavlov 2013
  h+(h2o)3       + o-  ---> h   + h2o + h2o + h2o          + o   6.00d-08  #Pavlov 2013
  h+(h2o)4       + o-  ---> h   + h2o + h2o + h2o + h2o    + o   6.00d-08  #Pavlov 2013
  h+(h2o)2(co2)  + o-  ---> h   + h2o + h2o + co2          + o   6.00d-08  #Pavlov 2013
#
  n+             + o3- ---> n   + o3                             6.00d-08  #Pavlov 2013
  o+             + o3- ---> o   + o3                             6.00d-08  #Pavlov 2013
  o(2p)+         + o3- ---> o   + o3                             6.00d-08  #Pavlov 2013
  o(2d)+         + o3- ---> o   + o3                             6.00d-08  #Pavlov 2013
  n2+            + o3- ---> n2  + o3                             6.00d-08  #Pavlov 2013
  no+            + o3- ---> no  + o3                             6.00d-08  #Pavlov 2013
  o2+            + o3- ---> o2  + o3                             6.00d-08  #Pavlov 2013
  co2+           + o3- ---> co2 + o3                             6.00d-08  #Pavlov 2013
  n4+            + o3- ---> n2  + n2 + o3                        6.00d-08  #Pavlov 2013
  o4+            + o3- ---> o2  + o2 + o3                        6.00d-08  #Pavlov 2013
  no+(h2o)       + o3- ---> no  + h2o                      + o3  6.00d-08  #Pavlov 2013
  no+(h2o)(h)    + o3- ---> no  + h2o + h                  + o3  6.00d-08  #Pavlov 2013
  no+(h2o)(n2)   + o3- ---> no  + h2o + n2                 + o3  6.00d-08  #Pavlov 2013
  no+(h2o)(co2)  + o3- ---> no  + h2o + co2                + o3  6.00d-08  #Pavlov 2013
  no+(h2o)2      + o3- ---> no  + h2o + h2o                + o3  6.00d-08  #Pavlov 2013
  no+(h2o)2(n2)  + o3- ---> no  + h2o + h2o + n2           + o3  6.00d-08  #Pavlov 2013
  no+(h2o)2(co2) + o3- ---> no  + h2o + h2o + co2          + o3  6.00d-08  #Pavlov 2013
  no+(h2o)3      + o3- ---> no  + h2o + h2o + h2o          + o3  6.00d-08  #Pavlov 2013
  no+(n2)        + o3- ---> no  + n2                       + o3  6.00d-08  #Pavlov 2013
  no+(co2)       + o3- ---> no  + co2                      + o3  6.00d-08  #Pavlov 2013
  o2+(h2o)       + o3- ---> o2  + h2o                      + o3  6.00d-08  #Pavlov 2013
  h3o+           + o3- ---> h2o + h                        + o3  6.00d-08  #Pavlov 2013
  h3o+(oh)       + o3- ---> h2o + h2o                      + o3  6.00d-08  #Pavlov 2013
  h3o+(n2)       + o3- ---> h   + h2o + n2                 + o3  6.00d-08  #Pavlov 2013
  h3o+(co2)      + o3- ---> h   + h2o + co2                + o3  6.00d-08  #Pavlov 2013
  h+(h2o)2       + o3- ---> h   + h2o + h2o                + o3  6.00d-08  #Pavlov 2013
  h+(h2o)3       + o3- ---> h   + h2o + h2o + h2o          + o3  6.00d-08  #Pavlov 2013
  h+(h2o)4       + o3- ---> h   + h2o + h2o + h2o + h2o    + o3  6.00d-08  #Pavlov 2013
  h+(h2o)2(co2)  + o3- ---> h   + h2o + h2o + co2          + o3  6.00d-08  #Pavlov 2013
#
  n+             + o4- ---> n                              + o2 + o2   6.00d-08  #Pavlov 2013
  o+             + o4- ---> o                              + o2 + o2   6.00d-08  #Pavlov 2013
  o(2p)+         + o4- ---> o                              + o2 + o2   6.00d-08  #Pavlov 2013
  o(2d)+         + o4- ---> o                              + o2 + o2   6.00d-08  #Pavlov 2013
  n2+            + o4- ---> n2                             + o2 + o2   6.00d-08  #Pavlov 2013
  no+            + o4- ---> no                             + o2 + o2   6.00d-08  #Pavlov 2013
  o2+            + o4- ---> o2                             + o2 + o2   6.00d-08  #Pavlov 2013
  co2+           + o4- ---> co2                            + o2 + o2   6.00d-08  #Pavlov 2013
  n4+            + o4- ---> n2  + n2                       + o2 + o2   6.00d-08  #Pavlov 2013
```

```
o4+             + o4- ---> o2  + o2                    + o2 + o2   6.00d-08  #Pavlov 2013
no+(h2o)        + o4- ---> no  + h2o                   + o2 + o2   6.00d-08  #Pavlov 2013
no+(h2o)(h)     + o4- ---> no  + h2o + h               + o2 + o2   6.00d-08  #Pavlov 2013
no+(h2o)(n2)    + o4- ---> no  + h2o + n2              + o2 + o2   6.00d-08  #Pavlov 2013
no+(h2o)(co2)   + o4- ---> no  + h2o + co2             + o2 + o2   6.00d-08  #Pavlov 2013
no+(h2o)2       + o4- ---> no  + h2o + h2o             + o2 + o2   6.00d-08  #Pavlov 2013
no+(h2o)2(n2)   + o4- ---> no  + h2o + h2o + n2        + o2 + o2   6.00d-08  #Pavlov 2013
no+(h2o)2(co2)  + o4- ---> no  + h2o + h2o + co2       + o2 + o2   6.00d-08  #Pavlov 2013
no+(h2o)3       + o4- ---> no  + h2o + h2o + h2o       + o2 + o2   6.00d-08  #Pavlov 2013
no+(n2)         + o4- ---> no  + n2                    + o2 + o2   6.00d-08  #Pavlov 2013
no+(co2)        + o4- ---> no  + co2                   + o2 + o2   6.00d-08  #Pavlov 2013
o2+(h2o)        + o4- ---> o2  + h2o                   + o2 + o2   6.00d-08  #Pavlov 2013
h3o+            + o4- ---> h2o + h                     + o2 + o2   6.00d-08  #Pavlov 2013
h3o+(oh)        + o4- ---> h2o + h2o                   + o2 + o2   6.00d-08  #Pavlov 2013
h3o+(n2)        + o4- ---> h   + h2o + n2              + o2 + o2   6.00d-08  #Pavlov 2013
h3o+(co2)       + o4- ---> h   + h2o + co2             + o2 + o2   6.00d-08  #Pavlov 2013
h+(h2o)2        + o4- ---> h   + h2o + h2o             + o2 + o2   6.00d-08  #Pavlov 2013
h+(h2o)3        + o4- ---> h   + h2o + h2o + h2o       + o2 + o2   6.00d-08  #Pavlov 2013
h+(h2o)4        + o4- ---> h   + h2o + h2o + h2o + h2o + o2 + o2   6.00d-08  #Pavlov 2013
h+(h2o)2(co2)   + o4- ---> h   + h2o + h2o + co2       + o2 + o2   6.00d-08  #Pavlov 2013
#
n+              + co3- ---> n                          + co2 + o   6.00d-08  #Pavlov 2013
o+              + co3- ---> o                          + co2 + o   6.00d-08  #Pavlov 2013
o(2p)+          + co3- ---> o                          + co2 + o   6.00d-08  #Pavlov 2013
o(2d)+          + co3- ---> o                          + co2 + o   6.00d-08  #Pavlov 2013
n2+             + co3- ---> n2                         + co2 + o   6.00d-08  #Pavlov 2013
no+             + co3- ---> no                         + co2 + o   6.00d-08  #Pavlov 2013
o2+             + co3- ---> o2                         + co2 + o   6.00d-08  #Pavlov 2013
co2+            + co3- ---> co2                        + co2 + o   6.00d-08  #Pavlov 2013
n4+             + co3- ---> n2  + n2                   + co2 + o   6.00d-08  #Pavlov 2013
o4+             + co3- ---> o2  + o2                   + co2 + o   6.00d-08  #Pavlov 2013
no+(h2o)        + co3- ---> no  + h2o                  + co2 + o   6.00d-08  #Pavlov 2013
no+(h2o)(h)     + co3- ---> no  + h2o + h              + co2 + o   6.00d-08  #Pavlov 2013
no+(h2o)(n2)    + co3- ---> no  + h2o + n2             + co2 + o   6.00d-08  #Pavlov 2013
no+(h2o)(co2)   + co3- ---> no  + h2o + co2            + co2 + o   6.00d-08  #Pavlov 2013
no+(h2o)2       + co3- ---> no  + h2o + h2o            + co2 + o   6.00d-08  #Pavlov 2013
no+(h2o)2(n2)   + co3- ---> no  + h2o + h2o + n2       + co2 + o   6.00d-08  #Pavlov 2013
no+(h2o)2(co2)  + co3- ---> no  + h2o + h2o + co2      + co2 + o   6.00d-08  #Pavlov 2013
no+(h2o)3       + co3- ---> no  + h2o + h2o + h2o      + co2 + o   6.00d-08  #Pavlov 2013
no+(n2)         + co3- ---> no  + n2                   + co2 + o   6.00d-08  #Pavlov 2013
no+(co2)        + co3- ---> no  + co2                  + co2 + o   6.00d-08  #Pavlov 2013
o2+(h2o)        + co3- ---> o2  + h2o                  + co2 + o   6.00d-08  #Pavlov 2013
h3o+            + co3- ---> h2o + h                    + co2 + o   6.00d-08  #Pavlov 2013
h3o+(oh)        + co3- ---> h2o + h2o                  + co2 + o   6.00d-08  #Pavlov 2013
h3o+(n2)        + co3- ---> h   + h2o + n2             + co2 + o   6.00d-08  #Pavlov 2013
h3o+(co2)       + co3- ---> h   + h2o + co2            + co2 + o   6.00d-08  #Pavlov 2013
h+(h2o)2        + co3- ---> h   + h2o + h2o            + co2 + o   6.00d-08  #Pavlov 2013
h+(h2o)3        + co3- ---> h   + h2o + h2o + h2o      + co2 + o   6.00d-08  #Pavlov 2013
h+(h2o)4        + co3- ---> h   + h2o + h2o + h2o + h2o + co2 + o   6.00d-08  #Pavlov 2013
h+(h2o)2(co2)   + co3- ---> h   + h2o + h2o + co2      + co2 + o   6.00d-08  #Pavlov 2013
#
n+              + co4- ---> n                          + co2 + o2  6.00d-08  #Pavlov 2013
o+              + co4- ---> o                          + co2 + o2  6.00d-08  #Pavlov 2013
o(2p)+          + co4- ---> o                          + co2 + o2  6.00d-08  #Pavlov 2013
o(2d)+          + co4- ---> o                          + co2 + o2  6.00d-08  #Pavlov 2013
n2+             + co4- ---> n2                         + co2 + o2  6.00d-08  #Pavlov 2013
no+             + co4- ---> no                         + co2 + o2  6.00d-08  #Pavlov 2013
o2+             + co4- ---> o2                         + co2 + o2  6.00d-08  #Pavlov 2013
co2+            + co4- ---> co2                        + co2 + o2  6.00d-08  #Pavlov 2013
n4+             + co4- ---> n2  + n2                   + co2 + o2  6.00d-08  #Pavlov 2013
o4+             + co4- ---> o2  + o2                   + co2 + o2  6.00d-08  #Pavlov 2013
no+(h2o)        + co4- ---> no  + h2o                  + co2 + o2  6.00d-08  #Pavlov 2013
no+(h2o)(h)     + co4- ---> no  + h2o + h              + co2 + o2  6.00d-08  #Pavlov 2013
no+(h2o)(n2)    + co4- ---> no  + h2o + n2             + co2 + o2  6.00d-08  #Pavlov 2013
no+(h2o)(co2)   + co4- ---> no  + h2o + co2            + co2 + o2  6.00d-08  #Pavlov 2013
no+(h2o)2       + co4- ---> no  + h2o + h2o            + co2 + o2  6.00d-08  #Pavlov 2013
no+(h2o)2(n2)   + co4- ---> no  + h2o + h2o + n2       + co2 + o2  6.00d-08  #Pavlov 2013
no+(h2o)2(co2)  + co4- ---> no  + h2o + h2o + co2      + co2 + o2  6.00d-08  #Pavlov 2013
no+(h2o)3       + co4- ---> no  + h2o + h2o + h2o      + co2 + o2  6.00d-08  #Pavlov 2013
no+(n2)         + co4- ---> no  + n2                   + co2 + o2  6.00d-08  #Pavlov 2013
no+(co2)        + co4- ---> no  + co2                  + co2 + o2  6.00d-08  #Pavlov 2013
```

```
  o2+(h2o)       + co4- ---> o2  + h2o                    + co2 + o2  6.00d-08  #Pavlov 2013
  h3o+           + co4- ---> h2o + h                      + co2 + o2  6.00d-08  #Pavlov 2013
  h3o+(oh)       + co4- ---> h2o + h2o                    + co2 + o2  6.00d-08  #Pavlov 2013
  h3o+(n2)       + co4- ---> h   + h2o + n2               + co2 + o2  6.00d-08  #Pavlov 2013
  h3o+(co2)      + co4- ---> h   + h2o + co2              + co2 + o2  6.00d-08  #Pavlov 2013
  h+(h2o)2       + co4- ---> h   + h2o + h2o              + co2 + o2  6.00d-08  #Pavlov 2013
  h+(h2o)3       + co4- ---> h   + h2o + h2o + h2o        + co2 + o2  6.00d-08  #Pavlov 2013
  h+(h2o)4       + co4- ---> h   + h2o + h2o + h2o + h2o  + co2 + o2  6.00d-08  #Pavlov 2013
  h+(h2o)2(co2)  + co4- ---> h   + h2o + h2o + co2        + co2 + o2  6.00d-08  #Pavlov 2013
#
  n+             + no2- ---> n                            + no2       6.00d-08  #Pavlov 2013
  o+             + no2- ---> o                            + no2       6.00d-08  #Pavlov 2013
  o(2p)+         + no2- ---> o                            + no2       6.00d-08  #Pavlov 2013
  o(2d)+         + no2- ---> o                            + no2       6.00d-08  #Pavlov 2013
  n2+            + no2- ---> n2                           + no2       6.00d-08  #Pavlov 2013
  no+            + no2- ---> no                           + no2       6.00d-08  #Pavlov 2013
  o2+            + no2- ---> o2                           + no2       6.00d-08  #Pavlov 2013
  co2+           + no2- ---> co2                          + no2       6.00d-08  #Pavlov 2013
  n4+            + no2- ---> n2 + n2                      + no2       6.00d-08  #Pavlov 2013
  o4+            + no2- ---> o2 + o2                      + no2       6.00d-08  #Pavlov 2013
  no+(h2o)       + no2- ---> no  + h2o                    + no2       6.00d-08  #Pavlov 2013
  no+(h2o)(h)    + no2- ---> no  + h2o + h                + no2       6.00d-08  #Pavlov 2013
  no+(h2o)(n2)   + no2- ---> no  + h2o + n2               + no2       6.00d-08  #Pavlov 2013
  no+(h2o)(co2)  + no2- ---> no  + h2o + co2              + no2       6.00d-08  #Pavlov 2013
  no+(h2o)2      + no2- ---> no  + h2o + h2o              + no2       6.00d-08  #Pavlov 2013
  no+(h2o)2(n2)  + no2- ---> no  + h2o + h2o + n2         + no2       6.00d-08  #Pavlov 2013
  no+(h2o)2(co2) + no2- ---> no  + h2o + h2o + co2        + no2       6.00d-08  #Pavlov 2013
  no+(h2o)3      + no2- ---> no  + h2o + h2o + h2o        + no2       6.00d-08  #Pavlov 2013
  no+(n2)        + no2- ---> no  + n2                     + no2       6.00d-08  #Pavlov 2013
  no+(co2)       + no2- ---> no  + co2                    + no2       6.00d-08  #Pavlov 2013
  o2+(h2o)       + no2- ---> o2  + h2o                    + no2       6.00d-08  #Pavlov 2013
  h3o+           + no2- ---> h2o + h                      + no2       6.00d-08  #Pavlov 2013
  h3o+(oh)       + no2- ---> h2o + h2o                    + no2       6.00d-08  #Pavlov 2013
  h3o+(n2)       + no2- ---> h   + h2o + n2               + no2       6.00d-08  #Pavlov 2013
  h3o+(co2)      + no2- ---> h   + h2o + co2              + no2       6.00d-08  #Pavlov 2013
  h+(h2o)2       + no2- ---> h   + h2o + h2o              + no2       6.00d-08  #Pavlov 2013
  h+(h2o)3       + no2- ---> h   + h2o + h2o + h2o        + no2       6.00d-08  #Pavlov 2013
  h+(h2o)4       + no2- ---> h   + h2o + h2o + h2o + h2o  + no2       6.00d-08  #Pavlov 2013
  h+(h2o)2(co2)  + no2- ---> h   + h2o + h2o + co2        + no2       6.00d-08  #Pavlov 2013
#
  n+             + no3- ---> n                            + no2 + o   6.00d-08  #Pavlov 2013
  o+             + no3- ---> o                            + no2 + o   6.00d-08  #Pavlov 2013
  o(2p)+         + no3- ---> o                            + no2 + o   6.00d-08  #Pavlov 2013
  o(2d)+         + no3- ---> o                            + no2 + o   6.00d-08  #Pavlov 2013
  n2+            + no3- ---> n2                           + no2 + o   6.00d-08  #Pavlov 2013
  no+            + no3- ---> no                           + no2 + o   6.00d-08  #Pavlov 2013
  o2+            + no3- ---> o2                           + no2 + o   6.00d-08  #Pavlov 2013
  co2+           + no3- ---> co2                          + no2 + o   6.00d-08  #Pavlov 2013
  n4+            + no3- ---> n2  + n2                     + no2 + o   6.00d-08  #Pavlov 2013
  o4+            + no3- ---> o2  + o2                     + no2 + o   6.00d-08  #Pavlov 2013
  no+(h2o)       + no3- ---> no  + h2o                    + no2 + o   6.00d-08  #Pavlov 2013
  no+(h2o)(h)    + no3- ---> no  + h2o + h                + no2 + o   6.00d-08  #Pavlov 2013
  no+(h2o)(n2)   + no3- ---> no  + h2o + n2               + no2 + o   6.00d-08  #Pavlov 2013
  no+(h2o)(co2)  + no3- ---> no  + h2o + co2              + no2 + o   6.00d-08  #Pavlov 2013
  no+(h2o)2      + no3- ---> no  + h2o + h2o              + no2 + o   6.00d-08  #Pavlov 2013
  no+(h2o)2(n2)  + no3- ---> no  + h2o + h2o + n2         + no2 + o   6.00d-08  #Pavlov 2013
  no+(h2o)2(co2) + no3- ---> no  + h2o + h2o + co2        + no2 + o   6.00d-08  #Pavlov 2013
  no+(h2o)3      + no3- ---> no  + h2o + h2o + h2o        + no2 + o   6.00d-08  #Pavlov 2013
  no+(n2)        + no3- ---> no  + n2                     + no2 + o   6.00d-08  #Pavlov 2013
  no+(co2)       + no3- ---> no  + co2                    + no2 + o   6.00d-08  #Pavlov 2013
  o2+(h2o)       + no3- ---> o2  + h2o                    + no2 + o   6.00d-08  #Pavlov 2013
  h3o+           + no3- ---> h2o + h                      + no2 + o   6.00d-08  #Pavlov 2013
  h3o+(oh)       + no3- ---> h2o + h2o                    + no2 + o   6.00d-08  #Pavlov 2013
  h3o+(n2)       + no3- ---> h   + h2o + n2               + no2 + o   6.00d-08  #Pavlov 2013
  h3o+(co2)      + no3- ---> h   + h2o + co2              + no2 + o   6.00d-08  #Pavlov 2013
  h+(h2o)2       + no3- ---> h   + h2o + h2o              + no2 + o   6.00d-08  #Pavlov 2013
  h+(h2o)3       + no3- ---> h   + h2o + h2o + h2o        + no2 + o   6.00d-08  #Pavlov 2013
  h+(h2o)4       + no3- ---> h   + h2o + h2o + h2o + h2o  + no2 + o   6.00d-08  #Pavlov 2013
  h+(h2o)2(co2)  + no3- ---> h   + h2o + h2o + co2        + no2 + o   6.00d-08  #Pavlov 2013
#
$  END OF REACTIONS
```

```
#
######################### REFERENCE LIST ##############################################################
#
# Anderson, G.P., S. A. Clough, F. X. Kneizys, J. H. Chetwynd, and E. P. Shettle (1986), AFGL
Atmospheric Constituent Profiles (0-120km), AFGL-TR-86-0110, Air Force Geophysical Laboratory,
Hanscom AFB, MA.
#
# Baggaley, W. J. (1975), The excitation of the oxygen metastable OI(1S) state in meteors
#
# Baulch, D., R. Cox, P. Crutzen, R. Hampson, J. Kerr, J. Troe, R. J. Watson (1982), Phys. Chem.
Ref. Data, 11, 327.
#
# Bo¬®hringer H., F. Arnold (1982), Temperature dependence of three-body associative reactions
from 45 to 400 K. The reactions N2+ + 2N2 ---> N4+ + N2 and O2+ + 2O2 ---> O4+ + O2, J. Chem.
Phys., 77, 5534-5541.
#
# Bo¬®hringer H, Durup-Ferguson M, Ferguson EE, Fahey DW (1983) Collisional relaxation of
vibrationally excited O2 ? ions. J Chem Phys 79(9):4201,Äi4213
#
# Cao, Y. S. and R. Johnsen (1991), Recombination of N4,Äù ions with electrons, J. Chem. Phys.,
95(10), 7356-7359.
#
# Cohen, N., K. J. Westerberg (1983), Phys. Chem. Ref. Data, 12, 531.
#
#  Dheandhanoo, S., R. Johnsen (1983) Laboratory measurements of the association rate
coefficients of NO+, O2+, N+, and N2+ ion with N2 and CO2 at temperatures between 100 K and 400
K. Plan. Space Sci., 31, 933-938.
#
# Duleancy, J. L., M. A. Biondi, R. Johnsen (1988), Electron-temperature dependence of the
recombination of electrons with O4+ ions, Phys. Rev. A., 37(7), 2539-2542.
#
# Eliasson, B., U. Kogelschatz (1986), Basic Data for Modeling of Electrical Discharges in Gases:
Oxygen, Asea Brown Boveri, Baden, Switzerland.
#
# Eyet, N. et al (2011) The importance of NO+(H2O)4 in the conversion of NO+(H2O)N to H2O+(H2O)n:
I. Kinetics measurements and statistical rate modeling, J. Phys. Chem. A 115, 7582-7590.
#
# Fehsenfeld FC, Ferguson EE (1972) Thermal energy reaction rate constants for H? and CO? with O
and NO. J Chem Phys 56(3):3066,Äi3070
#
# Fehsenfeld FC, Ferguson EE (1972) Thermal energy reaction rate constants for H? and CO? with O
and NO. J Chem Phys 56(3):3066,Äi3070
#
# Ferguson EE, Bohme DK, Fehsenfeld FC, Dunkin DB (1969) Temperature dependence of slow ion-atom
interchange reactions. J Chem Phys 50(11):5039,Äi5040
#
# Gallagher, J., E. Beaty, J. Dutton, L. J. Pitchford (1983), Phys. Chem. Ref. Data, 12, 109.
#
# Hampson, R. F., D. Garvin (1978), Reaction Rate and Photochemical Data for Atmospheric
Chemistry, NBS Special Publication 513; U.S. Government Printing Office, Washington, DC.
#
# Heicklen, J. (1976), Atmospheric Chemistry, Academic Press, New York.
#
# Henry, R. J. W. (1970), Photoionization cross-sections for atoms and ions of carbon, nitrogen,
oxygen, and neon, Astrophys J., 161, 1153-1155.
#
# Hunton, D. M., M. B. McElroy (1966), Quenching of metastable states of atomic and molecular
oxygen and nitrogen, Rev. Geophys., 4, 303-328.
#
# Kopp E (1997) On the abundance of metal ions in the lower ionosphere. J Geophys Res
102(5):9667,Äi9674
#
# McFarland, M., D. L. Albritton, F. C. Fehsenfeld, E. E. Ferguson, A. L. Schmeltekopf (1973)
Flow-drift technique for ion mobility and ion-molecule reaction rate constant measurements. II.
Positive ion reactions of N+, O+, and H2+ with O2 and O+ with N2 form thermal to ~2 eV. J. Chem.
Phys., 59, 6620-6628.
#
# McFarland, M., D. L. Albritton, F. C. Fehsenfeld, E. E. Ferguson, A. L. Schmeltekopf (1977)
Energy dependence and branching ratio of the N2+ + O reaction, J. Geophys. Res., 79, 2925-2926.
#
```

Midey AJ, A. A. Viggiano (1999) Rate constants for the reaction of O2+ with NO from 300 to 1400 K. J Chem Phys 110(22):10746,Ä¡10748.
#
Midey AJ, I. Dotan, A. A. Viggiano (2004) Reactions of N+, N2+, and N3+ with NO from 300 to 1400 K, J. Chem. Phys., 112, 3040-3045, doi:10.1021/jp710539s.
#
Neau, A., A. Al Khalili, et al. (2000), Dissociative recombination of D3O+ and H3O+: absolute cross sections and branching ratios, J. Chem. Phys., 113(5), 1762-1770.
#
O'Keefe, A., G. Mauclaire, D. Parent, M. T. Bowers (1986), Product energy disposal in the reaction of N+(3P) and O2(3S), J. Chem. Phys., 81, 2442-2444.
#
Ojekull, J., P. U. Andersson, et al. (2007), Dissociative recombination of H+(H2O)3 and D+(D2O)3 water cluster ions with electrons: cross sections and branching ratios, J. Chem. Phys., 127(19) 194301, doi:10.1063/1.2803901.
#
Ojekull, J., P. U. Andersson, et al. (2008), Dissociative recombination of water cluster ions with free electrons: Cross sections and branching ratios, J. Chem. Phys., 128(4), 044311-044311. Doi:10.1063/1.2823062.
#
Pavlov, A. V. (2013), Photochemistry of ions at D-region altitudes of the ionosphere: A Review, Surv. Geophys., doi:10.1007/s10712-013-9253.
#
Picone, J. M.,¬†A. E. Hedin, D. P. Drob, and¬†A. C. Aikin, NRLMSISE-00 empirical model of the atmosphere: Statistical comparisons and scientific issues, J. Geophys. Res., 107(A12), 1468, doi:10.1029/2002JA009430, 2002.
#
Richards, P. G., J. A. Fennelly, D. G. Torr (1994a), EUVAC: A solar EUV flux model for aeronomic calculations, J. Geophys. Res., 99, 8981-8992.
#
Richards, P. G., J. A. Fennelly, D. G. Torr (1994b), Correction to ,ÄúEUVAC: A solar EUV flux model for aeronomic calculations,Äù, J. Geophys. Res., 99, 13,283.
#
Sabadil, H., P. Bachmann, H. Kastelewicz (1985), Beitr. Plasmaphys., 20, 283. Frimer, A. Singlet O2, Vol. I, Physical-Chemical Aspects; CRC Press: Boca Raton, FL.
#
Scott, G. B. I., D. S. Fairley, C. G. Freeman, M. J. McEwan, V. G. Anicich (1998), Gas-phase reactions of some positive ions with atomic and molecular nitrogen, J. Chem. Phys., 109, 9010-9014.
#
Seaton, M. J., and D. E. Osterbrock (1957), Relative (OII) intensities in gaseous nebulae, Astrophys. J., 125, 66-83.
#
Shemansky, D. E. (1969), J. Chem. Phys., 51, 689.
#
Sheehan, C. H., J-P St.-Maurice (2004), Dissociative recombination of N2,Äù, O2,Äù, and NO,Äù: rate coefficients for ground state and vibrationally excited ions, J. Geophys. Res., 109, 3302, doi:10.1029/2003JA010132.
#
Smith WH, Bromander J, Curtis LJ, Berry HG, Buchta R (1971) Lifetime measurements and absolute oscillator strengths for some vacuum-ultraviolet transitions in O I and O II. Astrophys J 165(5), 217-221
#
Sojka, J. J., J. Jensen, M. David, R. W. Schunk, T. Woods, and F. Eparvier (2013), Modeling the ionospheric E and F1 regions: Using SDO-EVE observations as the solar irradiance driver, J. Geophys. Res. Space Physics, 118, 5371-5391, doi:10.1002/jgra.50480.
#
Sojka, J. J., J. B. Jensen, M. David, R. W. Schunk, T. Woods, F. Eparvier, M. P. Sulzer, S. A. Gonzalez, and J. V. Eccles (2014), Ionospheric model-observation comparisons: E layer at Arecibo incorporation of SDO-EVE solar irradiances, J. Geophys. Res. Space Physics, 119, 3844-3856, doi:10.1002/2013JA019528.
#
Streit,
#
Swider, W., and C. L. Foley (1978), Steady-state multi-ion disturbed D-region model, AFGL-TR-78-0155, Air Force Geophysics Laboratory, Hanscom AFB, MA.
#
Tachiev, G. I., C. F. Fischer (2002), Astron. Astrophys. 385, 716.
#
Torr,
#

```
# Viggiano AA, Knighton WB, Williams S, Arnold ST, Midey AJ, Dotan I (2003)A reexamination of the
temperature dependence of the reaction of N+ with O2. Int J Mass Spectrom 223-224:397-402
#
# Zipf, E. C. (1969), Can. J. Chem, 47, 1863.
#
##########################################################################################################
```

Bottomside Ionosphere with Winds, X-rays, and Metals

Version 2.0

User's Guide

October 10, 2020

(This page is intentionally blank)

(This page is intentionally blank)

Table of Contents

1 Version Guide for BIWXM

Version Table for BIWXM User's Guide

Version	Date	Person	Changes
V0.1	October 2018	James Vincent Eccles	Initial Document named V0.1. Chemistry solver solution for D region altitudes with EUV and X-ray ionization.
V0.9	October 2019	James Vincent Eccles	Transport additions to solve for D, E, F regions and topside.
V1.0	October 2020	James Vincent Eccles and Jan J. Sojka	Updates to solar spectrum, addition of particle ionization, ExB convection, and 3D ionosphere solution for mid and high latitudes.
V2.0	December 2020	James Vincent Eccles	Finished complete debug and testing of BIWXM_3D ability for polar region.

2 Bottomside Ionosphere with Winds, X-rays, Metals

2.1 BIWXM Introduction

The *Bottomside Ionosphere with Winds, X-rays, Metals* (BIWXM) model ionosphere solves for ionosphere electron density and ion constituent densities, velocities and temperatures. The BIWXM is a physics-based model was developed by Primarily by James Vincent Eccles, a scientist at Space Environment Corporation to provide a bottomside ionosphere profile with features observed in the real ionosphere for use primarily within radio propagation models. The BIWXM results are suitable for high frequency (HF) radio wave (3-30 MHz) ray-tracing codes and Very Low Frequency (VLF) radio propagation codes (3-30 kHz). The Winds, X-rays, and Metals descriptor of the model indicates that the model is designed to reflect bottom side structures generated by strong gradients in the horizontal neutral winds, by solar X-ray flares in the D region, and by dense metal ion layers if the physical drivers are accurately prescribed to reflect space weather variations of the thermosphere, solar spectrum, and energetic particle precipitation. The ionosphere solution is aimed at the altitude range of 50 to 500 km, but the solution range is 30 to 3000 km. The lower altitudes are required for severe X-ray events and the higher altitudes are required to properly solve for the F region peak altitudes. The full altitude range solves the chemistry and transport of all ion species or it can be accelerated by choice to solve for the chemically produced profiles without transport for D region species or very minor ion species of the E and F1 region (N_2^+ for example)

The Bottomside Ionosphere with Winds, X-rays, Metals model is mostly a new model from beginning to end, but some features of the core codes are based on Data-Driven D-Region model (DDDR) created by James Vincent Eccles as the physics-based solution of the D region for calculating HF non-deviative absorption. The DDDR is the physics-based code within the ABBYNORMAL OR ***AB****sorption* ***BY*** *the D and E Region of HF Signals with* ***NORMAL*** *Incidence* [Eccles et al., 2005]. This Version 2.0 of the Bottomside Ionosphere with Winds, X-rays, Metals can generate a 3D ionosphere description for mid and high latitudes and is designed to run in on a multi-CPU machine to generate electron densities for the geo-longitude and geo-latitude nodes above 30 degrees geomagnetic latitude. It can be used for the southern hemisphere as well. The BIWXM1D code solves for a vertical profile that accounts for magnetic field inclination. The BIWXM_TR code runs many 1D trajectories and merges these many solutions into a 3D regular grid solution, but with variable spacing in the altitude nodes.

The 1D version of the BIWXM model solves a vertical profile with an inclined magnetic field. The solution solves the non-linear density profiles, velocity and temperature profiles for selected species. There are internal empirical models that define important 'spheres' that the ionosphere is embedded within. The magnetic field is defined by the IGRF (Version13) so it includes a proper declination and inclination. NRL MSIS00e defines the major neutral atmosphere constituent densities (H, N, O, N2, O2). HWM14 defines the neutral atmosphere horizontal wind motions. CTMT has been used but this does not seem

to provide better tides than HWM14 with the exception of adding lunar tides, which HWM14 does not provide.

2.2 BIWXM Setup

2.2.1 BIWXM Software and Public Software

The BIWXM is written in FORTRAN. Some public domain subroutines (MSIS, ODEPACK) and some BIWXM subroutines are written in FORTRAN77 syntax and are indicated by the `.f` suffix on the code file names. Some BIWXM subroutines are written with FORTRAN90 syntax and are indicated by the `.f90` suffix. Any modern FORTRAN compiler will automatically acknowledge the FORTRAN77 and FORTRAN90 subroutines. The development of BIWXM has used the GNU gfortran compiler as the primary development compiler.

2.2.2 Development Environment

The BIWXM model was developed and tested on a multi-core generic computer with Dual CPUs under Ubuntu Linux versions 18.04 and 20.04.

2.2.3 Build Dependencies

The development *gfortran* version is based on GNU *gfortran/gcc* libraries. The GNU *make* utility is used to compile. The BIWXM model precompiled executables use *–static-libgfortran –static-libgcc* flags to strive for portable executables. The precompiled executables are placed in the *./biwxm/bin_precompiled/* directory. The *make.flags* file can be altered for use with the Intel FORTRAN compiler, *ifort*.

2.2.4 Suggested Resources

The BIWXM is designed to solve the D, E and F regions and the topside ionosphere for magnetic latitudes above +/-30 degrees (1) in a single vertical profile or (2) in a many profile distribution with a regular gridded 3D output at a user requested resolution. The 3D resolution can be 300, 200, 100, or 50 km in the horizontal direction with use of increasing number of profiles used to define the 3D region. The vertical resolution is also requested by the user, but is a variable grid that increases with altitude above 100 km. The D region resolution below 70 km is 3 km and 1 km above 70, then from 95 km up the user selects a desired resolution, which increases with altitude. It is recommended that 0.5 to 2.0 km resolution be used. The internal numerical methods selects the appropriate time step for an accurate and stable solution. The user can select the cadence of the output from 1 minute to 60 minutes.

2.2.5 BIWXM 1D Resources

For a 1D BIWXM run, the output files are ascii and organized to hold all information useful to the user and necessary to initiate a new run of the 1D BIWXM using the last output from the previous day run. Running a 1km resolution (E region) run from 30 to 2500km altitude, the single profile model takes 7 minutes for a day run at 5-minute output cadence on a single processor operating at 4GHz.

2.2.6 BIWXM 3D Resources

Note that depending on the selection of horizontal and altitude resolutions of the 3D output produces very large files. The selection of a 3D run (MLat > 45 deg) with horizontal resolution of 50 km and 2 km altitude selection produces a file of 442 MB for each output file of trajectories and another file of the rectangular gridded output of 231 MB for the Northern latitudes above 45 deg magnetic. Each time step of the 3D solution produces has two *netCDF* output files. A day of results with a 15-minute cadence will take about 68 GB of model output or 200 GB for 5-minute cadence. The first day of a BIWXM run is always suspect of contamination by initial conditions (no ionosphere), thus, two days should always be run. If a continuous realtime use of BIWXM is setup with cron, then old days must eventually be deleted.

It is recommended that the BIWXM 3D code run on one computer under a recent version of GNU/LINUX with 24 or more cores with 1TB disk space assigned in total. The 3D results are voluminous.

2.2.7 Setup

The BIWXM is distributed in two compressed tar files: one for the deployment of the source code and directories for compiling and running the code (*BIWXM_VX.X.tar.gz*). VX.X identifies the version and patch subversion. This tar file has the netCDF outputs generated by the BIWXM model for these standard test periods.

These are the instructions to setup the BIWXM on a LINUX-based computer. First place the tar files in a directory for extraction.

STEP 1: Extract Software
The tar files use bzip2 compression. Extract both files using the following commands:

tar –jxf BIWXM_VX.X.tar.bz2

These directories are produced with the following directory structure:

(essential)
./BIWXM/bin/
./BIWXM/data/
./BIWXM/inputs/
./BIWXM/log/
./BIWXM/output/
./BIWXM/scratch/
./BIWXM/src/

(extra directories)
./BIWXM/bin_precompiled/
./BIWXM/doc/
./BIWXM/images/

./BIWXM/plotfiles/
./BIWXM/observations/
./BIWXM/sets/

These are for the following uses for these directories:

bin:	The executable programs of BIWXM
data:	The information of running the test periods and historical runs
inputs:	The physics information for the BIWXM model and various internal empirical model data files.
log:	Log directory for 3D runs to log individual trajectories.
output:	BIWXM program output director
scratch:	scratch area for programs that generate plot-able files
src:	The FORTRAN codes for BIWXM
bin_precompiled:	Holds precompiled programs for LINUX machines.
doc:	The documents of the BIWXM are in this directory.
images:	directory to hold images from plotted runs.
plotfiles:	Holds developer plot files (uses plotl).
observations:	Some observations for comparison runs.
sets:	Holds a copy of set files and various chemical system sets.

STEP 2: Compile the Software
We first suggest skipping this step because there are executables that may already be suitable for your computer. Copy the contents of *./BIWXM/bin_precompiled/* into *./BIWXM/bin/* then Go to STEP 3.

To compile the code, enter the *./BIWXM/src/ directory.* and clean old object files

make clean

The BIWXM code outputs the 3D ionosphere files in NetCDF files. BIWXM requires the NetCDF (FORTRAN90) to be installed on your computer. The compilation of BIWXM is accomplished using the *make* utility. The NetCDF library and include directory should be identified in the *make.flags* file. Edit the make.flags file:

1. Set the directory definition to point to the BIWXM/src directory.
2. Set the fortran include and library definitions to point to the NetCDF install.
3. Choose your compile flags.

then *make* the BIWXM executables:

make

The make procedures will copy the executables to the *./BIWXM/bin/* directory.

STEP 3. First Test.
In the *./BIWXM/* directory you can verify that the code is working properly using the following script

time ./first_run.sh

This is just a test script but is sets up a 1D run at a particular geographic position for a 3-day run to model a quiet spring day in the mid latitudes. The first day is not useful, but the second and third day are useful. This script creates a set of files in the output directory for and in the scratch directory for you to examine. It will run to BIWXM model for March 15, 2015 on day 74 of the year.

This script depends on a number of graphics programs that should be in the *./bin_precompiled/* and in *./bin/* directory (*plotll* , *plotl* , *ps2png, ps2jpg*)

2.3 BIWXM Usage

The executable programs of the BIWXM are placed in *./BIWXM/bin/* the main programs are:

conditions.x:	Program that reads data files in ./BIWXM/data/ to setup run with geophysical indices, solar wind values, IMF values, GOES X-ray Flux, GOES Solar Proton Flux.
biwxm1d.x	Program that generates the ionospheric altitude profiles at a particular geophysical location
biwxm1d.x	Program that collects a day of time-tagged profile files for various plots of those profiles. (Copy to another file name and change as needed.)
biwxm_tr.x	Runs the *biwxm1d.x* many times to construct a mid/high latitude region that covers the polar region.
tr_to_xy.x:	Reads the netCDF files (trajectory file) produced by *biwxm_tr.x* holding the many profiles generated and produces a regular grid solution in an x-y cartesian grid with (x,y) = (0,0) at the geographic pole all in a second regular gridded file. It also reduces the profiles that are clumped in the trajectory file and fills rarified regions.
see_tr.x:	Reads the time-tagged regional netCDF files produced by *biwxm_tr.x* generates files of ionospheric parameters for plotting.
see_xy.x:	Reads the time-tagged regional netCDF files produced by *tr_to_xy.x* generates files of ionospheric parameters for plotting. It can produce results in solar magnetic coordinates.
terminator.x	Program to generate the solar terminator locations for plotting on a geographic grid or plotting on x-y solar magnetic coordinates.

mappolar.x	Program to generate outlines of continents in files for plotting on a geographic grid or on the x-y polar region grid in solar magnetic coordinates.
cgs_to_si_reactions.x:	Program to read a reactions.set files with reaction rates written in cgs and rewrite them in SI.
plotl	A plotting program that works with plotting scripts in ./BIWXM/plotfiles/. See http://plotl.com for comprehensive descriptions.
ps2png, ps2jpg, ps2tiff	are included for convenience of test plotting.

2.3.1 Setup Files and running the ./bin/biwxm1d code

The model has a number of setup files that define the system. The several ascii setup files are:

start_location.set	defines the glon and glat of start of day. This gets updated at the end of the day run if the trajectory is convecting.
time.set	UT Start HHMM, cadence of output in minutes, # of steps of outputs. This is used mostly for biwxm1d.x output cadence.
biwxm.set	defines the spatial grid and has flags for drivers.
species.set	defines the species within the system.
reactions.set	defines the chemical reactions of the system.
conditions.set	defines geoindices, solar wind, IMF, solar x-rays, solar protons. It is created by *./bin/conditions.x*

The above setup files are ASCII files and are read via a free format FORTRAN READ statement. There might be a better set of species and reactions that include metastable species, but the current file provides for D, E, F region and topside. This includes negative ion and metal ion chemistry through simplified species/reactions list. Note there can be a set of neutral species solved for (minor species only) like nitric oxide [NO]. However, this is very slow so the BIWXM has been reduced to be primarily an ion model. However, minor species that are metastable species for important detailed chemistry can be added. We think the improvements in MSIS2020 with the addition of NO will be the best path forward for BIWXM. This permits a run to be accomplished in a reasonable time on a reasonable computer.

So, let's set up a run. Chose a date between 2010 and 2019 and run conditions.x.

./bin/conditions.x 2015 74

for single day. This program (conditions.x) generates geoindices and other inputs for the model in the *condition.set* file. The following lines are the first 10 lines of that file. There is a header line and then 1440 lines of indices for every biwxm step of 60 seconds. Note that conditions.f averages the solar wind conditions and IMF B field for 5-minute averages. The Weimer high

latitude convection model updates the potential pattern every 5 minutes.

You can run BIWXM serially to produce several days of continuous 1D model results. However, if the model is convecting the 1d profile in the high latitude polar region, then after each day of the run one should copy *end_location.set* to *start_location.set*. The lines of the *conditions.set* are read with a free format with the following read statement:

```
OPEN(1,file='conditions.set')
READ(1,*)
DO
  READ(1,*,iostat=ios)iyr,imo,ida,idoy,ihr,imi, &
  f107,f107p,f107a,xkp,xkpnwl,ap,apdaily, &
  dsw,vsw,by,bz,tilt,xray1,xray2,pf01,pf05,pf10,pf30,pf50,pf99
  if (ios/=0) EXIT
ENDDO
```

The definitions of these variables are as follows:

FIRST RECORD:

```
Header for the following column data.
```

EACH REMAINING RECORD:

```
IYR          ! 4-digit year
IMO          ! Month
IDA          ! Day of Month
IDOY         ! Day of Year
IHR          ! UT Hour of Day
IMI          ! UT Minute of Hour
F107         ! F10.7 of current day
F107P        ! F10.7 of previous day (for MSIS)
F107A        ! 90 (or 81) day average of F10.7
xKp          ! Newell Kp value calculated from solar wind
Ap           ! Ap Geomagnetic Indices calculated from xKp
ApDAILY      ! 24-hour average of Ap
dsw          ! solar wind density (#/cc)
vsw          ! solar wind velocity (km/s)
By           ! IMF By
Bz           ! IMF Bz
Tilt         ! earth tilt
Xray1        ! Short wavelength bin of GOES Xray Flux
Xray2        ! Long wavelength bin of GOES Xray Flux
P01          ! GOES Proton Flux of Protons >=1MeV
P05          ! GOES Proton Flux of Protons >=5MeV
P10          ! GOES Proton Flux of Protons >=10MeV
P30          ! GOES Proton Flux of Protons >=30MeV
P50          ! GOES Proton Flux of Protons >=50MeV
P99          ! GOES Proton Flux of Protons >=100MeV
```

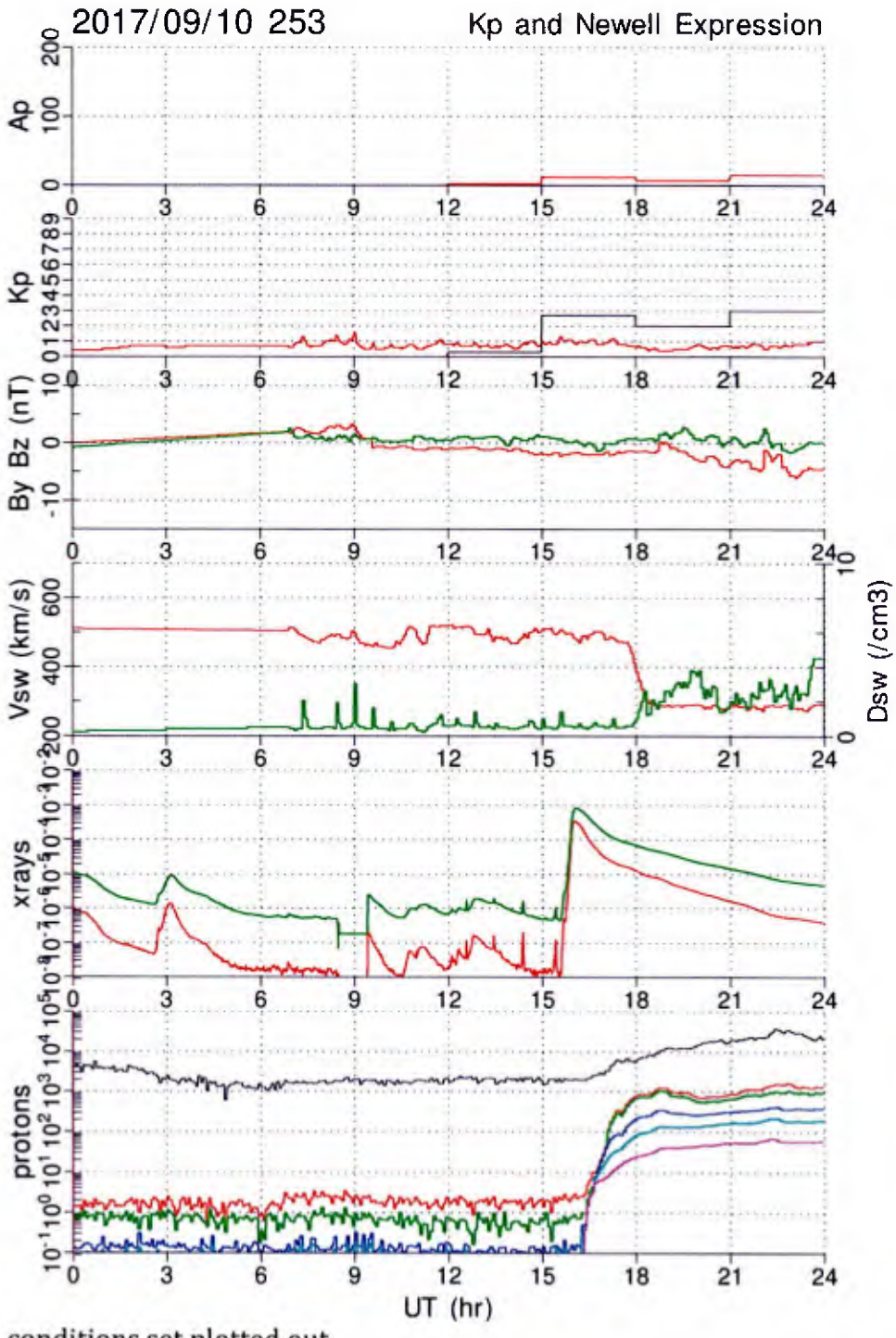

Figure 2.1 conditions.set plotted out.

Figure 2.1 is a plot of these data in a 1-day run of BIWXM. These are plotted directly out of the *BIWXM.set* file.

The next program to run is *./bin/biwxm1d.x* but there are several files to edit for what the user desires. First, *biwxm.set*, which is printed below:

```
        ! altitude information
185     ! nz - altitude nodes
30      ! z0 node
1.0     ! dz0 resolution in km
1.040   ! zfact increasing spacing with altitude
                ! flags
0       ! atmosphere flag (0 - msis+hwm, no other option)
1.0     ! factor on fe layer (0 to 1)
0.02    ! factor on gcr      (0 to 1) (Galactic Cosmic Rays default 0.02)
1.0     ! factor on e precip (0 to 1) (Auroral e precipitation)
1.0     ! factor on spe      (0 to 1) (Solar Proton Events)
1.0     ! factor on xrays    (0 to 1) (Solar Xray flares)
1.0     ! factor on euv      (0 to 1) (Solar EUV)
1       ! flag   on convection (0 or 1) must be integer
        !        0 - no convecting trajectory (ExB not calculated)
        !        1 - convection of trajectory (ExB calculated)
        !        2 - no convecting trajectory (ExB calculated)
```

These are expected lines as are the blank lines.

nz	number of altitude nodes
z0	first altitude (must be 30 km or greater)
dz0	spacing near 100 km (1. or 2. km)
zfact	multiplier for increasing altitude spacing
aflag	atmosphere flag (0 – msis+hwm is only option currently)
factor_fe	factor on neutral empirical Fe layer (0 to 2 – default: 1)
factor_gcr	factor on ionization by galactic cosmic rays (0 to 1 – default: 1e-4)
factor_eprec	factor on ionization by e precipitation (0 to 1 – default: 1)
factor_spe	factor on ionization by SPE (0 to 1 – 0.25)m
factor_xrays	factor on xray fluxes (0.05 to 10 nm). (0 to 1)
factor_euv	factor on EUV fluxes (10 to 121.4 nm). (0 to 1)

Second, *start_location.set* to indicate trajectory position at start of run. If convection is used, then high latitude trajectories will move along convection potential lines and the *end_location.set* file will be written at the end of the run. If the run is a contiguous day run, then copy *end_location.set* from the previous day run to *start_location.set.* Next, generate the *conditions.set* file for the day run desired via *./bin/conditions.x*. This program reads data files within *./BIWXM/data/*. Finally, run the BIWXM model *./bin/biwxm1d.x*.

There are other setup files. The species.set file defines the chemical system. The reactions.set file defines the chemical reactions and rates to be used. Currently, the BIWXM models is designed for solving the ions and electron parameters in a vertical profile. If neutrals are to be added, then contact Vince Eccles as minor neutral gases can be solved for as well, but several components of the code need to be inserted for these species. Additionally, there is ncpu.set that indicates to the 3D BIWXM run how many CPU cores are available to run profiles in parallel. It is recommended that one uses something less than the total number of cores within the computer to permit other users to manage their login

and edit sessions with free cores. Note that the code does not access threads. gfortran compilers have not optimize for the symmetric parallel use of threads.

The *biwxm1d..x* program is 'noisy'. It prints to the screen information on the progress of the calculation. This can be redirected to a *foo* file.

The output files generated by ./bin/biwxm1d.x are placed in ./output/. These are text files containing the results of the numerical model. Outputs will be at a 5-minute cadence and be time-tagged for the 'end-of-the-period' output time. All species are represented in the outputs.

./output/ds20172530000.txt	! contains densities (#/m^3)
./output/vs20172530000.txt	! contains southward velocities (m/s)
./output/ve20172530000.txt	! contains eastward velocities (m/s)
./output/vz20172530000.txt	! contains vertical velocities (m/s)
./output/ts20172530000.txt	! contains temperatures (ion, neutral, electron)

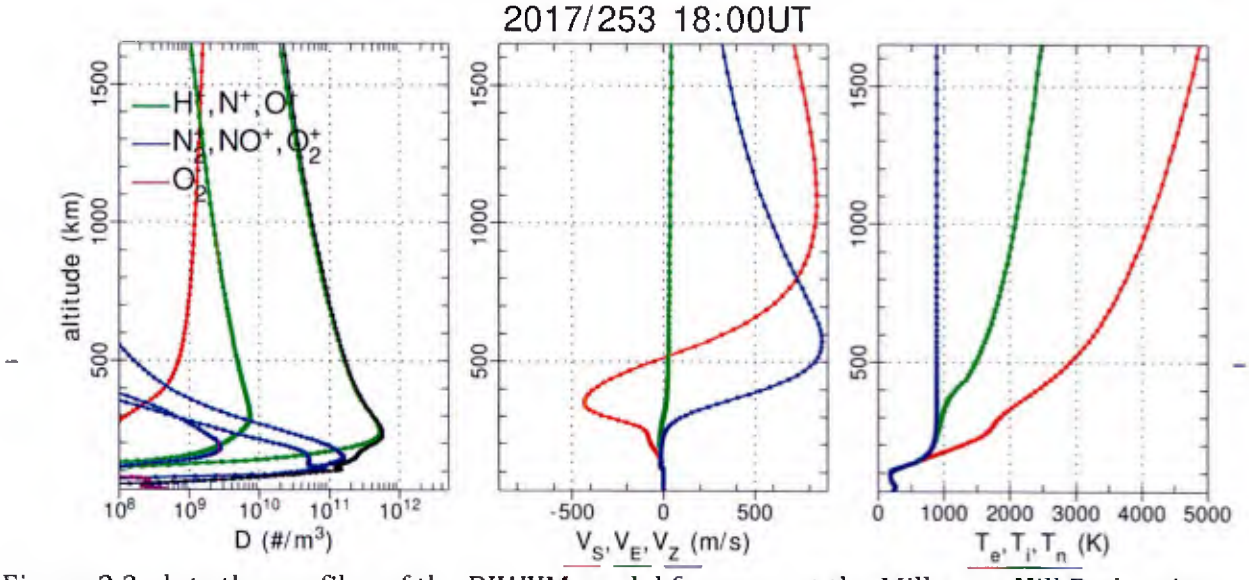

Figure 2.2 plots the profiles of the BIWXM model for a run at the Millstone Hill Radar site. The left-hand panel provides ion densities, right hand panel provides temperatures, and the middle panel plots south, east, and vertical velocities of the O+ ion.

2.3.2 Setup Files and running the ./bin/biwxm_tr.x code (3D BIWXM)

The BIWXM single profile code can be run many times to construct a 3D ionospheric representation. The *./bin/biwxm_tr.x* performs this task. The *biwxm_tr* code first initializes the 3d output files, then calls many *biwxm1d.x* runs to provide a sufficiently dense solution of many trajectories, then constructs a regular 3D grid solution of the ionosphere. The individual trajectory information at each output time step is held in a time-tagged netCDF file.

./output/trj20131451200.nc
./output/trj20131451205.nc
./output/trj20131451210.nc
./output/trj20131451215.nc
./output/trj20131451320.nc

These files hold all the information of the biwxm1d.x output for all profiles run. There are additional setup files required by biwxm_tr.x to establish the characteristics of the run.

- ncpu.set --- indicates the number of CPU cores available for launching parallel single profile runs (biwxm1d.x) to produce the 3d ionosphere.
- biwxm_tr.set --- indicates the fundamental resolution of the 3D run in degrees. This should be 2 or 1 or 0.5 degrees. The number of profiles is generated to accomplish the requested resolution.

To run the 3D BIWXM model, one must run the conditions program once, then run the biwxm_tr.x program. Depending on the resolution requested and the number of cores being used, the run can take hours to days of wall-clock time to produce the 3D representation of the ionosphere above MLat 45 degrees north. Figure 2.3.1 plots the ionospheric parameters associated with a 3D run with a resolution of 0.5 degrees.

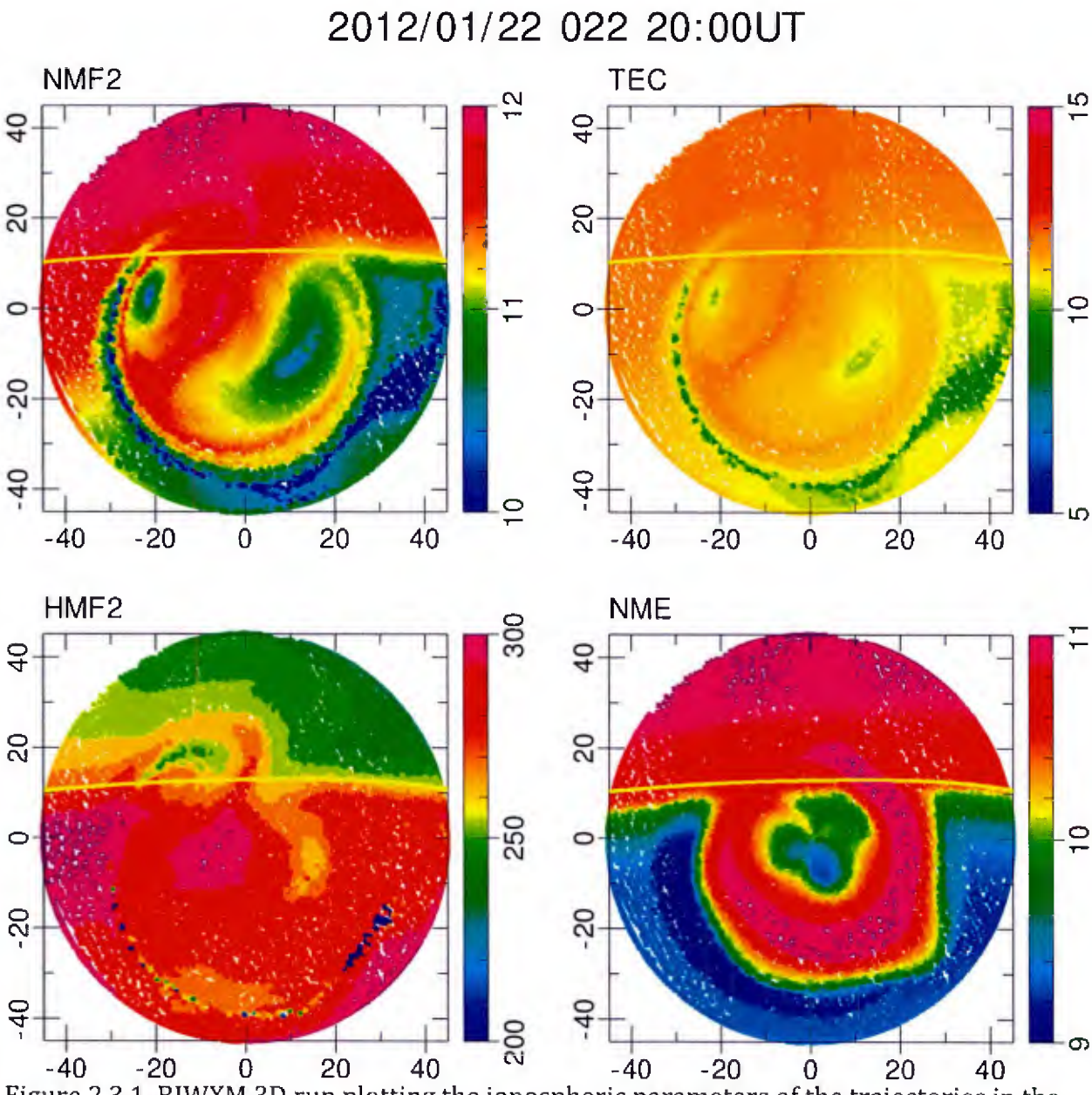

Figure 2.3.1. BIWXM 3D run plotting the ionospheric parameters of the trajectories in the trj20120222000.nc file. (a) log(NmF2) values, (b) TEC values, (c) HmF2 values in km, and (d) log(NmE) values.

Every hour of model time the biwxm_tr.x model code reads the last hour of output files and generates a regular gridded representation of the ionosphere in the polar x, y, altitude grid where

$$x = \Theta * \cos\phi$$
$$y = \Theta * \sin\phi$$

with Θ is the geographic colatitude (90-λ) and ϕ is the geographic longitude. This is a call from within *biwxm_tr.x* to a second program, *tr_to_xy.x*. The *tr_to_xy.x* program collects the trajectories for the regular gridded representation, but it also examines if there are regions with no profiles due to clumping of convecting trajectory paths or too many profiles and

redistributes a few of the profiles in the *biwxm_tr.x* run to keep a reasonable distribution of profiles throughout the whole region. The regular gridded results are time-tagged files named:

./output/xy3d20131451200.nc
./output/xy3d20131451205.nc
./output/xy3d20131451210.nc
./output/xy3d20131451215.nc
./output/xy3d20131451320.nc

One can examine the contents of the trj files or the *xy3d* files by using the *ncdump* utility.

ncdump output/trj20200222000.nc > trj.txt
ncdump output/xy3d20200222000.nc > xy3d.txt

The netCDF files can be very large and the text files will be at least twice as large. For example, using the biwxm_tr.set resolution of 0.5 degrees, one gets 25433 profiles within each trjyyyydddhhmm.nc file which is 544MB. The xy3dyyyydddhhmm.nc files are 274MB. This provides the following ASCII information on the content of the trj file (data excluded):

```
netcdf trj20120222000 {
dimensions:
      StringLen = 32 ;
      AltitudeDim = 160 ;
      TrajDim = 25433 ;
variables:
      char Model_tr(StringLen) ;
      float UThr_tr ;
      float Resolution_tr ;
      float Altitudes(AltitudeDim) ;
      float GeoLongitudes_tr(TrajDim) ;
      float GeoLatitudes_tr(TrajDim) ;
      float MagLocalTimes_tr(TrajDim) ;
      float MagLatitudes_tr(TrajDim) ;
      float e-_density_tr(TrajDim, AltitudeDim) ;
      float H+_density_tr(TrajDim, AltitudeDim) ;
      float N+_density_tr(TrajDim, AltitudeDim) ;
      float O+_density_tr(TrajDim, AltitudeDim) ;
      float N2+_density_tr(TrajDim, AltitudeDim) ;
      float NO+_density_tr(TrajDim, AltitudeDim) ;
      float O2+_density_tr(TrajDim, AltitudeDim) ;
      float Fe+_density_tr(TrajDim, AltitudeDim) ;
      float M2-_density_tr(TrajDim, AltitudeDim) ;
      float H+_vsouth_tr(TrajDim, AltitudeDim) ;
      float N+_vsouth_tr(TrajDim, AltitudeDim) ;
      float O+_vsouth_tr(TrajDim, AltitudeDim) ;
      float N2+_vsouth_tr(TrajDim, AltitudeDim) ;
      float NO+_vsouth_tr(TrajDim, AltitudeDim) ;
      float O2+_vsouth_tr(TrajDim, AltitudeDim) ;
      float Fe+_vsouth_tr(TrajDim, AltitudeDim) ;
      float M2-_vsouth_tr(TrajDim, AltitudeDim) ;
      float H+_veast_tr(TrajDim, AltitudeDim) ;
```

```
        float N+_veast_tr(TrajDim, AltitudeDim) ;
        float O+_veast_tr(TrajDim, AltitudeDim) ;
        float N2+_veast_tr(TrajDim, AltitudeDim) ;
        float NO+_veast_tr(TrajDim, AltitudeDim) ;
        float O2+_veast_tr(TrajDim, AltitudeDim) ;
        float Fe+_veast_tr(TrajDim, AltitudeDim) ;
        float M2-_veast_tr(TrajDim, AltitudeDim) ;
        float H+_vup_tr(TrajDim, AltitudeDim) ;
        float N+_vup_tr(TrajDim, AltitudeDim) ;
        float O+_vup_tr(TrajDim, AltitudeDim) ;
        float N2+_vup_tr(TrajDim, AltitudeDim) ;
        float NO+_vup_tr(TrajDim, AltitudeDim) ;
        float O2+_vup_tr(TrajDim, AltitudeDim) ;
        float Fe+_vup_tr(TrajDim, AltitudeDim) ;
        float M2-_vup_tr(TrajDim, AltitudeDim) ;
        float Te_tr(TrajDim, AltitudeDim) ;
        float Ti_tr(TrajDim, AltitudeDim) ;
```

The xy3d is simpler, and the ascii result of the ncdump provides (data excluded):

```
netcdf xy3d20120222000 {
dimensions:
        StringLen = 32 ;
        RegionDim = 113 ;
        AltitudeDim = 160 ;
variables:
        char Model(StringLen) ;
        float xGeo(RegionDim) ;
        float yGeo(RegionDim) ;
        float Altitudes(AltitudeDim) ;
        float Resolution ;
        float UThr ;
        float GeoLongitudes(RegionDim, RegionDim) ;
        float GeoLatitudes(RegionDim, RegionDim) ;
        float MagLocalTimes(RegionDim, RegionDim) ;
        float MagLatitudes(RegionDim, RegionDim) ;
        float e-_density(AltitudeDim, RegionDim, RegionDim) ;
        float H+_density(AltitudeDim, RegionDim, RegionDim) ;
        float N+_density(AltitudeDim, RegionDim, RegionDim) ;
        float O+_density(AltitudeDim, RegionDim, RegionDim) ;
        float N2+_density(AltitudeDim, RegionDim, RegionDim) ;
        float NO+_density(AltitudeDim, RegionDim, RegionDim) ;
        float O2+_density(AltitudeDim, RegionDim, RegionDim) ;
        float Fe+_density(AltitudeDim, RegionDim, RegionDim) ;
        float M2-_density(AltitudeDim, RegionDim, RegionDim) ;
        float H+_vsouth(AltitudeDim, RegionDim, RegionDim) ;
        float N+_vsouth(AltitudeDim, RegionDim, RegionDim) ;
        float O+_vsouth(AltitudeDim, RegionDim, RegionDim) ;
        float N2+_vsouth(AltitudeDim, RegionDim, RegionDim) ;
        float NO+_vsouth(AltitudeDim, RegionDim, RegionDim) ;
        float O2+_vsouth(AltitudeDim, RegionDim, RegionDim) ;
        float Fe+_vsouth(AltitudeDim, RegionDim, RegionDim) ;
        float M2-_vsouth(AltitudeDim, RegionDim, RegionDim) ;
        float H+_veast(AltitudeDim, RegionDim, RegionDim) ;
        float N+_veast(AltitudeDim, RegionDim, RegionDim) ;
        float O+_veast(AltitudeDim, RegionDim, RegionDim) ;
```

```
float N2+_veast(AltitudeDim, RegionDim, RegionDim) ;
float NO+_veast(AltitudeDim, RegionDim, RegionDim) ;
float O2+_veast(AltitudeDim, RegionDim, RegionDim) ;
float Fe+_veast(AltitudeDim, RegionDim, RegionDim) ;
float M2-_veast(AltitudeDim, RegionDim, RegionDim) ;
float H+_vup(AltitudeDim, RegionDim, RegionDim) ;
float N+_vup(AltitudeDim, RegionDim, RegionDim) ;
float O+_vup(AltitudeDim, RegionDim, RegionDim) ;
float N2+_vup(AltitudeDim, RegionDim, RegionDim) ;
float NO+_vup(AltitudeDim, RegionDim, RegionDim) ;
float O2+_vup(AltitudeDim, RegionDim, RegionDim) ;
float Fe+_vup(AltitudeDim, RegionDim, RegionDim) ;
float M2-_vup(AltitudeDim, RegionDim, RegionDim) ;
float Te(AltitudeDim, RegionDim, RegionDim) ;
float Ti(AltitudeDim, RegionDim, RegionDim) ;
float fof2(RegionDim, RegionDim) ;
float nmf2(RegionDim, RegionDim) ;
float hmf2(RegionDim, RegionDim) ;
float foe(RegionDim, RegionDim) ;
float nme(RegionDim, RegionDim) ;
float hme(RegionDim, RegionDim) ;
float TEC(RegionDim, RegionDim) ;
```

The programs that read these files for plotting are *./bin/see_tr.x* and *./bin/see_xy.x*. the FORTRAN is in *./src/see_tr.f90* and *./src/see_xy.f90*. The subroutines that create, write, and read the output files are *./src/include/rw_biwxm_trajs_nc.f90* and *./src/include/rw_biwxm_xy3d_nc.f90*.

The programs to see the parameter results are run with command line inputs:

./bin/see_tr.x <year> <day-of-year> <hour> <minute>

and

./bin/see_xy.x <year> <day-of-year> <hour> <minute>